Tooth tales told by dental diet proxies: an alpine community of sympatric ruminants as a model to decipher the ecology of fossil fauna

Gildas Merceron, Emilie Berlioz, Hubert Vonhof, Daniel Green, Mathieu Garel

Tooth tales told by dental diet proxies: an alpine community of sympatric ruminants as a model to decipher the ecology of fossil fauna

Gildas Merceron[1]*, Emilie Berlioz[1,2], Hubert Vonhof[3], Daniel Green[4], Mathieu Garel[5], Thomas Tütken[6]

1. PALEVOPRIM, UMR 7262 CNRS and University of Poitiers, 86073 France Cedex; gildas.merceron@univ-poitiers.fr
2. TRACES, CNRS and University of Toulouse, France; emilie.berlioz@univ-tlse2.fr
3. Department of Climate Geochemistry, Max Planck Institute for Chemistry, 55128 Mainz, Germany; hubert.vonhof@mpic.de
4. Department of Human Evolutionary Biology, Harvard University, Peabody Museum, 11 Divinity Avenue, Cambridge, MA 02138, U.S.A.; drgreen@fas.harvard.edu
5. OFB, Direction de la Recherche et Appui Scientifique, Unité Ongulés Sauvages – Gières, France ; mathieu.garel@ofb.gouv.fr
6. Applied and Analytical Paleontology, Institute of Geosciences, Johannes Gutenberg University, 55128 Mainz, Germany; tuetken@uni-mainz.de

*Corresponding author
Email address: gildas.merceron@univ-poitiers.fr

Abstract

Paleobiologists tend to use dietary information as an ecological indicator because diet is a fundamental link between an organism and its environment. However, the ecological information from fossilized hard tissues is often difficult to interpret, because links between environment, diet, and hard tissue biology are insufficiently studied in modern communities. To address this dilemma, we investigated dietary proxies commonly used by paleobiologists in a 4-ruminant community from the French Alps. Dental microwear textural analyses are applied to 82 specimens of roe deer, red deer, chamois, and mouflons. Intra-tooth serial enamel stable carbon and oxygen isotope analyses of the structurally bound carbonate were applied on eleven specimens, with isotope-based niche reconstructions, and inverse modeling of original seasonally variable oxygen isotope inputs.

While microwear complexity largely overlaps, both inter-individual dispersion and heterogeneity of complexity together with the anisotropy track dietary differences. The red deer is likely more engaged in grazing than the two bovids, which both plot as mixed feeders. When combined, dental microwear and carbon stable isotope analyses accurately reflect known ecological separation between the chamois and the roe deer. Both stable isotopes suggest niche separation by increasing enrichment from roe deer to red deer, to chamois; mouflons appear to feed as generalists. In roe deer, which shows the highest enamel oxygen isotope range (5.7 ‰), variation is nevertheless constrained compared to oxygen isotope ranges observed in regional precipitation, where the mean annual range reaches 9.9 ‰. However, through inverse modeling we estimate seasonal input ranges that average 9.7 ‰, a result strikingly similar to regional values. Altogether, our data demonstrate that given appropriate sampling strategies and modeling approaches, microwear and isotopic data can be effective tools for demonstrating niche separation among multiple sympatric herbivorous taxa.

Keywords: Niche, Teeth, Stable Isotopes, Dental Microwear Textures, Ungulates, Europe

1. Introduction

Exploring the diet of extinct species is essential to understand how they interacted with their ecosystems, and how biotic and abiotic factors have both shaped their evolution. Most soft tissues including stomach contents are rarely preserved in the fossil record, and vertebrate paleontologists therefore base many paleodietary reconstructions on dental morphology. Based on functional interpretations paleontologists identify plausible underlying mechanisms driving evolution, and propose environmental reconstructions that constrain climate models. For instance, the relative abundances of ruminants with low- and high-crowned cheek teeth supposedly reflecting grazing versus browsing behavior have been used to assess spatial and chronological variations in vegetation covers and climatic conditions (e.g., Fortelius et al., 2002; Kaya et al., 2018).

Alternative approaches provide taxon-free tools to reconstruct the ecological traits. Among them, the most widely used in mammal paleontology are traditional and non-traditional stable isotopes (see Ben-David and Flaherty, 2012 and citations therein; Martin et al., 2017) and dental microwear texture analyses (Ungar et al., 2008; Calandra and Merceron, 2016; DeSantis, 2016; Kaiser et al., 2016). However, prior to their application to fossils, these proxies require validation using either in vivo experimentations (Merceron et al., 2016; Ramdarshan et al., 2016, 2017; Schulz et al., 2013; Winkler et al., 2019) or well-constrained modern communities of species with known ecological habits and life history traits (Merceron et al., 2010; Berlioz et al., 2017; Bignon-Lau et al., 2017; Percher et al., 2018).

The present paper is a case study to explore how dental tissues reflect ecological partitioning, through dietary habits and habitat use, among a modern community of four sympatric ruminants. We here focus on two species of cervids (*Cervus elaphus*, and *Capreolus capreolus*) and two of bovids (*Ovis gmelini musimon*, and *Rupicapra rupicapra*) from the Bauges Natural Regional Park (BNRP) in the French Alps. These species have

different feeding behaviors and habitat use due to species-specific body-mass, digestive morpho-physiological features and social-spatial behaviors (Redjadj et al., 2014 and citations therein).

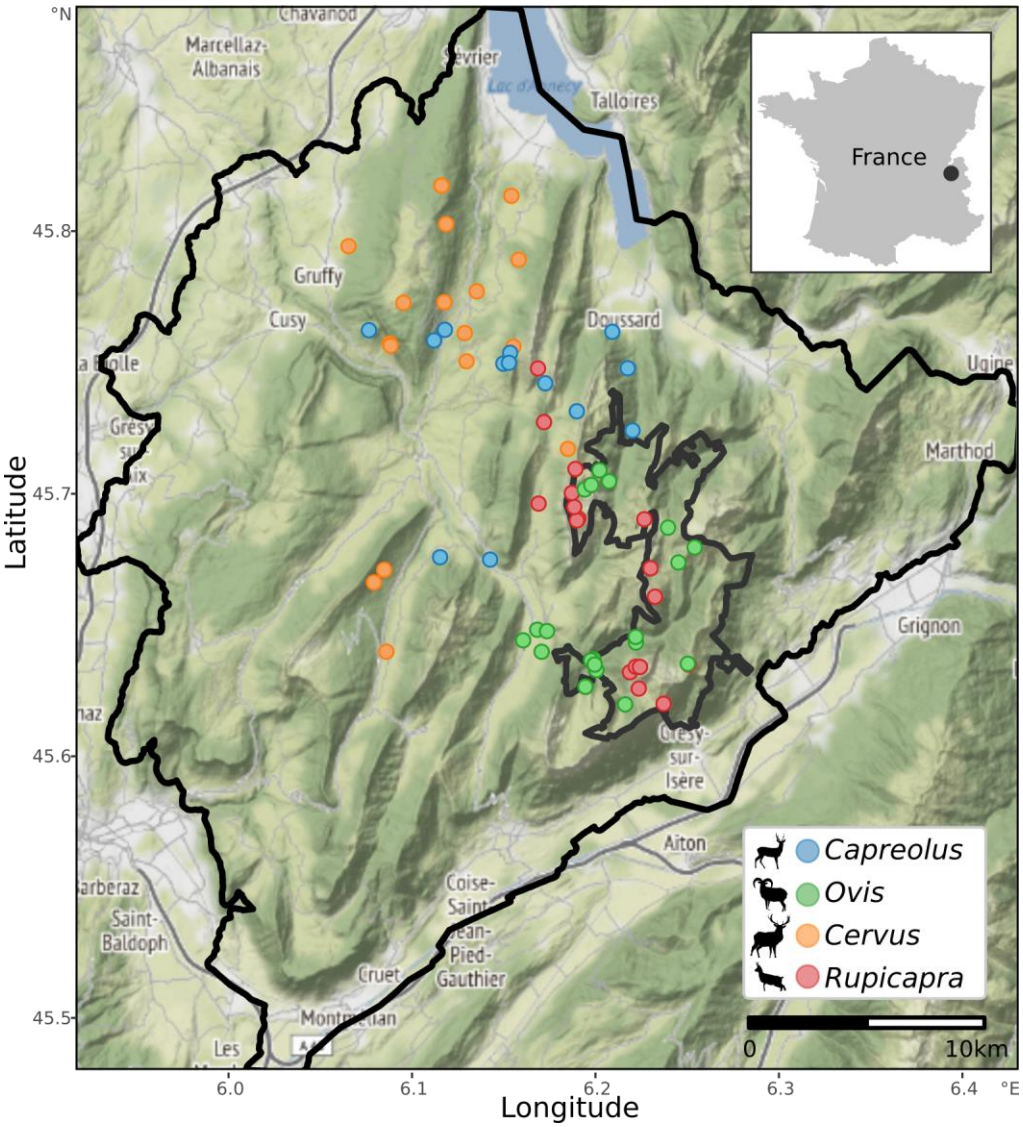

Figure 1. Location of specimens of roe deer (*Capreolus capreolus*, n = 18), red deer (*Cervus elaphus*, n = 21), chamois (*Rupicapra rupicapra*, n = 21) and mouflon (*Ovis gmelini musimon*, n = 22) from Bauges Natural Regional Park (BNRP). The inner limits correspond to the National Game and Wildlife Reserve within the BNRP. White zones represent urbanized areas, dark green forest and light green either lowland open fields or higher alpine meadows.

As Redjadj et al. (2014) have shown inter-specific differences in diet and habitat within the Bauges ruminant community, we expect to observe corresponding differences in dental microwear textures (Merceron et al., 2016; Ramdarshan et al., 2016; Schulz et al.,

2013; Scott, 2012) and stable carbon isotopes ($^{13}C/^{12}C$ ratio expressed as $\delta^{13}C$ value in permil relative to VPDB; Vienna PeeDee Belemnite) in enamel (Bonafini et al., 2013; Drucker and Bocherens, 2009). In addition, we expect the enamel oxygen isotopic composition ($^{18}O/^{16}O$ ratio expressed as $\delta^{18}O$ value in permil relative to VSMOW, Vienna Standard Mean Ocean Water) to primarily reflect the $\delta^{18}O$ values of the ingested water, including drinking and/or leaf water. Physiology (Kohn, 1996; Green et al., 2018a) and altitudinal ranges (Dansgaard, 1964; Rozanski et al., 1993; Gat, 1996; Bowen, 2010) will further impact body water and enamel $\delta^{18}O$ compositions (See text-SI). The community of sympatric ruminants at the BNRP representing 82 wild-shot individuals with known sex, age, place and date of death, sampled over few months mostly during fall 2014 and 2015, provides a unique opportunity to investigate ecological partitioning through different dietary proxies all issued from dental tissues. This will allow us to draw conclusions how well a combined dental wear and stable isotope approach on such a well-constrained faunal sample does reflect the environmental conditions in mid-latitude mountainous C_3 plant ecosystem.

2. Material and methods

2.1. Material

The Bauges Natural Regional Park (BNRP; 45.69 °N, 6.14 °E) is a typical subalpine massif located in the French Alps, with altitudes ranging from 250 m to 2217 m (see Figure 1 and Text-SI). Several studies have investigated multiple aspects of behavioral ecology of the ruminants (chamois, red deer, roe deer and mouflon) inhabiting the BNRP. Among them, Redjadj et al. (2014; see Text-SI and Table S1) made a comparative analysis of the feeding ecology of these four large herbivores through a gender-balanced stomach content analysis covering late summer until early winter period from 2003 to 2008. It is worth mentioning here that the specimens considered in Redjadj et al. (2014) are not the same analyzed in the present

112 study. However, we used to interpret at best between species differences in dental dietary
113 proxies. It is also worth noting that stomach content or feces analyses reflect dietary
114 composition of the last few hours and days, respectively. However, the dietary proxies
115 extracted from dental tissues we investigate here reflect larger time windows: from at least
116 weeks, to months, to just over a year (Kierdorf and Kierdorf, 2000; Davis and Pineda Munoz,
117 2016).

118 *Cervus elaphus* is a mixed-feeding species (including both monocots and dicots)
119 with spatial variation in its diet (Gebert and Verheyden-Tixier, 2001). *Capreolus capreolus* is
120 a selective browser (Tixier et al., 1997). *Ovis gmelini musimon* is a mixed-feeding species.
121 Marchand et al. (2013) concluded that although grasses are the major food type, foliages from
122 shrubs and herbaceous dicots are the secondarily preferred food resources. *Rupicapra*
123 *rupicapra* is a mixed feeder grazing and browsing depending resource availabilities and
124 energetic requirements (Pérez-Barberia et al., 1997; see Text SI and Table S1). The largest
125 ruminant (adult males: 151 kg; adult females: 98 kg; Text SI and Table S1) at the BNRP, the
126 red deer *Cervus elaphus*, is a mixed-feeding species (including both monocots and dicots)
127 with spatial variation in its diet. Grasses account for about 30 % of the annual diet in many
128 regions through Europe but can surpass 80 % in Mediterranean habitats (Azorit et al., 2012;
129 Bugalho and Milne, 2003; Gebert and Verheyden-Tixier, 2001). At the BNRP, Redjadj et al.
130 (2014) found out that during late summer and early fall (the period during which most of the
131 specimens were shot), herbaceous monocots and forbs represent about 40 and 6 %,
132 respectively, of the stomach content as dry matter weight. Fruits, mainly apples and to a lesser
133 extent acorns (Redjadj et al., 2014) may account for up to 20 %. Foliages from various
134 evergreen and deciduous trees and shrubs (cumulative proportions reaching 23.6 %),
135 dominated by evergreen shrubs, notably brambles (*Rubus fruticosus*; Table S1), also form a
136 major fraction of the diet. It is worth noting that Suter et al. (2004) indicates that herbaceous

monocots represent between 50 and 60 % of summer diet of red deer in the Alps, which is complemented with herbaceous dicots (forbs) that could represent up to 20 %. Although comparisons between the two studies are difficult as the sampling methods differ, the seasonal shift from graze to browse from summer to winter are reported for many Alpine populations (Suter et al., 2004).

The second cervid, the roe deer *Capreolus capreolus* (adult males: 22.8 kg; adult females: 21.4 kg; Text SI and Table S1), is a selective browser (Cibien, 1984; Cornelis et al., 1999; Cransac et al., 2001; Storms et al., 2008; Tixier et al., 1997). Its diet mostly includes dicot foliage, mosses, mushrooms, fruits including seeds. Herbaceous monocots barely reach 10 % of its diet; this occurs, however, only in spring. In late summer and early fall, roe deer from the BNRP mainly focus on evergreen shrubs (bramble leaves) and forbs at about 44 and 25 % of the stomach content expressed as dry matter weight, respectively. Evergreen shrubs reach almost 60 %, and forbs surpass 10 % in late fall and winter. What is surprising at the BNRP is the very low amount of fruits in the roe deer diet for the two periods (3.4 and 5.8 % of the diet, respectively) compared to the greater fruit intake among red deer at BNRP, (Redjadj et al., 2014), and to roe deer populations in other locations (Tixier and Duncan, 1996). As expected, grasses represent less than 6 % of the roe deer diet for each of the two seasons at the BNRP (Table S1).

The mouflons, *Ovis gmelini musimon* (adult males: 42.8 kg; adult females: 31.3 kg; Text SI and Table S1) is a mixed-feeding species. Marchand et al. (2013) reviewed the feeding ecology of this wild sheep. Although grasses are the major food type, foliages from shrubs and herbaceous dicots are the secondarily preferred food resources. At the BNRP, grasses represent 42 and 29 % (expressed as percentage of dry matter weight) of their diet for each of the two investigated periods (Redjadj et al., 2014). Evergreen shrubs (16.2 %) and forbs (15.7 %) are the secondarily preferred foods in late summer and early fall. In late fall

and winter, evergreen trees (mostly conifer foliages; 28.1 %) counterbalance the drop in proportions of both forbs and grass component compared to the first period (Table S1; Redjadj et al., 2014).

The chamois *Rupicapra rupicapra* (adult males: 34.5 kg; adult females: 29.7 kg; Text SI and Table S1) is a mixed feeder grazing and browsing depending resources availabilities and energetic requirements (Pérez-Barberia et al., 1997). For instance, recent studies show that the chamois in Pyrenees may include less than 20 % grasses in its summer and fall diets (Espunyes et al., 2019). Besides, grasses represent 44 % and more than 50 % in summer and fall, respectively, of its diet at the BNRP (Table S1; Redjadj et al., 2014). Forbs (22.4 %) and evergreen shrubs (19.6 %) complement the diet for the first period whereas the drop in forbs is counterbalanced with evergreen trees (17.5 %) composing the secondary food items (Table S1).

Mandibles were collected from early September to end of March during three hunting seasons (2008/2009, 2014/2015 and 2015/2016), from adult animals (with worn facets on M_2 and erupted or erupting M_3)shot during the legal hunting season both within and outside the National Game and Wildlife Reserve (Figure 1). Most of the specimens were sampled from late September to November 2015 (see Appendix 2). All samples come from animals tagged with official annual hunting quotas delivered by the county prefects in agreement with the environmental code (Art. R425-2 to 425-141 13). No animals were harvested solely for the purpose of this study. A total of 11 and 82 adult specimens (with erupted and worn second molars) were used for serial intra-tooth enamel stable isotope and dental microwear texture analyses, respectively (see SI-Text and Appendices 1 and 2).

2.2. Methods

2.2.1. Enamel carbon and oxygen stable isotope analyses

About 100 µg of enamel powder per sample were serially extracted with a hand-held microdrill, sampled along the crown from apex to cervix on both second and third lowers (see Figures 2 and 3; Table 1; see Text SI and Appendix 1). The spatial location of sample positions on each tooth was recorded to within 0.1 mm precision. No bleach treatment was applied. Isotope analyses of structural carbonate in tooth enamel samples were performed on a Thermo DeltaV mass spectrometer coupled to a Gasbench II gas preparation unit in which a cold trap system at liquid nitrogen temperature is integrated. The system is setup as outlined in Fiebig et al. (2005; see Text-SI).

Enamel formation (amelogenesis) of second and third molars differ in duration from one species to another depending on the body mass and molar heights (see Text-SI). The amelogenesis may last about 4 months for the roe deer second molar up to more than a year for the third molar of the other ruminants because they are larger and have higher tooth crown. Kierdorf and Kierdorf (2000) report that for the roe deer, enamel formation (amelogenesis) of M2 begins *in utero* and terminates around 4 months of age. The roe deer M3 is estimate to form between 4–9 months of age. For the red deer, the second molar begins forming prior to 3 months of age and completes formation around 9 months of age; the third molar begins forming at 9 months of age and completes prior to 26 months. We estimate the fractionation factor ε between the carbon stable isotope composition of food resources ($\delta^{13}C_{diet}$) and enamel carbonate using a body mass-dependent equation calibrated for foregut-fermenting mammals (Tejada-Lara et al., 2018; Table 1; see Text-SI and Appendix 1). While there is uncertainty in the optimal parameterization of ε (Clauss et al., 2020; Manthi et al., 2019) in our calculations this offset differs by less than 1.1 ‰ between taxa. In parallel to carbon isotope analysis of tooth enamel, for some individuals food remains stuck between cusps and teeth in the jaw were sampled also for carbon isotope analysis, if present, to directly assess the $\delta^{13}C$ values of ingested plants (see Text-SI and Table S2). Both food remains from

212 the teeth/jaw and $\delta^{13}C_{enamel}$ represent an unknown interval of time. We argue the plant
213 remains stuck in teeth is an epiphenomenon meaning the direct comparisons of these data
214 should be done with high caution. In any case, the $\delta^{13}C_{enamel}$ value of the very last sample to
215 mineralize on the M_3 is the most appropriate value to be compared with $\delta^{13}C$ measured from
216 food remains stuck between cusps and teeth. Based on the enamel oxygen isotope
217 composition, we propose an estimation of the oxygen isotope composition of the
218 environmental water ($\delta^{18}O_{ew}$) ingested by the ruminants from the BNRP following the
219 regression between enamel (i.e. structurally bound carbonate in the bioapatite) and ingested
220 water of Iacumin et al. (Iacumin et al., 1996; Table 1; Text-SI).

221 We also consider the niche breadth B_A (Levins, 1968) and the ecological
222 overlapping O_{Bauges} (Pianka, 1973) based on both $\delta^{18}O_{ew}$ and $\delta^{13}C_{diet}$ (see also Dantas et al.,
223 2017), and mixSIAR modeling based on enamel $\delta^{18}O$ and $\delta^{13}C$ measurements (Jackson et al.,
224 2011). The niche breadth B_A estimating inter-individual dispersion and the ecological
225 overlapping O_{Bauges} are computed with the relative proportions of values plotting within pre-
226 defined isotopic bins (Table 2; Figure 4; see text-SI). Instead of using a mean value per
227 individual, which is a computation of *n* values representing an unknown time span, we here
228 simulate every *n* intra-tooth values in stable isotope composition along the M_3 as a single
229 snapshot of stable isotope composition (of the diet or environmental water ingested) of *n*
230 individuals randomly sampled. This means that the value sampled n_i is representative of an
231 individual *i* among a given population at any season around the year.

232 Lastly, we combine serial enamel $\delta^{18}O$ values with inverse modeling to estimate
233 $\delta^{18}O$ seasonality, a longtime goal of vertebrate isotope ecology (e.g. Passey et al., 2005;
234 Zazzo et al., 2010; Blumenthal et al., 2019). Specifically, we employ Bayesian inference with
235 a synchrotron-based empirical model of ruminant molar enamel formation (illustrated for *Ovis*
236 and *Rupicapra* in Figure 5), originally derived from a population of domesticated sheep, to

237 better infer potential seasonal variations in environmental $\delta^{18}O$ values that contribute to
238 measured spatial variations in tooth $\delta^{18}O$ (Green et al., 2018b; See Text-SI).

239 *2.2.2. Dental Microwear Texture Analysis*

240 Following standard procedures, replicas of the investigated dental facet on the
241 lower second molars were produced and then scanned using the surface profilometer confocal
242 DCM8 Leica Microsystems "TRIDENT" with a 100 × lens (Leica Microsystems) at the
243 Palevoprim lab, CNRS and University of Poitiers, France (see details in Merceron et al.,
244 2016; See text-SI and Appendix 3). We target the disto-buccal facet of the protoconid or of
245 the hypoconid in case the former one was damaged. We do avoid grouping different dental
246 facets as they have different functions during mastication and thus significant differences in
247 dental microwear textures as shown by Ramdarshan et al. (2017).

248 After treating surfaces (see details in Merceron et al., 2016), the Dental Microwear
249 Texture Analysis (DMTA) was performed using the Scale-Sensitive Fractal Analysis using
250 Toothfrax and Sfrax software (Surfract, http://www.surfract. com) following Scott et al.
251 (2006). Four variables were extracted from the surface: complexity (Asfc), anisotropy
252 (epLsar), heterogeneity of complexity (HAsfc calculated with a 9-cell mesh) and Textural fill
253 volume (Tfv; Table 3, Appendix 3). Dispersion of the values are calculated following Plavcan
254 and Cope (2001) Levene equations (see Text-SI). After box-cox transformations, one-way
255 analyses of variance (ANOVAs) and pairwise comparisons were performed for each texture
256 parameter (Table 4, Figure 6; see Text-SI and Table S3). Furthermore, seasonal variations in
257 DMTA are explored on the mouflons as 10 of them were sampled in late summer/early fall
258 and 12 others in winter 2009 (see Text-SI and Table S4).

259

260 **3. Results**

261 *3.1. Enamel carbon isotope composition*

Individual mean molar enamel carbon isotope compositions ($\delta^{13}C_{enamel}$) for all four ruminant species range from –18.4 ‰ to – 14.3 ‰ VPDB (Table 1). The chamois (*Rupicapra rupicapra*) has the highest mean $\delta^{13}C_{enamel}$ values both on lower M_2 and M_3 among the four ruminant species while the roe deer (*Capreolus capreolus*) has the lowest values. The moufflons (*Ovis gmelini musimon*) M_2 and M_3, and red deer (*Cervus elaphus*) M_3, show intermediate values (Table 1; Figures 2 and 4). It is worth noting that a single high $\delta^{13}C_{enamel}$ value (−6.9 ‰ VPDB; not shown in Figure 2 but in Table 1 and Appendix 1) on a single specimen (15MO8843) likely constitutes an undetected analytical error. The isolated high $\delta^{13}C_{enamel}$ value, if not an analytical artefact, is perhaps either due the high intake of alpine CAM plants or the few native C_4 plants at high altitudes and mid-to-high latitudinal biomes (Osmond et al., 1975; Pyankov et al., 2010) which can have variable $\delta^{13}C$ values, depending on local and seasonal conditions, or due to the consumption of cultivated maize in valleys. Also, moufflons are known to perform seasonal altitudinal movements (Darmon et al. 2014) and as there are a few areas of cultivated maize in the valleys and the possible existence of some places where hunters spread maize for preventing damages caused by wild boar, we cannot firmly exclude a high consumption of maize for short period. Apparently semi-continuous isotopic compositions across sampled M_2 and M_3 reflect a relatively continuous record of body fluid isotopic compositions during the earlier formation of the M_2, and the later formation of the M_3.

The carbon isotope composition of the food resources exploited ($\delta^{13}C_{diet}$) are calculated following the body mass-dependent diet-to-bioapatite fractionation equations for foregut fermenting mammals following Tejada-Lara et al. (2018; Table 2). The calculated mean $\delta^{13}C_{diet}$ values by tooth and specimen range from –30.5 ‰ and –26.6 ‰ VPDB. The estimation of the seasonal variations in $\delta^{13}C_{diet}$ of food resources are given in Table 1 (Appendix 1).

Table 1. Enamel carbon and oxygen stable isotope composition $\delta^{13}C_{enamel}$ (‰ vs. VPDB) and $\delta^{18}O_{enamel}$ (‰ vs. VSMOW; mean *m*, standard deviation *sd*, minimal *min* and maximal *max* values, and amplitude Δ) of serial samples along second (M_2) and third (M_3) lower molars of the sympatric ruminants from the Bauges NRP, Alps, France. Carbon stable isotope composition of the food resources $\delta^{13}C_{diet}$ are calculated following Tejada-Lara et al. (2018 in supplementary material) with a shift depending on bodymass. An estimation of the oxygen stable isotope composition of the environmental water $\delta^{18}O_{ew}$ (‰ vs. VSMOW) is calculated after Iacumin et al. (1996).

				$\delta^{13}C_{enamel}$					$\delta^{13}C_{diet}$	$\delta^{18}O_{enamel}$					$\delta^{18}O_{ew}$
Species	Specimen	Tooth	N	**m**	**sd**	**max**	**min**	**Δ**		**m**	**sd**	**max**	**min**	**Δ**	**m**
C. capreolus	CC2613	M_2	6	-16.6	0.4	-17.0	-16.2	0.9	-28.7	22.8	0.3	23.1	22.3	0.8	-10.9
		M_3	6	-18.4	0.5	-18.9	-17.6	1.3	-30.5	19.9	0.4	20.4	19.3	1.1	-13.7
	CC2653	M_2	6	-18.4	0.2	-18.7	-18.1	0.6	-30.5	22.8	0.9	24.0	21.6	2.4	-10.9
		M_3	6	-18.0	1.6	-18.8	-14.7	4.1	-30.2	19.3	1.6	22.5	18.3	4.2	-14.3
C. elaphus	CE4821	M_3	9	-15.9	0.2	-16.2	-15.6	0.6	-29.1	22.3	0.5	23.0	21.7	1.3	-11.4
	CE0104	M_3	8	-16.4	0.3	-16.9	-16.0	0.9	-29.6	21.7	1.4	23.7	19.6	4.1	-12.0
	CE4951	M_3	10	-15.7	0.3	-16.2	-15.4	0.8	-28.9	22.6	0.6	23.4	21.4	2.0	-11.1
	CEF7104	M_3	14	-16.0	0.3	-16.6	-15.5	1.1	-29.2	21.5	0.9	23.1	20.1	3.0	-12.1
	CEM2616	M_3	10	-16.1	0.4	-16.7	-15.5	1.2	-29.3	22.3	1.2	23.9	20.5	3.4	-11.3
O. gmelini	MO8843	M_2	16	-15.8	2.5	-17.2	-6.9	10.3	-28.2	21.3	1.5	24.0	19.5	4.5	-12.4
		M_3	16	-15.7	0.8	-16.6	-14.7	1.9	-28.1	22.5	1.0	23.9	20.6	3.3	-11.1
	MO8847	M_2	12	-16.3	1.0	-17.5	-15.2	2.3	-28.8	21.0	1.5	23.1	18.9	4.2	-12.7
		M_3	15	-15.9	0.7	-17.1	-15.0	2.1	-28.4	21.6	1.5	23.8	19.2	4.6	-12.1
R. rupicapra	IS8932	M_2	10	-14.9	0.4	-15.2	-14.1	1.1	-27.2	21.7	0.6	22.7	21.0	1.7	-12.0
		M_3	11	-14.3	0.4	-14.7	-13.7	1.0	-26.6	22.9	0.7	23.9	21.7	2.2	-10.7
	IS8952	M_2	9	-14.4	0.2	-14.8	-13.9	0.8	-26.7	23.8	0.7	25.0	22.7	2.3	-9.9
		M_3	9	-14.4	0.3	-14.7	-13.8	0.9	-26.7	22.1	0.8	23.2	21.2	2.0	-11.5

The inter-individual and inter-species differences between the estimated enamel carbon isotopic compositions calculated from values from food remains stuck between teeth are quite similar with the $\delta^{13}C_{enamel}$ measured on the last enamel part to mineralize next the M_3 cervix (Table S2). Food item $\delta^{13}C$ composition differences reflect enamel patterns overall, with highest values observed in the chamois and mouflons, and lowest in the red and roe deer. All differences are < 2 ‰ VPDB.

The most narrow niche breath B_A based on $\delta^{13}C_{diet}$ is that of the chamois, with especially high values and nearly no or little ecological overlapping with the other sympatric

ruminants investigated. The mouflons and the red deer have the highest ecological overlapping when considering $\delta^{13}C_{diet}$ (Table 2).

Table 2. Niche breadth (B_A) per species are given in brackets next to the taxon name and ecological overlapping of the Bauges ruminants (O_{Bauges}) are given for $\delta^{18}O_{ew}$ and $\delta^{13}C_{diet}$ respectively below and above the diagonal.

$\delta^{18}O_{ew}\backslash\delta^{13}C_{diet}$	***C. capreolus* (0.119)**	***C. elaphus* (0.161)**	***O. gmelini* (0.233)**	***R. rupicapra* (0.060)**
***C. capreolus*(0.405)**		0.087	0.016	0.108
***C. elaphus* (0.472)**	0.284		0.542	0
***O. gmelini* (0.552)**	0.300	0.851		0.082
***R. rupicapra* (0.389)**	0.085	0.918	0.929	

3.2. Enamel oxygen isotope composition

The chamois (*Rupicapra rupicapra*) has the highest mean $\delta^{18}O_{enamel}$ value (23.8 ‰ VSMOW) and the roe deer (*Capreolus capreolus*) the lowest mean value (19.3 ‰ VSMOW). The mouflons (*Ovis gmelini musimon*) show the highest intra-tooth variability $\Delta^{18}O_{enamel}$ (from 3.3 ‰ to 4.6 ‰ Table 2; Figure 3). The $\delta^{18}O_{H2O}$ values (inferred from inverse modeling from enamel $\delta^{18}O_{enamel}$) of water ingested by the roe deer are the lowest of all analyzed ruminants (−14.3 ‰ to −10.9 ‰ VSMOW) but display the highest intra-tooth differences when $\delta^{18}O$ values of M_2 and M_3 are merged. High variations in oxygen isotope composition of water sources are also estimated for the mouflons. The highest $\delta^{18}O_{H2O}$ values for the ingested water are recorded by the chamois.

Regarding the niche breadth B_A based on $\delta^{18}O_{ew}$, the narrowest breadth is recorded for the chamois and the widest for the mouflons. Ecological overlapping is higher between the mixed feeding red deer, the mouflon and the chamois (Table 2). These patterns can be observed by comparing $\delta^{13}C$ and $\delta^{18}O$ measurements across all single serial intra-tooth enamel samples. Among BNRP taxa, $\delta^{13}C$ and $\delta^{18}O$ enrichment or depletion tend to co-segregate (Figure 4). For example, species like the chamois with higher enamel $\delta^{13}C$

compositions have higher $\delta^{18}O$ values with little $\delta^{18}O$ variation, whereas species like roe deer or mouflons have lower minimum $\delta^{18}O$ values, and greater ranges of $\delta^{18}O$ values.

Reconstruction of estimated ingested seasonal $\delta^{18}O_{H2O}$ compositions recover what appear to be annual cycles (Figure 5; Figure S1 and Figure S2), with average ranges of $\delta^{18}O$ variation in all teeth equal to 9.7 ± 4.5 ‰ 1 S.D. The highest degree of variation is reconstructed for the mouflons, where within-tooth reconstructed $\delta^{18}O$ ranges are 12.9 ± 2.9 ‰ 1 S.D. The lowest variation is observed among the chamois where reconstructed $\delta^{18}O$ ranges are from 7.4 ± 1.9 ‰. Intermediate ranges are observed for the red deer (9.3 ± 3.2 ‰) and roe deer (9.46 ± 7.8 ‰), with greater variability in roe deer resulting from a single very high value at the cuspal margin of a M_3.

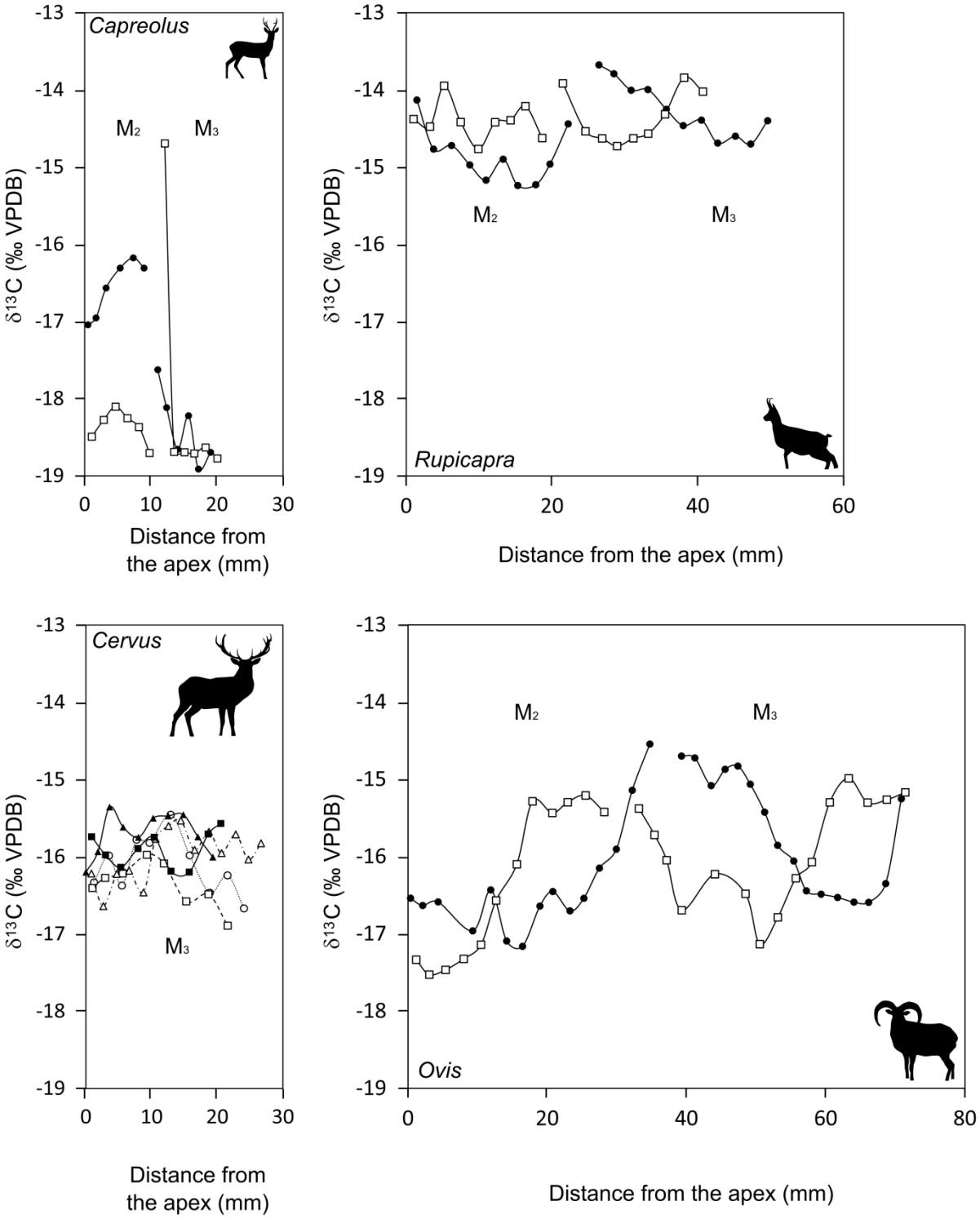

Figure 2. Variations in enamel carbon isotope composition ($\delta^{13}C_{enamel}$ ‰ VPDB) along the lower M_3 for red deer (*Cervus elaphus*), and of lower M_2 (left curves) and M_3 (right curves) for the three other species of ruminants (*Ovis gmelini musimon*, *Rupicapra rupicapra*, *Capreolus capreolus*) from the Bauges NRP expressed in mm from the apex of the M_2. For all taxa except the red deer, the height dimension of the lower M_2 is added to the distance to the M_3 apex of the samples along the M_3.

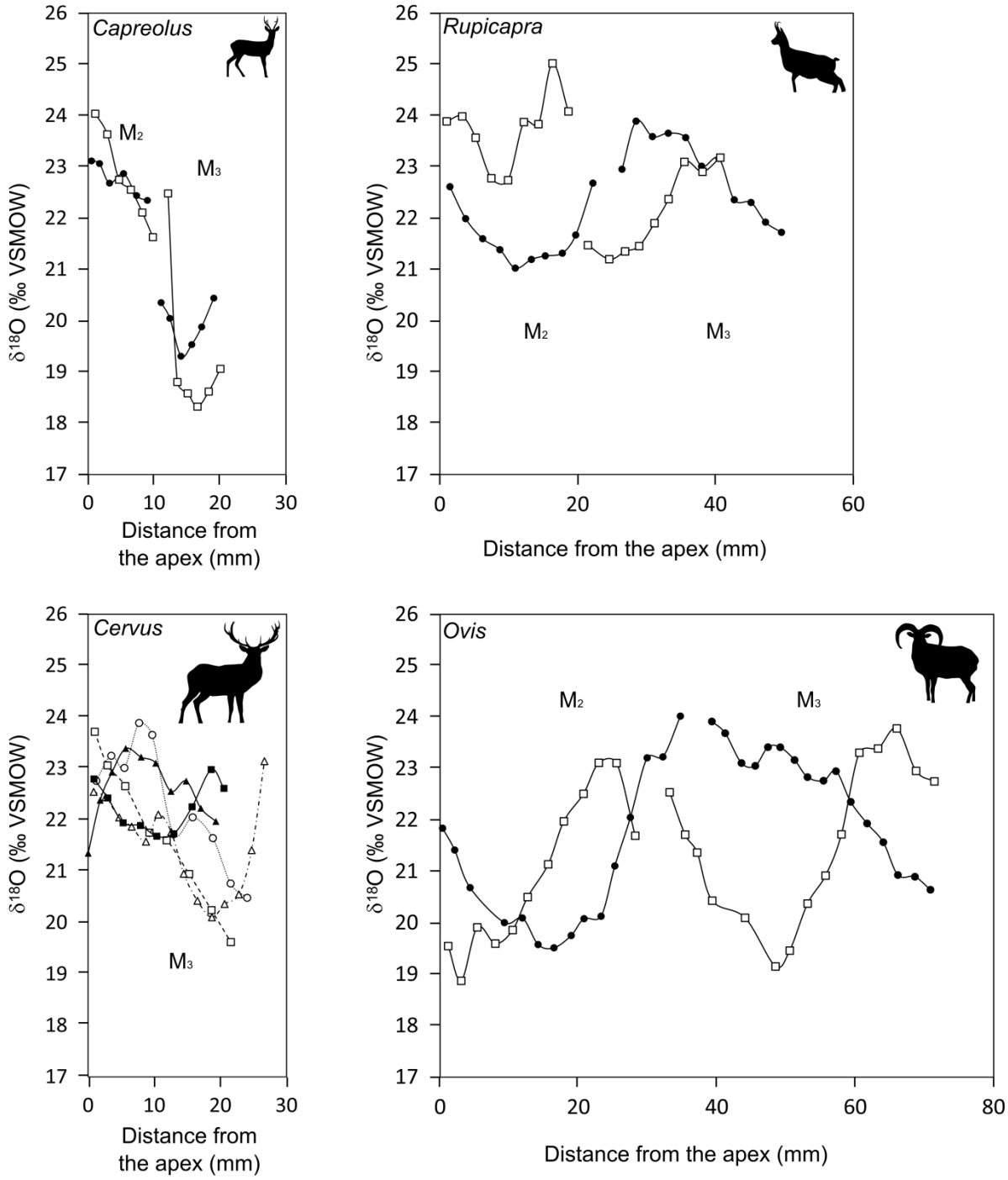

Figure 3. Variations in enamel oxygen isotope composition ($\delta^{18}O$ ‰ VSMOW) along the lower M_3 of the red deer (*Cervus elaphus*) and along the lower M_2 (left curves) and M_3 (right curves) of the three other species of ruminants (*Ovis gmelini musimon*, *Rupicapra rupicapra*, *Capreolus capreolus*) from the Bauges NRP expressed in mm from the apex of M_2. For all taxa except the red deer, the height dimension of the lower M_2 is added to the distance to the M_3 apex of the samples along the M_3.

3.3. DMTA

Among the four species, the red deer (*Cervus elaphus*) shows the lowest values of complexity (Asfc), and the roe deer (*Capreolus capreolus*) the highest. The two bovids

(*Rupicapra rupicapra* and *Ovis gmelini musimon*) significantly contrast with the two cervids with lower values in anisotropy (epLsar; Tables 3 and 4; Table S3). The roe deer and the two bovids have lower heterogeneity of complexity ($HAsfc_{9\text{-cells}}$; Table 3; Table S3) than the red deer. There is no difference in textural fill volume (Tfv; Tables 3 and 4; Table S3). Regarding dispersions, the roe deer has the highest values for Disp-Asfc and Disp-Tfv, and the red deer the lowest ones (Tables 3 and 4; Table S3). Regarding the two other indices, the mouflons has the highest Disp-epLsar, the roe deer and the chamois the lowest. The dispersion in Heterogeneity of Complexity (Disp-$HAsfc_{9\text{-cells}}$) is maximal for the red deer and minimal for the mouflons (Table 3). One way ANOVA on box-cox transformed data detects significant differences in Anisotropy (epLsar), Heterogeneity of Complexity ($HAsfc_{9\text{-cells}}$), and Dispersion in Complexity (Disp-Asfc, Tables 3 and 4, Figure 6; Table S3). Mouflons, the only sample for which we could test seasonal variations, show significant differences in textural fill volume (Tfv); the ones sampled in late fall and early winter having higher values (Table S4).

Table 3. Descriptive statistics (mean m and standard deviation sd) as well as dispersion of dental microwear texture parameters per species and per seasonal group for the mouflons.

		Asfc			epLsar			$HAsfc_{9\text{-cells}}$			Tfv (μm^3)		
	N	m	sd	disp	m*	sd*	disp	m	sd	disp	m	sd	disp
C. capreolus	*18*	2.61	2.49	0.43	6.05	2.34	0.38	0.36	0.14	0.09	36152	19052	1.08
C. elaphus	*21*	1.36	0.57	0.18	5.99	2.63	0.42	0.55	0.48	0.13	36891	10049	0.24
R. rupicapra	*21*	1.79	0.97	0.23	4.26	1.78	0.38	0.39	0.22	0.10	36645	13018	0.36
O. gmelini musimon (all individuals)	*22*	2.02	0.88	0.25	3.76	2.56	0.54	0.33	0.10	0.06	34363	14738	0.44
Sample (late summer-early fall 2015)	*12*	2.01	0.74		3.33	0.21		0.35	0.11		27092	14338	
Sample (winter 2008-2009)	*10*	2.03	1.06		4.27	0.30		0.30	0.10		43089	10026	

*original values ($\times 10^{-3}$)

Table 4. Summary of the analyses of variances on the box-cox transformed DMTA variables from ruminants of the Bauges NRP (complete results in Table S3).

	dof	F	p
Asfc			
Taxa	3	1.917	0.133
Residuals	78		
epLsar		F	p
Taxa	3	5.0279	***<0.05***
Residuals	78		
$HAsfc_{9\text{-cells}}$		F	p
Taxa	3	2.907	***<0.05***
Residuals	78		
Tfv		F	p
Taxa	3	0.1328	0.940
Residuals	78		
disp-Asfc		F	p
Taxa	3	2.7877	***<0.05***
Residuals	78		
disp epLsar		F	p
Taxa	3	0.7830	0.506
Residuals	78		
$disp\text{-}HAsfc_{9\text{-cells}}$		F	p
Taxa	3	0.6366	0.593
Residuals	78		
disp Tfv		F	p
Taxa	3	0.8252	0.483
Residuals	78		

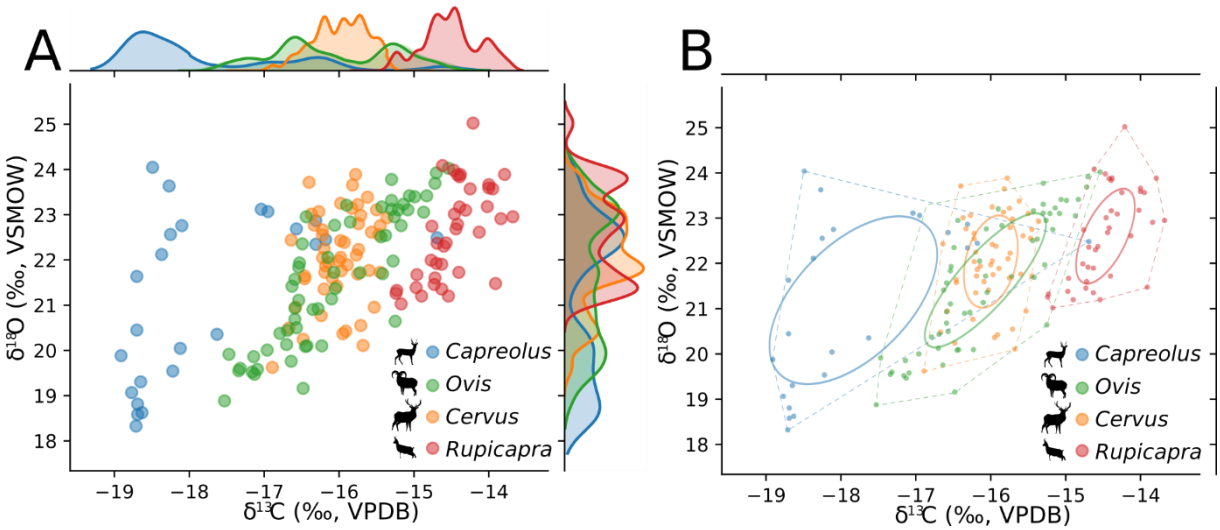

Figure 4. A: Enamel carbonate carbon ($\delta^{13}C$) and oxygen isotope ($\delta^{18}O$) values from red deer *Cervus elaphus*, mouflons *Ovis gmelini musimon*, chamois *Rupicapra rupicapra*, and roe deer *Capreolus capreolus*. Overall, measurements segregate species by greater (chamois) or lesser (roe deer) carbon and oxygen isotopic enrichment. Kernel density estimates on each axis demonstrate that $\delta^{13}C$ distinguish chamois, red deer and roe deer relatively clearly, with mouflons feeding between these groups. B: mixSIAR modeling estimating isotope-based niche separation among taxa. The full range of observed variation is shown as a dashed line, while predictive ellipses in full lines show 40 % predictive ellipses for measurements from each population.

4. Discussion

4.1. Inter-specific differences in diet

All $\delta^{13}C_{enamel}$ of permanent molars support that the four ruminants feed only on C_3 vegetation (Tables 1 and 5, Figure 2). Considering the relation specific to foregut-fermenting mammals and body mass (Tejada-Lara et al., 2018) of the species at the BNRP (Redjadj et al., 2014), the shift between diet and enamel carbon stable isotope composition varies from 12.1 ‰ for the roe deer to 13.2 ‰ for the red deer (Table 1; Appendix 1). Thus, the mean calculated $\delta^{13}C_{diet}$ of the food resources for all four species ranges from about −30.5 ‰ to −26.6 ‰, which supports the exclusive use of C_3 food resources, as C_3 plants have $\delta^{13}C$ values (Table 1; Appendix 1) ranging from −37 ‰ to −20 ‰ (with a mean value of −27 ‰; see Kohn, 2010 for a review): far below the range seen for C_4 plants (from −18 ‰ to −8 ‰ with a mean value of −13 ‰; Smith and Epstein, 1971). The dominance of C_3 vegetation is expected as BNRP dicots and monocots share similar C_3 metabolic pathways (Pyankov et al., 2010).

As Kierdorf and Kierdorf (2000) report that the amelogenesis of the second molar of the roe deer begins *in utero* and continues about four months after birth, enamel $\delta^{13}C$ and $\delta^{18}O$ values likely reflect a mixture of pre-weaning and post-weaning values. Thus the $\delta^{13}C_{diet}$ and $\delta^{18}O$ values derived from the roe deer M_2s are potentially biased by a milk suckling enrichment effect, which may contribute to the especially large range of roe deer $\delta^{18}O$ compositions (Figs. 2–3; SI text Fig. S2): roe deer are thought to wean between 4–7 months of age (Espmark, 1969). Because the other species are larger and have taller molar crowns, we assume that a high proportion of their M_2 crown mineralizes after weaning and indeed reflects food resources that compose the diet of these species.

The dental microwear texture analysis complements the ecological picture provided by $\delta^{13}C_{enamel}$ values. First, the two cervids have higher anisotropy than the two bovids (Tables

3 and 5). The two cervids, however, differ from each other in having contrasting complexities; the red deer having lower values than the roe deer (Table 3, Figure 6). High anisotropy on shearing molar facets have been empirically and experimentally associated with grass-eating habits (Scott, 2012; Merceron et al., 2016). In the present case, the combination of high anisotropy and low complexity for the red deer would advocate for a dominance of monocots in the diet. By contrast, Redjadj et al. (2014) have found that monocots represent no more than 40 % of diet in fall and winter. Our data would instead support a higher amount (Table 5), at least similar to the summer diet for Alpine red deer during which grasses may account for up to 60 %; the remaining diet would be dominated by herbaceous dicots (Suter et al., 2004). This is consistent with the fact that most of the red deer studied in the present study were shot in October, so that dental microwear textures likely reflect summer food resources. Several studies have challenged the hypothesis that anisotropy (epLsar) reflects only grass consumption. For instance, Hedberg and DeSantis (2017) describing koalas or Merceron et al. (2010) describing roe deer have shown that high anisotropy (epLsar) on shearing molar facets is not specifically related to grass-eating habits but to tough leaf-eating habits requiring a shearing motion during mastication. This appears to explain our observations at the BNRP. Roe deer from the BNRP avoid fruits (3.4 and 5.8 % of the diet for the two periods; Table S1) and mainly feed on forbs and evergreen shrubs, notably bramble foliage (*Rubus fruticosus*). In addition to anisotropy, roe deer complexity (Asfc) and most specifically the dispersion of complexity (disp-Asfc) are more than double those observed in the red deer (Table 3, Figure 6). This supports mechanically more diverse foods for the roe deer compared with the red deer. Several specimens of roe deer browsing mostly on soft food have low values in complexity (Asfc), whereas specimens with higher complexity consumed harder food items (Ramdarshan et al., 2016). Indeed, while the high disp-Asfc seen in roe deer suggests important inter-individual differences regarding mechanical food properties, the lower

heterogeneity of complexity ($HAsfc_{9\text{-}cells}$) supports a dietary spectrum, for any given individual, that is constrained by its high feeding selectivity coupled with a low spatial heterogeneity in resources (Table 5). This reflects smaller roe deer home range compared with the red deer. In contrast, most of the red deer specimens share a mechanically diverse spectrum of foods (low disp-Asfc and high $HAsfc_{9\text{-}cells}$), which reflects wider spatial heterogeneity in resources and larger home range for all red deer individuals (Table 5).

The two bovids significantly contrast with the cervids with lower values in anisotropy (epLsar). Their complexity values plot between the limits defined by the two deer (Table 3, Figure 6). Chamois and mouflon fed on a mixed diet that was overall less tough, most likely less abrasive but harder than that consumed by the red deer (Table 5). This reflects the low to medium dietary portion (from 30 to 50 %) of herbaceous monocots for these bovids during fall and winter (La Morgia and Bassano, 2009; Marchand et al., 2013; Redjadj et al., 2014; Espunyes et al., 2019). Cransac et al. (1997) found out that for mouflons reintroduced in the Caroux-Espinouse Mediterranean mountain habitats, in Southern France, herbaceous monocots may account for less dietary intake in summer than in fall and winter. This is exactly opposite the timing of herbaceous monocot consumption among red deer in the Alps (Suter et al., 2004). Pérez-Barbería et al. (1997) found out that the shrub component increases from spring to summer and grasses and forbs increase in early fall in the diet of Cantabrian chamois. Besides, chamois and mouflons have lower heterogeneity of complexity ($HAsfc_{9\text{-}cells}$) than the red deer, suggesting a dietary spectrum with a reduced diversity of mechanical properties (Tables 3 and 5, Figure 6).

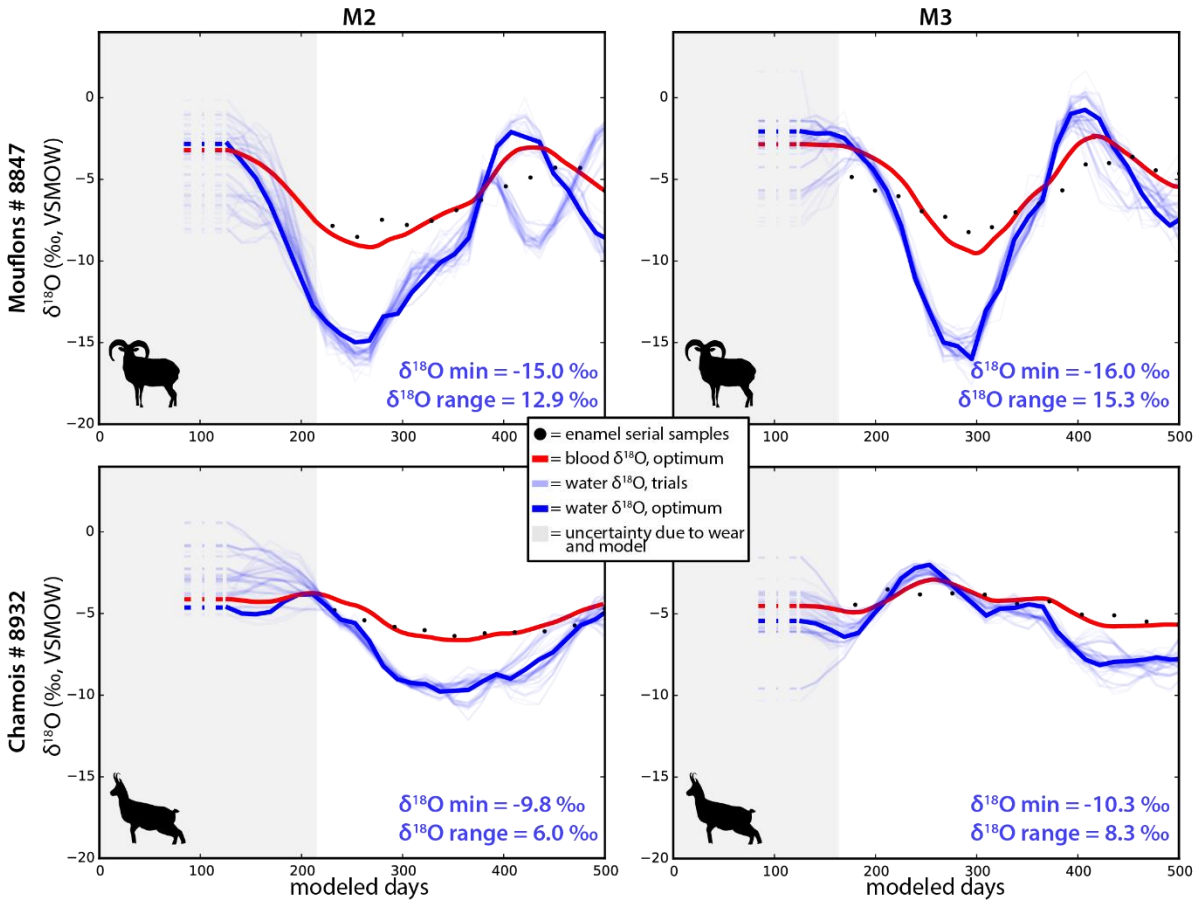

Figure 5. Measurements of enamel oxygen isotope compositions ($\delta^{18}O$ ‰, here shown as phosphate $\delta^{18}O$-equivalent on the VSMOW scale, with an estimated PO_4-water offset of 19.1 ‰ subtracted from each measurement) are made serially down the tooth crown (black circles). These measurements are combined with a model of tooth formation to infer likely (light blue) and best guess (dark blue) histories of ingested seasonal $\delta^{18}O$ compositions in environmental and plant water. The $\delta^{18}O$ of blood water over time (red) is also estimated. Periods of uncertainty resulting from significant tooth wear or limitations in the synchrotron-based model of enamel formation are shown in light gray. Uncertainty also increases towards the end of the tooth, when enamel growth slows and incorporates ever greater periods of time into smaller spatial increments. Results suggest that compared to the chamois, mouflons ingest a greater range of environmental water $\delta^{18}O$ compositions, and in particular ingest lower $\delta^{18}O$ values, likely derived from snow in high altitude areas.

4.2. Inter-specific differences in habitat use

The carbon and oxygen isotopic compositions of the four ruminants appear to mirror their behavior and range at BNRP (Tables 1 and 5, Figure 4). Roe deer have by far the lowest $\delta^{13}C$ values of all the taxa, reflecting their browsing behavior in forested habitats (Table 5). Interestingly, roe deer also show the greatest range of $\delta^{18}O$ values: the M_2 $\delta^{13}C$ and

511 $\delta^{18}O$ measurements of both sampled individuals are higher than their M_3 measurements
512 (Table 1, Figures 2–4). This pattern would be consistent with $\delta^{13}C$ trophic enrichment and
513 elevated milk water $\delta^{18}O$ ingestion resulting from suckling during M_2 formation (Kierdorf and
514 Kierdorf, 2000), and relatively rapid M_3 formation in the following winter. By contrast
515 chamois enamel samples are the most ^{13}C- and ^{18}O-enriched and show less variation (Table 1,
516 Figures 2–4). This result is also observed in inverse modeling (Figure 5) and suggests the
517 consumption of both plant and water resources that are subject to low humidity and
518 evaporative enrichment. High $\delta^{18}O$ measurements among the chamois, who live at high
519 altitudes, may reflect a greater proportion of water obtained from vegetation and metabolic
520 water production. Mouflons and red deer have measured molar and reconstructed $\delta^{13}C$ and
521 $\delta^{18}O$ values that are intermediate between the high values observed in the chamois and the
522 low values of the roe deer (Figure 4–5).

523 The isotopic ecology of vegetation in the BNRP helps to explain these general
524 patterns. Understory plants are exposed to lower light intensity and higher CO_2 concentration
525 (^{13}C-depleted CO_2 from biomass degradation) favoring the fractionation of light ^{12}C into plant
526 tissue during photosynthesis (Van der Merwe and Medina, 1991). Therefore, $\delta^{13}C$ values of
527 subcanopy C_3 plants under dense tree cover can be up to 5 ‰ lower than for the same species
528 of plants in more open habitats (Bonafini et al., 2013). Such differences in carbon isotope
529 fractionation in open versus under canopy conditions is then recorded in the dental tissues of
530 the mammalian herbivore species which browse or graze on these plants. When $\delta^{13}C_{enamel}$ on
531 third molars are considered (the M_3 mineralizes after weaning for all four species), the roe
532 deer (–18.4 ‰ and –18.0 ‰ VPDB) appears as the most forest-dwelling ruminant at the
533 BNRP with an estimated $\delta^{13}C_{diet}$ ranging from –30.5 ‰ to –30.2 ‰ (Tables 1 and 5, Figure 2,
534 Appendix 1). It is worth noting that the specimen CC 2613 likely shifts its home range to a
535 more open area while growing as its M_3 (–16.6 ‰ VPDB) has recorded less negative

536 $\delta^{13}C_{enamel}$ values compared to the M_2 (–18.4 ‰ VPDB). With roe deer having a significantly
537 smaller home range (from 20 to 60 ha depending on gender and density; Kjellander et al.,
538 2004) than red deer, the variations in $\delta^{13}C_{enamel}$ between individuals likely reflect the
539 differences in tree cover from one habitat to another. Specimen CC 2613 was shot at the "Roc
540 des Boeufs" station, an area between 1000 m and 1600 m high with a lower tree cover than
541 the Golet Station from 1200 m to 1600 m high where the second specimen comes from.
542 Although the five red deer were shot at different stations in the BNRP and their higher tooth
543 crowns indeed have the potential to record more dietary variations during a longer time span,
544 their low inter- and intra-tooth variation in $\delta^{13}C_{enamel}$ compared with the roe deer, strongly
545 suggest that the red deer has i) a wider home range, covering several micro-habitats buffering
546 by then any micro-habitat scale effects and ii) a slightly more open habitats than the roe deer
547 (Table 5).

548 The chamois displays the highest $\delta^{13}C_{enamel}$ values, indicating use of the largest
549 fraction of food resources from open habitats of the four ruminant species (Tables 1 and 5,
550 Figure 2). With intermediate $\delta^{13}C_{enamel}$ values (Table 1, Figure 2, Appendix 1), mouflons
551 show intra-tooth variations in $\delta^{13}C_{enamel}$ of about 3.0 ‰ across all samples, whereas variation
552 in the chamois is lower, at 1.6 ‰. This reflects seasonal altitudinal displacement (Table 5), as
553 mouflons move up to higher altitude settings in late spring and return to lower altitudes in
554 winter (Darmon et al., 2014). This variability in the mouflons is supported by reconstructions
555 of blood and environmental water $\delta^{18}O$ values (Table 5, Fig. 5; SI text and Figure S1). It is
556 worth noting that the high $\delta^{13}C_{enamel}$ value in one of the two mouflons, if not an artefact, is
557 also associated with an increase in $\delta^{18}O_{enamel}$ (not shown in Figures 2 and 3, see Table 1 and
558 Appendix 1), supporting not only a shift to a diet with higher $\delta^{13}C$ values but likely a change
559 of habitat (i.e. ingested water) as well.

Although all ruminants at the BNRP have grown up in a pure C_3 ecosystem, the species differ in their niche breadth B_A, with the chamois having the most constrained niche breadth characterized by the consumption of pure C_3 food resources in open habitats all around the year (Tables 2 and 5; Figure 4). The mouflon has the widest niche breadth and has a minor ecological overlapping with the chamois. The ecological overlapping is actually the highest between the mouflon and the red deer, though mouflons $\delta^{13}C$ values indicate that it may be feeding in between niches occupied by the three other taxa (Figure 4). There is also a low ecological overlapping between the two cervids, the roe deer occupying more closed habitats than the red deer (Tables 2 and 5).

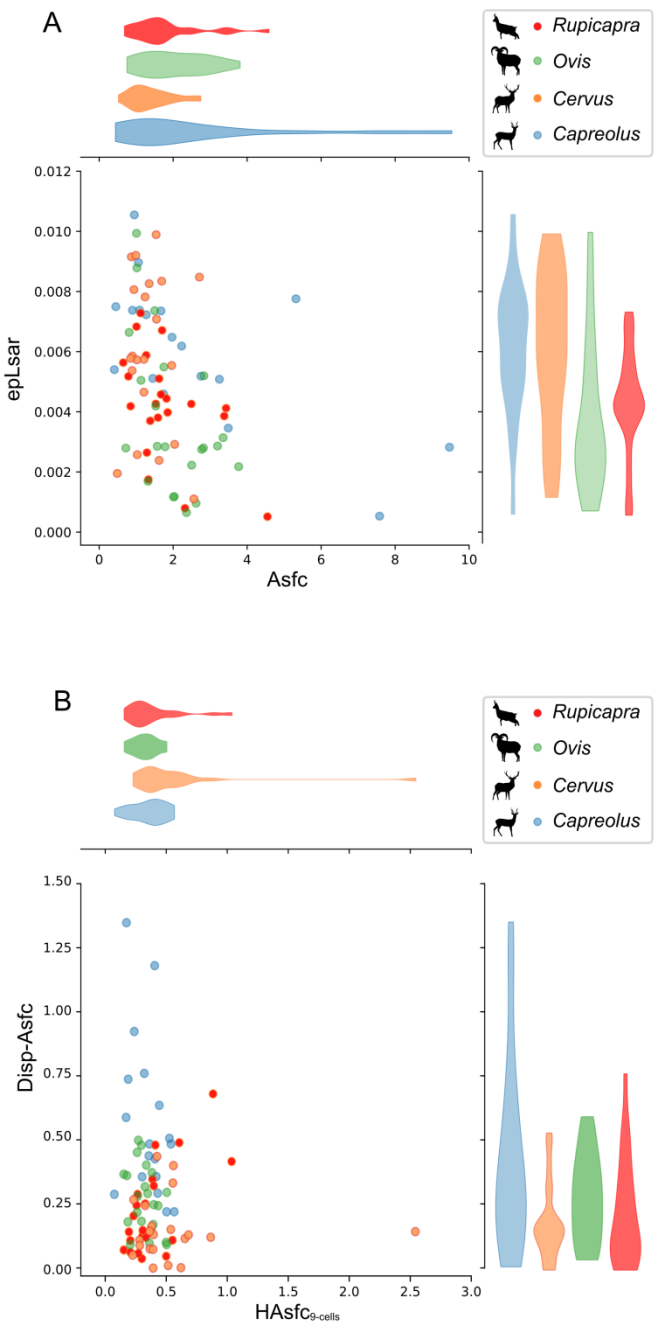

Figure 6. Dental microwear texture complexity and anisotropy values (Asfc, epLsar, A) and disparity and heterogeneity of complexity (Disp-Asfc, HAsfc, B) from red deer *Cervus elaphus*, mouflons *Ovis gmelini musimon*, chamois *Rupicapra rupicapra*, and roe deer *Capreolus capreolus*. Overall, anisotropy significantly segregates the two bovids from the cervids. While complexity shows no significant variation, disparity of complexity significantly discriminates the roe deer from the red deer, and heterogeneity of complexity the red deer from the two bovids.

4.3. Seasonal variations in diet, habitat, and altitudes

The large intra-tooth variation in $\delta^{13}C_{enamel}$ support that the most mobile species is the mouflon (Tables 1 and 5, Figure 2). Regarding DMTA, mouflons are the only species for

584 which the sampling in two seasons makes an assessment of the inter-season variation
585 possible. The sheep from late fall and early winter have significantly higher textural fill
586 volume (Tfv) than specimens sampled in late summer and early fall (Table S4). Knowing that
587 mouflons tend to decrease their consumption of grasses from 42 % to 29 % from late summer
588 to winter counterbalanced by more conifer foliage up to 28.1 %, we might interpret this
589 increase of textural fill volume as a trend towards more browsing (Tables S1 and S4).
590 However, the absence of significant difference in the other variables on one hand, and the fact
591 that the samples not only differ in season but also in year of sampling (2009 vs. 2015) make it
592 difficult to interpret differences in textural fill volume. Moreover, earlier works yielded
593 contrasted results regarding this variable, with grazers having higher values than browsers in
594 one study (Merceron et al., 2016) and lower values in the other (Scott, 2012).

595 Because mouflons, red deer and chamois molars form over longer periods (about
596 10 to 15 months for the M_3 versus less than 6 months for the roe deer M_3), they are especially
597 useful for the reconstruction of local seasonal patterns (Figure 5, Figure S1–S2). A sample of
598 472 measurements from nearby Thonon-les-Bains (about 80 km from the BNRP) monthly
599 recorded precipitation $\delta^{18}O$ values ranging from -17.8 to -0.4 ‰ between 1963 and 2012
600 (IAEA/WMO, 2020). Mean precipitation $\delta^{18}O$ range from the site at any given year is 9.9 ±
601 2.9 ‰ 1 S.D. Only 37 % of total site variation is recorded directly by enamel carbonate $\delta^{18}O$
602 values across all taxa, and 39 % using $\delta^{18}O_{ew}$ values. By contrast, inverse modeling recovers a
603 significant portion of this variation. Using serial M_2 and M_3 measurements from the chamois,
604 which have the lowest measured enamel $\delta^{18}O$ range, we reconstruct ingested water $\delta^{18}O$
605 values ranging from -10.3 to 0.8 ‰ across all individuals. Even from a single chamois M_2, we
606 recover a range of 9.5 ‰, or 96 % of the average yearly variation found in Thonon-les-Bains
607 precipitation (Figure 5, Figures S1 and S2). Reconstructions from the mouflons, which are
608 known to migrate across altitudes seasonally, reproduce an even greater proportion of local

609 isotopic and hydrological variation: average reconstructed mouflon $\delta^{18}O$ ranges across all four
610 teeth are 12.93 ‰. Across all teeth from all taxa sampled isotopically in this study, we
611 estimate average annual oscillations of 9.7 ± 4.5 ‰, a result strikingly similar to the average
612 annual precipitation range of 9.9 ‰ observed at Thonon-les-Bains (Table 5, Figure 5, Figure
613 S1 and S2).

614 It is possible that our modeling parameters may under- or overestimate
615 reconstructed seasonal $\delta^{18}O$ variability. We hold ingested carbohydrate $\delta^{18}O$ values
616 contributing to metabolic water production as constant, while these values probably shift by
617 several permil or more over the course of the growing season, or may vary with altitude
618 during the migration of the mouflons. In this case, reconstructed water $\delta^{18}O$ may vary more in
619 model outcomes to account for measured enamel $\delta^{18}O$ compositions. Alternatively, we may
620 under- or overestimate the fraction of body water oxygen derived from liquid water, which
621 would tend to amplify or dampen, respectively, reconstructed ingested water $\delta^{18}O$
622 compositions. Importantly, the mineralization model that we use for reconstruction of
623 seasonal patterns is empirical and based upon mineralization observations in a population of
624 sheep. The cervids analyzed here have less hypsodont molars, and in the case of roe deer form
625 very quickly. One result of this rapid tooth formation process is that uncertainty in our
626 reconstructed $\delta^{18}O$ inputs for roe deer are high at the end of our reconstruction interval (SI
627 text, Fig. S2). Though our inverse method attempts to account for possible taxonomic
628 variability (SI text), it is possible that differences in cervid mineralization may impact our
629 results, for instance by overestimating input $\delta^{18}O$ variability if roe deer enamel maturation
630 occurred more rapidly than expected. Lastly, we observe that inverse modeling is highly
631 sensitive to individual values: reconstructions from the M_3 of one roe deer, CC 2653, are
632 based on a very high cuspal value, and produce an estimated isotopic range of 20.7 ‰, very
633 possibly a ringing artifact that is common during inverse modeling (Figure S2). Even in this

case however, inverse model estimates of blood $\delta^{18}O$ change only amount to 7–9 ‰, a result directly measured in experimental sheep when they consumed some quantity of snow (Green *et al.*, 2018a). Inverse modeling does appear robust in several respects. Reconstructed values are not overly sensitive to variation in estimated tooth wear, with more or less wear producing inversion results within 1 ‰ of one another. Ecological patterns observed in raw enamel carbonate $\delta^{18}O$ measurements are replicated by inverse modeling, where for instance $\delta^{18}O$ variation is reduced in the chamois, and amplified in the mouflons. Reconstructed water $\delta^{18}O$ compositions produced by individual teeth recover nearly the whole range of $\delta^{18}O$ variation observed in nearby precipitation, suggesting that this method may be a powerful tool for reconstructing past seasonality in contexts where precipitation $\delta^{18}O$ are not available.

Table 5. Summary of ecological data and ecological inferences made based on dental proxies of the sympatric ruminants of the BNRP, France.

	Ecological data *		**Interpretations of dental ecological proxies**		
Taxon	Diet (late summer to early winter)	Habitat use	$\delta^{13}C - \Delta^{13}C$	$\delta^{18}O - \Delta^{18}O$	DMTA on shearing molar facets
Capreolus capreolus (Roe deer)	Selective browser -mostly browse on leaves -fruits and seeds < 6 % -herbaceous monocots < 6 %	-low altitude -mostly below 1200 m	-C_3 diet -forested habitats	-varied water inputs -variability not clearly seasonal	-tough foliage-dominated browsing habits -low variations in food resources at (small) home range scale -high inter-individual variations indicating disparity in food resources between (small) home ranges
Cervus elaphus (Red deer)	Mixed feeder -fruits 20% - herbaceous monocots ≈ 40 % In summer**: -herb. monocots 50-60 % -herb. dicots 20 %	-low altitude -mostly below 1200 m -move seasonally at higher altitudes than the roe deer	-C_3 diet -mixed habitats -low altitudinal range	-apparently annual seasonality -intermediate ecology	-grazing habits -low inter-individual variations reflecting gregarious behavior and access to foods similar to most individuals
Ovis gmelini musimon (Mouflon)	Mixed feeder -herb. monocots 32-40 % -mostly browse on deciduous/evergreen trees and shrubs	-high altitude -mostly above 1200 m -move seasonally at lower altitudes than the chamois	-C_3 diet -mixed habitats -high altitudinal range	-varied water inputs -interstitial niche exploitation	-mixed feeding habits -diet richer in lignified tissues than deer ones -diet less rich in herbaceous monocots than the red deer and the chamois diets
Rupicapra rupicapra (Chamois)	Mixed feeder -herb. monocots 42-50 % -mostly browse on forbs, evergreen trees and shrubs	-high altitude -mostly above 1200 m	-C_3 diet -open habitats -low altitudinal range	-limited water inputs -apparently annual seasonality	-mixed feeding habits -diet richer in lignified tissues than deer ones -diet likely richer in herbaceous monocots than the mouflons diet

* Both habitat use and dietary data (stomach content analysis) are from Redjadj et al. (2014) – Although they also come from BNRP, the present study was not conducted on the very same individuals as the ones studied by Redjadj et al. (2014).

** data from Suter et al. (2004). This paper summarizes the variations of summer diet of red deer *Cervus elaphus* in the eastern Swiss Alps. The authors concluded that the herbaceous monocots content is maximal in summer. The dietary difference, and notably the amount of herbaceous monocots and dicots between summer and fall for red deer is essential to be emphasized here because due to the dental microwear turnover (much lower than stomach content), DMTA of red deer shot in September and October does not track fall but summer diet.

5. Conclusions

This study provides insights into the feeding ecology of a modern sympatric ruminant community in a C_3 plant ecosystem providing a comparative stable isotope and dental wear dataset (see summary in Table 5), which could serve as a model to interpret past mammalian herbivore communities. For instance, the contrasting $\delta^{13}C$ values of the roe deer and the chamois mirror their different habitats whereas the red deer and the mouflons show intermediate values, with the latter showing the highest intra-tooth amplitude reflecting its altitudinal seasonal displacements. Dental microwear textures detect some significant differences in diet between species. The two bovids plot as mixed feeding species displaying both intermediate complexity and anisotropy, which is expected for species that ingest less than 50 % herbaceous monocots. This contrasts with the apparent discrepancy between dental proxies and stomach content analysis found for the mixed feeding red deer, where low microwear complexity together with high anisotropy may reflect a summer diet bias towards more grazing habits. Based on comparisons with earlier works on present-day populations of ruminants and experimental controlled food testing on domesticated sheep used as a model for ruminants, the red deer at the BNRP is supposed to be more engaged in grazing than suggested earlier by stomach content analyses. Regarding the roe deer, both mean and inter-individual dispersion of complexity and its anisotropy mirrors stomach content analysis which attests to browsing habits with a low amount of fruits.

Variation in enamel $\delta^{18}O$ compositions appears to reflect the complexity of landscape use in all animals except the roe deer, whose enriched M_2 values likely reflect early life milk consumption. While $\delta^{18}O$ variability is reduced in enamel compared to regional precipitation, inverse modeling appears to fully recover annual $\delta^{18}O$ ranges, while preserving inter-species differences in migratory behavior. Altogether, despite some temporal biases introduced by the timing of enamel deposition or wear, in most cases isotopic and microwear proxies

678 successfully recover ecological niche spaces occupied by all four ruminants in this alpine
679 setting. These results highlight the potential of combined proxies and modeling for
680 reconstructing different ecological aspects (diet, habitat tree cover, home range, seasonal
681 displacement, social behaviors) using dental remains.
682
683 **Acknowledgments**
684 This project has received funding from the French Agency for Research (TRIDENT Project;
685 ANR-13-JSV7-0008-01, PI: G. Merceron, http://anr-trident.prd.fr/) and the European
686 Research Council (ERC) under the European Union's Horizon 2020 Research and Innovation
687 Programme (Grant Agreement 681450, PI: T. Tütken). E. Berlioz was funded by the PHC
688 PROCOPE 2017 - 37786VC. The authors thank G. Reynaud and L. Painault (PALEVOPRIM,
689 Poitiers) for administrative guidance, and C. Gilbert (PALEVOPRIM, Poitiers), J. E. Martin
690 and A. Hassler (LGL: TPE, Lyon) for discussion as well as N. Bourgon for kindly processing
691 C and O isotope data with SIBER to generate predictive ellipses. We would like to thank the
692 OGFH, the Groupement d'Intérêt Cynégétique des Bauges, the Office National des Forêts,
693 hunters, wildlife technicians (T. Chevrier, T. Amblard and J.-M. Jullien), students and
694 volunteers who contributed to collecting ungulate data in BNPR. We would like to thank K.
695 Uno and two anonymous reviewers for helpful comments that help to improve the manuscript.

References

Azorit, C., Tellado, S., Oya, A., Moro, J., 2012. Seasonal and specific diet variations in sympatric red and fallow deer of southern Spain: a preliminary approach to feeding behaviour. Anim. Prod. Sci. 52, 720–727.

Ben-David, M., Flaherty, E.A., 2012. Stable isotopes in mammalian research: a beginner's guide. J. Mammal. 93, 312–328. https://doi.org/10.1644/11-MAMM-S-166.1

Berlioz, E., Azorit, C., Blondel, C., Ruiz, M.S.T., Merceron, G., 2017. Deer in an arid habitat: dental microwear textures track feeding adaptability. Hystrix Ital. J. Mammal. 28, 222–230.

Bignon-lau, O., Catz, N., Berlioz, E., Veiberg, V., Strand, O., Merceron, G., 2017. Dental microwear textural analyses to track feeding ecology of reindeer: a comparison of two contrasting populations in Norway. Mammal Res. 62, 111–120.

Blumenthal S.A., Cerling T.E., Smiley T.M., Badgley C.E., Plummer T.W. 2019. Isotopic records of climate seasonality in equid teeth. Geoch. Cosmochim. Acta 260, 329–48.

Bonafini, M., Pellegrini, M., Ditchfield, P., Pollard, A.M., 2013. Investigation of the 'canopy effect'in the isotope ecology of temperate woodlands. J. Archaeol. Sci. 40, 3926–3935.

Bowen, G.J., 2010. Isoscapes: spatial pattern in isotopic biogeochemistry. Annu. Rev. Earth Planet. Sci. 38, 161–187.

Bugalho, M.N., Milne, J.A., 2003. The composition of the diet of red deer (*Cervus elaphus*) in a Mediterranean environment: a case of summer nutritional constraint? For. Ecol. Manag. 181, 23–29.

Calandra, I., Merceron, G., 2016. Dental microwear texture analysis in mammalian ecology. Mammal Rev. 46, 215–228.

Cibien, C., 1984. Variations saisonnières de l'utilisation de l'espace en fonction des disponibilités alimentaires chez le chevreuil (*Capreolus capreolus* L.). Université François Rabelais, Académie de Tours-Orléans, Tours.

Clauss, M., Dittmann, M.T., Vendl, C., Hagen, K.B., Frei, S., Ortmann, S., Müller, D.W., Hammer, S., Munn, A.J., Schwarm, A., 2020. Comparative methane production in mammalian herbivores. animal 14, s113–s123.

Cornelis, J., Casaer, J., Hermy, M., 1999. Impact of season, habitat and research techniques on diet composition of roe deer (*Capreolus capreolus*): a review. J. Zool. 248, 195–207.

Cransac, N., Cibien, C., Angibault, J.-M., Morrelet, N., Vincent, J.-P., Hewison, A.J.M., 2001. Variations saisonnières du régime alimentaire du chevreuil (*Capreolus capreolus*) selon le sexe en milieu forestier à forte densité (forêt domaniale de Dourdan). Mammalia 65, 1–12.

Cransac, N., Valet, J.P., Cugnasse, J.-M., Rech, J., 1997. Seasonal diet of mouflon (*Ovis gmelini*): comparison of population sub-units and sex-age classes. Rev. Ecologie.

Dansgaard, W., 1964. Stable isotopes in precipitation. Tellus 16, 436–468.

Dantas, M.A.T., Cherkinsky, A., Bocherens, H., Drefahl, M., Bernardes, C., Melo-França, L. de M., 2017. Isotopic paleoecology of the Pleistocene megamammals from the Brazilian Intertropical Region: Feeding ecology ($\delta^{13}C$), niche breadth and overlap. Quat. Sci. Rev. 170, 152–163. https://doi.org/10.1016/j.quascirev.2017.06.030

Darmon, G., Bourgoin, G., Marchand, P., Garel, M., Dubray, D., Jullien, J.-M., Loison, A., 2014. Do ecologically close species shift their daily activities when in sympatry? A test on chamois in the presence of mouflon. Biol. J. Linn. Soc. 111, 621–626.

Davis, M., Pineda Munoz, S., 2016. The temporal scale of diet and dietary proxies. Ecol. Evol. 6, 1883–1897.

DeSantis, L.R.G., 2016. Dental microwear textures: reconstructing diets of fossil mammals. Surf. Topogr. Metrol. Prop. 4, 023002. https://doi.org/10.1088/2051-672X/4/2/023002
Drucker, D.G., Bocherens, H., 2009. Carbon stable isotopes of mammal bones as tracers of canopy development and habitat use in temperate and boreal contexts. For. Canopies For. Prod. Ecosyst. Health Clim. Cond. U. S. Am. Nova Sci. Publ. Inc 2–8.
Espmark, Y., 1969. Mother-young relations and development of behaviour in roe deer (*Capreolus capreolus* L.) (PhD Thesis). Stockholm University.
Espunyes, J., Bartolomé, J., Garel, M., Gálvez-Cerón, A., Aguilar, X.F., Colom-Cadena, A., Calleja, J.A., Gassó, D., Jarque, L., Lavín, S., 2019. Seasonal diet composition of Pyrenean chamois is mainly shaped by primary production waves. PLoS ONE 14, e0210819.
Fiebig, J., Schöne, B.R., Oschmann, W., 2005. High-precision oxygen and carbon isotope analysis of very small (10–30 μg) amounts of carbonates using continuous flow isotope ratio mass spectrometry. Rapid Commun. Mass Spectrom. Int. J. Devoted Rapid Dissem. ---Minute Res. Mass Spectrom. 19, 2355–2358.
Fortelius, M., Eronen, J., Jernvall, J., Liu, L., Pushkina, D., Rinne, J., Tesakov, A., Vislobokova, I., Zhang, Z., Zhou, L., 2002. Fossil mammals resolve regional patterns of Eurasian climate change over 20 million years. Evol. Ecol. Res. 4, 1005–1016.
Gat, J.R., 1996. Oxygen and hydrogen isotopes in the hydrologic cycle. Annu. Rev. Earth Planet. Sci. 24, 225–262.
Gebert, C., Verheyden-Tixier, H., 2001. Variations of diet composition of red deer (*Cervus elaphus* L.) in Europe. Mammal Rev. 31, 189–201.
Green, D.R., Olack, G., Colman, A.S., 2018a. Determinants of blood water $\delta^{18}O$ variation in a population of experimental sheep: Implications for paleoclimate reconstruction. Chem. Geol. 485, 32–43.
Green, D.R., Smith, T.M., Green, G.M., Bidlack, F.B., Tafforeau, P., Colman, A.S., 2018b. Quantitative reconstruction of seasonality from stable isotopes in teeth. Geochim. Cosmochim. Acta 235, 483–504.
Hedberg, C., DeSantis, L.R.G., 2017. Dental microwear texture analysis of extant koalas: clarifying causal agents of microwear. J. Zool. 301, 206–214.
Iacumin, P., Bocherens, H., Mariotti, A., Longinelli, A., 1996. Oxygen isotope analyses of co-existing carbonate and phosphate in biogenic apatite: a way to monitor diagenetic alteration of bone phosphate? Earth Planet. Sci. Lett. 142, 1–6.
IAEA/WMO, 2020. Global Network of Isotopes in Precipitation [WWW Document]. URL https://nucleus.iaea.org/wiser (accessed 4.20.20).
Jackson, A.L., Inger, R., Parnell, A.C., Bearhop, S., 2011. Comparing isotopic niche widths among and within communities: SIBER–Stable Isotope Bayesian Ellipses in R. J. Anim. Ecol. 80, 595–602.
Kaiser, T.M., Clauss, M., Schulz-Kornas, E., 2016. A set of hypotheses on tribology of mammalian herbivore teeth. Surf. Topogr. Metrol. Prop. 4, 014003. https://doi.org/10.1088/2051-672X/4/1/014003
Kaya, F., Bibi, F., Žliobaitė, I., Eronen, J.T., Hui, T., Fortelius, M., 2018. The rise and fall of the Old World savannah fauna and the origins of the African savannah biome. Nat. Ecol. Evol. 2, 241.
Kierdorf, U., Kierdorf, H., 2000. Comparative analysis of dental fluorosis in roe deer (*Capreolus capreolus*) and red deer (*Cervus elaphus*): interdental variation and species differences. J. Zool. 250, 87–93.
Kjellander, P., Hewison, A.J.M., Liberg, O., Angibault, J.-M., Bideau, E., Cargnelutti, B., 2004. Experimental evidence for density-dependence of home-range size in roe deer

(*Capreolus capreolus* L.): a comparison of two long-term studies. Oecologia 139, 478–485. https://doi.org/10.1007/s00442-004-1529-z
Kohn, M.J., 2010. Carbon isotope compositions of terrestrial C3 plants as indicators of (paleo)ecology and (paleo)climate. Proc. Natl. Acad. Sci. U. S. A. 107, 19691–19695.
Kohn, M.J., 1996. Predicting animal $\delta^{18}O$: Accounting for diet and physiological adaptation. Geochim. Cosmochim. Acta 60, 4811–4829.
La Morgia, V., Bassano, B., 2009. Feeding habits, forage selection, and diet overlap in Alpine chamois (*Rupicapra rupicapra* L.) and domestic sheep. Ecol. Res. 24, 1043–1050.
Levins, R., 1968. Evolution in changing environments: some theoretical explorations. Princeton University Press.
Manthi, F.K., Sanders, W.J., Plavcan, J.M., Cerling, T.E., Brown, F.H., 2019. Late Middle Pleistocene elephants from Natodomeri, Kenya and the disappearance of *Elephas* (Proboscidea, Mammalia) in Africa. J. Mamm. Evol. 1–13.
Marchand, P., Redjadj, C., Garel, M., Cugnasse, J.-M., Maillard, D., Loison, A., 2013. Are mouflon *Ovis gmelini musimon* really grazers? A review of variation in diet composition. Mammal Rev. 43, 275–291.
Martin, J.E., Tacail, T., Balter, V., 2017. Non-traditional isotope perspectives in vertebrate palaeobiology. Palaeontology 60, 485–502. https://doi.org/10.1111/pala.12300
Merceron, G., Escarguel, G., Angibault, J.-M., Verheyden-Tixier, H., 2010. Can dental microwear textures record inter-individual dietary variations? PLoS ONE 5, e9542.
Merceron, G., Ramdarshan, A., Blondel, C., Boisserie, J.-R., Brunetiere, N., Francisco, A., Gautier, D., Milhet, X., Novello, A., Pret, D., 2016. Untangling the environmental from the dietary: dust does not matter. Proceeding R. Soc. Lond. B 283, 20161032.
Osmond, C.B., Ziegler, H., Stichler, W., Trimborn, P., 1975. Carbon isotope discrimination in alpine succulent plants supposed to be capable of crassulacean acid metabolism (CAM). Oecologia 18, 209–217.
Passey B.H., Cerling T.E., Schuster G.T., Robinson T.F., Roeder B.L., Krueger S.K. 2015. Inverse methods for estimating primary input signals from time-averaged isotope profiles. Geoch. Cosmochim. Acta 69, 4101–16.
Percher, A.M., Merceron, G., Nsi Akoue, G., Galbany, J., Romero, A., Charpentier, M.J., 2018. Dental microwear textural analysis as an analytical tool to depict individual traits and reconstruct the diet of a primate. Am. J. Phys. Anthropol. 165, 123–138.
Pérez-Barberia, F.J., Olivan, M., Osoro, K., Nores, C., 1997. Sex, seasonal and spatial differences in the diet of Cantabrian chamois *Rupicapra pyrenaica parva*. Acta Theriol. (Warsz.) 42, 37–46.
Pianka, E.R., 1973. The structure of lizard communities. Annu. Rev. Ecol. Syst. 4, 53–74.
Plavcan, J.M., Cope, D.A., 2001. Metric variation and species recognition in the fossil record. Evol. Anthropol. Issues News Rev. Issues News Rev. 10, 204–222.
Pyankov, V.I., Ziegler, H., Akhani, H., Deigele, C., Lüttge, U., 2010. European plants with C4 photosynthesis: geographical and taxonomic distribution and relations to climate parameters: European Plants with C_4 Photosynthesis. Bot. J. Linn. Soc. 163, 283–304. https://doi.org/10.1111/j.1095-8339.2010.01062.x
Ramdarshan, A., Blondel, C., Brunetière, N., Francisco, A., Gautier, D., Surault, J., Merceron, G., 2016. Seeds, browse, and tooth wear: a sheep perspective. Ecol. Evol. 6, 5559–5569.
Ramdarshan, A., Blondel, C., Gautier, D., Surault, J., Merceron, G., 2017. Overcoming sampling issues in dental tribology: Insights from an experimentation on sheep. Palaeontol. Electron. 20, 1–19.
Redjadj, C., Darmon, G., Maillard, D., Chevrier, T., Bastianelli, D., Verheyden, H., Loison, A., Saïd, S., 2014. Intra- and Interspecific Differences in Diet Quality and

Composition in a Large Herbivore Community. PLoS ONE 9, e84756. https://doi.org/10.1371/journal.pone.0084756
Rozanski, K., Araguás-Araguás, L., Gonfiantini, R., 1993. Isotopic patterns in modern global precipitation. Geophys. Monogr. 78, 1–36.
Schulz, E., Piotrowski, V., Clauss, M., Mau, M., Merceron, G., Kaiser, T.M., 2013. Dietary abrasiveness is associated with variability of microwear and dental surface texture in rabbits. PLoS ONE 8, e56167.
Scott, R.S., Ungar, P., Bergstrom, T.S., Brown, C.A.; Childs, B.E.; Teaford, M.F., Walker, A. 2006. Dental microwear texture analysis: technical considerations. J. Hum. Evol. 51, 339–49.
Scott, J.R., 2012. Dental microwear texture analysis of extant African Bovidae. Mammalia 76, 157–174.
Smith, B.N., Epstein, S., 1971. Two categories of $^{13}C/^{12}C$ ratios for higher plants. Plant Physiol. 47, 380–384.
Storms, D., Aubry, Ph., Hamann, J.-L., Saïd, S., Fritz, H., Saint-Andrieux, Ch., Klein, F., 2008. Seasonal variation in diet composition and similarity of sympatric red deer *Cervus elaphus* and roe deer *Capreolus capreolus*. Wildl. Biol. 14, 237–250.
Suter, W., Suter, U., Kriisi, B., Schütz, M., 2004. Spatial variation of summer diet of red deer *Cervus elaphus* in the eastern Swiss Alps. Wildl. Biol. 10, 43–50. https://doi.org/10.2981/wlb.2004.008
Tejada-Lara, J.V., MacFadden, B.J., Bermudez, L., Rojas, G., Salas-Gismondi, R., Flynn, J.J., 2018. Body mass predicts isotope enrichment in herbivorous mammals. Proc. R. Soc. B Biol. Sci. 285, 20181020.
Tixier, H., Duncan, P., 1996. Are European roe deer browsers? A review of variations in the composition of their diets. Rev. Ecol. Terre Vie 51, 3–17.
Tixier, H., Duncan, P., Scehovic, J., Yani, A., Gleizes, M., Lila, M., 1997. Food selection by a roe deer (*Capreolus capreolus*): effects of plant chemistry, and consequences for the nutritional value of their diet. J. Zool. 242, 229–245.
Ungar, P.S., Scott, R.S., Scott, J.R., Teaford, M.F., 2008. Dental microwear analysis: historical perspectives and new approaches, in: Irish, J.D., Nelson, G.C. (Eds.), Volume on Dental Anthropology. Cambridge University, Cambridge, pp. 389–425.
Van der Merwe, N.J., Medina, E., 1991. The canopy effect, carbon isotope ratios and foodwebs in Amazonia. J. Archaeol. Sci. 18, 249–259.
Winkler, D.E., Schulz-Kornas, E., Kaiser, T.M., De Cuyper, A., Clauss, M., Tütken, T., 2019. Forage silica and water content control dental surface texture in guinea pigs and provide implications for dietary reconstruction. Proc. Natl. Acad. Sci. 116, 1325–1330. https://doi.org/10.1073/pnas.1814081116
Winkler, D.E., Schulz-Kornas, E., Kaiser, T.M., Codron, D., Leichliter, J., Hummel, J. Martin, L.M., Clauss, M., Tütken, T. 2020. The turnover of dental microwear texture: Testing the ”last supper” effect in small mammals in a controlled feeding experiment. This volume
Zazzo A., Balasse M., Passey B. H., Moloney A.P., Monahan F.J., Schmidt O. 2010. The isotope record of short-and long-term dietary changes in sheep tooth enamel: implications for quantitative reconstruction of paleodiets. Geoch. Cosmochim. Acta 74, 3571–86.

SUPPLEMENTARY INFORMATION

Tooth tales told by dental diet proxies: an alpine community of sympatric ruminants as a model to decipher the ecology of fossil fauna

Gildas Merceron[1]*, Emilie Berlioz[1,2], Hubert Vonhof[3], Daniel Green[4], Mathieu Garel[5], Thomas Tütken[7]

1. Material and methods

1.1. Material

1.1.1. The Bauges Natural Regional Park (BNRP) and the sympatric ruminants

The Bauges Natural Regional Park (BNRP; 45.69°N, 6.14°E, Figure 1) is a typical subalpine massif of ≈90,000 ha located in the northern French Alps. Altitudes range from 250 m to 2217 m. The climate is cold and humid: at 590 meters in altitude, the Météo-France weather station has recorded annual mean temperatures of 9.2 °C, where the coldest month mean is -0.14 °C in January and the warmest month mean 18.5 °C in July. The same station records annual mean rainfall to be 1369 mm. Snow covers the ground from November to April in subalpine pastures (≈1,630 m) with frost lasting in average 123 days per year (Thuiller et al., 2018). More than 70 % of the BNRP has a high tree cover up to 1,500 m. The tree species of European beech (*Fagus sylvatica*) and silver fir (*Abies alba*) represent about 50 % of forest cover. The non-forested habitats, mostly at the highest altitudes, are composed of open pastures, screes and cliffs. The study area also encompasses a National Game and Wildlife Reserve (NGWR; 5,205 ha; Figure 1), comprising the highest part of the massif.

Several studies have investigated multiple aspects of behavioral ecology of the four wild ruminant species (chamois, red deer, roe deer and mouflon) inhabiting the BNRP. Among them, Redjadj et al. (2014; Table S1) made a comparative analysis of the feeding ecology of these four large herbivores through a gender-balanced stomach content analysis covering late summer until early winter period from 2003 to 2008. It is worth mention that none of stomach contents from the specimens in the present study have been analyzed. Also, with the exception of the mouflons, most of the specimens were shot in early fall (late September and October; Appendix 2); we therefore expect dental microwear textures to reflect the summer diet, since these reflect dietary habits of the last few weeks to months of life (Teaford et al., 2017; Teaford and Oyen, 1989; Winkler et al., this volume). Redjadj et al. (2014) have shown a clear spatial distribution between cervids and bovids, the latter, and notably the chamois, occupying the highest areas. Among cervids the red deer goes least frequently to higher altitudes (Redjadj et al., 2014).

The largest ruminant (adult males: 151 kg; adult females: 98 kg) at the BNRP, the red deer *Cervus elaphus*, is a mixed-feeding species (including both monocots and dicots) with spatial variation in its diet. Grasses account for about 30 % of the annual diet in many regions through Europe but can surpass 80 % in Mediterranean habitats (Azorit et al., 2012; Bugalho and Milne, 2003; Gebert and Verheyden-Tixier, 2001). At the BNRP, Redjadj et al. (2014) found out that during late summer and early fall (the period during which most of the specimens were shot), herbaceous monocots and forbs represent about 40 and 6 %, respectively, of the stomach content as dry matter weight. Fruits, mainly apples and to a lesser extent acorns (Redjadj et al., 2014) may account for up to 20 %. Foliages from various evergreen and deciduous trees and shrubs (cumulative proportions reaching 23.6 %), dominated by evergreen shrubs, notably brambles (*Rubus fruticosus*; Table S1), also form a major fraction of the diet. It is worth noting that Suter et al. (2004) indicates that herbaceous monocots represent between 50 and 60 % of summer diet of red deer in the Alps, which is complemented with herbaceous dicots (forbs) that could represent up to 20 %. Although comparisons between the two studies are difficult as the sampling methods differ, the seasonal shift from graze to browse from summer to winter are reported for many Alpine populations (Suter et al., 2004).

The second cervid, the roe deer *Capreolus capreolus* (adult males: 22.8 kg; adult females: 21.4 kg), is a selective browser (Cibien, 1984; Cornelis et al., 1999; Cransac et al., 2001; Storms et al., 2008; Tixier et al., 1997). Its diet mostly includes dicot foliage, mosses, mushrooms, fruits including seeds. Herbaceous monocots barely reach 10 % of its diet; this occurs, however, only in spring. In late summer and early fall, roe deer from the BNRP mainly focus on evergreen shrubs (bramble leaves) and forbs at about 44 and 25% of the stomach content expressed as dry matter weight, respectively. Evergreen shrubs reach almost 60%, and forbs surpass 10 % in late fall and winter. What is surprising at the BNRP is the very low amount of fruits in the roe deer diet for the two periods (3.4 and 5.8 % of the diet, respectively) compared to the greater fruit intake among red deer at BNRP, (Redjadj et al., 2014), and to roe deer populations in other locations (Tixier and Duncan, 1996). As expected, grasses represent less than 6% of the roe deer diet for each of the two seasons at the BNRP (Table S1).

The mouflons, *Ovis gmelini musimon* (adult males: 42.8 kg; adult females: 31.3 kg) is a mixed-feeding species. Marchand et al. (2013) reviewed the feeding ecology of this wild sheep. Although grasses are the major food type, foliages from shrubs and herbaceous dicots are the secondarily preferred food resources. At the BNRP, grasses represent 42 and 29 % (expressed

as percentage of dry matter weight) of their diet for each of the two investigated periods (Redjadj et al., 2014). Evergreen shrubs (16.2 %) and forbs (15.7 %) are the secondarily preferred foods in late summer and early fall. In late fall and winter, evergreen trees (mostly conifer foliages; 28.1 %) counterbalance the drop in proportions of both forbs and grass component compared to the first period (Table S1; Redjadj et al., 2014).

The chamois *Rupicapra rupicapra* (adult males: 34.5 kg; adult females: 29.7 kg) is a mixed feeder grazing and browsing depending resources availabilities and energetic requirements (Pérez-Barberia et al., 1997). For instance, recent studies show that the chamois in Pyrenees may include less than 20 % grasses in its summer and fall diets (Espunyes et al., 2019). Besides, grasses represent 44 % and more than 50 % in summer and fall, respectively, of its diet at the BNRP (Table S1; Redjadj et al., 2014). Forbs (22.4 %) and evergreen shrubs (19.6 %) complement the diet for the first period whereas the drop in forbs is counterbalanced with evergreen trees (17.5 %) composing the secondary food items (Table S1).

Table S1. Mean percentage of the main food resource of the ruminants from the Bauges NRP in late summer/early fall and late fall and winter (for more details, see Redjadj et al., 2014).

		Period 1 (early September-mid November)							Period 2 (mid November-late January)						
Species	N*	Fr	Gr	Fo	DS	ES	DT	ET	Fr	Gr	Fo	DS	ES	DT	ET
C. capreolus	104	3.44	5.08	25.1	2.41	44.3	5.7	0.8	5.83	5.52	10.4	1	58.6	0.61	10.2
C. elaphus	158	19.5	39.8	6.17	1.94	13.5	4.12	4.02	12.5	33.4	1.84	0.96	26.1	1.54	15.7
O. gmelini	86	5.18	41.8	15.7	4.12	16.2	5.81	1.45	4.43	29	3.71	1.32	17.3	2.36	28.1
R. rupicapra	148	1.29	44.4	22.4	0.67	19.6	0.79	0.42	1.48	50.5	9	0.81	16.2	0.48	17.5

*N: number of stomach contents; Fr: fruits; Gr: grasses and herbaceous monocots; Fo: forbs; DS: deciduous shrubs; ES: evergreen shrubs; DT: deciduous trees; ES: evergreen trees.

1.1.2 Selection of BNRP specimens

Our study was based on tooth samples collected from animals shot during the legal hunting season both within and outside the NGWR (Fig. 1). All samples come from animals tagged with official annual hunting quotas delivered by the county prefects in agreement with the environmental code (Art. R425-2 to 425-141 13). No animals were harvested solely for the purpose of this study.

Mandibles were collected from early September to end of March during three hunting seasons (2008/2009, 2014/2015 and 2015/2016). A total of 11 and 82 adult specimens (with erupted and worn second molars) were used for enamel stable isotope and dental microwear texture analyses, respectively. Five red deer, two roe deer, two chamois and two mouflon molars

were serially sampled for enamel stable isotope analyses (Appendix 1). Eighteen roe deer, 21 red deer, 22 mouflons, and 21 chamois compose the sample for DMTA, which was performed on second molars (Appendix 2).

2. Methods

2. 1. Enamel carbon and oxygen stable isotope analyses

Stable carbon isotopes ($^{13}C/^{12}C$ ratio expressed as $\delta^{13}C$ value) in enamel reflect the $\delta^{13}C$ values of the ingested food resources that are mainly controlled by the photosynthetic pathway used by plants. The C_3 or Calvin-Benson-Bassham cycle results in more fractionation of ^{12}C and therefore lower $\delta^{13}C$ values, while the C_4 or Hatch-Slack cycle results in less fractionation of ^{12}C and therefore higher $\delta^{13}C$ values. Vegetation type and plant physiology can further control herbivore enamel $\delta^{13}C$ values: C_3 plants tend to be trees or shrubs and herbaceous dicots and monocots from either high altitudes or latitudes, whereas C_4 plants tend to be monocots, notably grasses. Even in a pure C_3 ecosystem, the degree of vegetation cover can be observed isotopically, where dense forest cover results in lower $\delta^{13}C$ values, and open environments result in higher $\delta^{13}C$ due to increased rates of evapotranspiration and stomatal conductance in leaves (Bonafini et al., 2013; Drucker and Bocherens, 2009). Given these considerations we expect enamel $\delta^{13}C$ values to be lower in the forest-dwelling roe deer and higher in the chamois, which occupies the most open Alpine habitat within this C_3 plant ecosystem (Redjadj et al., 2014 and citations therein).

About 100 µg of enamel powder per sample were serially extracted with a hand-held microdrill, sampled along the crown from apex to cervix on the third lower molars (M_3) of red deer, and on the second (M_2) and third (M_3) lower molars of mouflons, chamois, and roe deer. Six to 16 enamel samples per tooth were analyzed for roe deer and mouflon, respectively (Figures 1 and 2; Table 1; Appendix 1). The spatial location of sample positions on each tooth was recorded to within 0.1 mm precision. No bleach treatment was applied.

Isotope analyses of structural carbonate in tooth enamel samples were performed on a Thermo DeltaV mass spectrometer coupled to a Gasbench II gas preparation unit in which a cold trap system at liquid nitrogen temperature is integrated. The system is set up as outlined in Fiebig et al. (2005). With this technique, smaller than usual samples can be analyzed: in this study <200 microgram of non-pre-treated tooth enamel powder. Digestion of enamel powder

took place in >99 % H_3PO_4, at a temperature of 70 ºC. The sample digestion time between acidification and CO_2 sample transfer to the cold trap was ~90 minutes. Isotope data are calculated by direct comparison to a total of ≈20 replicates of at least two isotopically distinct $CaCO_3$ isotope standards analyzed in each run of 55 samples. A logarithmic fit through the isotope ratios versus peak size data of the standard replicates is used to remove fractionation effects due to sample size. The reproducibility of standards after these corrections typically is better than 0.3 ‰ for both $\delta^{18}O$ and $\delta^{13}C$ (1SD). This is a slightly higher uncertainty in comparison to the analysis, on the same equipment, of larger samples that do not require use of the cold trap (Breitenbach and Bernasconi, 2011; Spötl and Vennemann, 2003). For the precision requirements in this study, we believe the slightly higher uncertainty does not outweigh the benefits of achieving high-resolution growth incremental series by analysing the smaller amounts. We routinely analyzed a modern tooth enamel standard of an African elephant (AG-Lox, Gehler et al., 2012) in the runs as well, to verify that this enamel standard (i.e. structurally bound carbonate in bioapatite) has a similar reproducibility to pure carbonate standards. Daily averages of the the AG-Lox standard as measured with this technique yield a $\delta^{13}C_{enamel}$ value of -11.49 ± 0.11 ‰ (1SD) and a $\delta^{18}O_{enamel}$ value of -1.50 ± 0.19 ‰ (1SD). These precisions are slightly better than sample to sample uncertainties, as they are based on daily averages of multiple analyses of this standard. We observe that the AG-Lox isotope values reported for this technique compare, within error, to the values we find if we run larger amounts of AG-Lox on the same Gasbench system without using the cold trap. Another relevant observation is that the $\delta^{18}O_{enamel}$ values for AG-Lox on this system differ significantly from previous published values, obtained on a fundamentally different IRMS system (Wacker et al 2016). Interlaboratory differences for tooth enamel $\delta^{18}O_{enamel}$ values occur frequently, and are believed to relate to analytical conditions like digestion temperature and acid type (e. g., Demény et al., 2019). Reporting isotope values for tooth enamel standards like AG-Lox enables a better comparison of isotope data from different laboratories. The interlaboratory differences for tooth enamel $\delta^{13}C_{enamel}$ values tend to be much smaller, and would be insignificant for the $\delta^{13}C_{enamel}$ variation described in this study.

2.2 Modeling ruminant isotope ecology

Kierdorf and Kierdorf (2000) report that for the roe deer, enamel formation (amelogenesis) of M_2 begins *in utero* and terminates around 4 months of age. The roe deer M_3 is estimated to form between 4–9 months of age. For the red deer, the second molar begins

forming prior to 3 months of age and completes formation around 9 months of age; the third molar begins forming at 9 months of age and completes prior to 26 months. Here, we consider only M_3 of red deer. Depending on the breed, sheep second molars may mineralize over a 10–15 months period, and third molars over 10–15 months or more (Milhaud and Nezit, 1991). Assuming that caprine bovids have similar enamel growth rate and that chamois molars are smaller than those of mouflons, we consider it plausible that chamois second and third molars form over slightly less time than those of mouflons (see also Kierdorf et al., 2012).

Using a bodymass-dependent equation calibrated specifically for foregut mammals (Tejada-Lara et al., 2018; Table S1; Appendix 1), we calculate ε an estimation of the carbon stable isotope composition of the food resources ($\delta^{13}C_{diet}$) exploited by the ruminants.

$\varepsilon^* = \mathbf{2.34} + \mathbf{0.05}\ (\mathbf{BM})$; Bodymass expressed need to be ln-transformed, and then ε* needs to be inverted (e^x) to obtain the ‰ value to be applied for each species. We consider bodymass (intermediate value between male and female bodymass) measured on specimens sampled over several years in BNRP: 125 kg for the red deer, 22 kg for the roe deer, 32 kg for the chamois and 37 kg for the mouflon (see Table 1 and Appendix 1). The isolated high $\delta^{13}C_{enamel}$ value, if not an analytical artefact, is either due the high intake of alpine CAM plants or the few native C_4 plants at high altitudes and mid-to-high latitudinal biomes (Osmond et al., 1975; Pyankov et al., 2010) which can have variable $\delta^{13}C$ values, depending on local and seasonal conditions, or due to the consumption of cultivated maize in valleys. Also, mouflons are known to perform seasonal altitudinal movements (Darmon et al., 2014) and as there are a few areas of cultivated maize in the valleys and the possible existence of some places where hunters spread maize for preventing damages caused by wild boar, we cannot firmly exclude a high consumption of maize for short period.

In parallel to carbon isotope analysis of tooth enamel, food remains stuck between cusps and teeth in the jaw were sampled also for carbon isotope analysis to directly assess the $\delta^{13}C$ values of ingested food plants. Dried plant samples were homogenized in 2 ml Eppendorf vials using a Retsch ball mill. About 700 µg of plant powder were weight into a 3.3 x 5 mm tin capsule and tightly folded. Each plant sample was analyzed in triplicate for its carbon isotope composition using a Vario EL elemental analyzer (EA) coupled to a Finnigan MAT 253 isotope ratio mass spectrometer in continuous flow mode. Carbon isotope data ($^{13}C/^{12}C$ expressed as $\delta^{13}C$ value) are reported in the δ-notation in per mil (‰), relative to the international isotope reference standard Vienna Pee Dee Belemnite (VPDB). Sample $\delta^{13}C$ values were calibrated

against the two international glutamic acid standard reference materials USGS 40 and 41. The analytical precision of $\delta^{13}C$ values was better than +/- 0.1 ‰ (1 SD). The $\delta^{13}C$ values of these plant remains were measured from which an expected enamel $\delta^{13}C_{enamel}$ value is calculated according to the equation for foregut fermenting mammals from Tejada-Lara et al. (2018; Table S2). This hypothetical $\delta^{13}C_{enamel}$ is not compared with the mean $\delta^{13}C$ values of the serial enamel samples along the tooth crown that would represent a long time span but with the measured $\delta^{13}C_{enamel}$ value of the very last sample to mineralize on the M_3, meaning next to the cervix. Both, food remains from the teeth/jaw and $\delta^{13}C_{enamel}$, represent an unknown interval of time (even when the enamel is serially sampled). However, the carbon isotope composition of the enamel was incorporated when it was mineralized at least weeks if not months before food items were stuck in dental arches. Moreover, we may also argue the plant remains stuck in teeth is an epiphenomenon meaning the direct comparisons of these data should be done with high caution. In any case, the $\delta^{13}C_{enamel}$ value of the very last sample to mineralize on the M_3 is the most appropriate value to be compared with $\delta^{13}C$ measured from food remains lodged between cusps and teeth.

Table S2. Carbon stable isotope compositions of the food stuck between cuspids and teeth of different individuals of the ruminants from the Bauges NRP. Estimations of carbon stable isotope composition of the enamel (based on Tejada et al., 2018) that would have incorporated carbon atoms from a dietary bolus with a carbon stable isotope composition similar to the one of the food stuck are calculated compared with the carbon stable isotope composition of the very last sample on the third molar.

taxon	specimen	$\delta^{13}C$ vegetation	sd*	$\delta^{13}C_{enamel}$ estimation	$\delta^{13}C_{enamel}$ M_3 Last sample	$\Delta^{13}C_{diet\text{-}enamel}$
Cervus elaphus	CE 4821	-28.27	1.79	-15.30	-14.51	-0.79
Cervus elaphus	CEF 7104	-29.86	0.11	-16.88	-15.83	-1.05
Cervus elaphus	CEM 2616	-29.19	0.10	-16.21	-16.67	0.46
Cervus elaphus	CE 4951	-29.94	0.07	-16.96	-16.00	-0.96
Cervus elaphus	CE 0104	-30.06	0.43	-17.08	-16.89	-0.19
Capreolus capreolus	CC 2613	-28.36	0.04	-16.18	-16.30	0.12
Capreolus capreolus	CC 2653	-28.94	0.04	-16.76	-18.70	1.94
Rupicapra rupicapra	RR 8952	-28.58	0.05	-16.31	-14.50	-1.81
Rupicapra rupicapra	RR 8932	-27.23	0.06	-14.95	-14.43	-0.52
Ovis gmelini	OG 8843	-27.55	0.04	-15.44	-14.57	-0.87
Ovis gmelini	OG 8847	-27.65	0.01	-15.54	-15.54	0.00

* Standard deviation

In addition, we expect the enamel oxygen isotopic composition ($^{18}O/^{16}O$ ratio expressed as $\delta^{18}O$ value) to primarily reflect the $\delta^{18}O$ values of the ingested water, including drinking and/or leaf water. The $\delta^{18}O$ values of precipitation should be lower at low temperatures and high altitudes, and should vary across winter and summer seasons (Dansgaard, 1964; Rozanski et al., 1993; Gat, 1996; Bowen, 2010). Therefore, the altitudinal distribution of the species and their distinct spatial and temporal feeding behaviors can potentially be inferred from enamel $\delta^{18}O$ values. Additionally, enamel $\delta^{18}O$ values may reflect differences in feeding ecology and plant physiology. Compared to grazers, browsers gain most of their body water from the vegetation itself, where leaf water and plant structural carbohydrates are significantly ^{18}O-enriched relative to meteoric water (Farquhar and Lloyd, 1993; Farquhar and Gan, 2003; Song et al., 2013). Herbivores produce a portion of their body water from the metabolism of these carbohydrates and the inspiration of atmospheric oxygen (Gretebeck et al., 1997; Podlesak et al., 2008). Lastly, herbivore physiology itself may impact body water and enamel $\delta^{18}O$ compositions, as individuals increased loss of lose body water to the environment through panting and cutaneous evaporation have ^{18}O-enriched body water pools (Kohn et al., 1996; Green et al., 2018a).

Based on the enamel oxygen isotope composition, we propose an estimation of the oxygen isotope composition of the environmental water ($\delta^{18}O_{ew}$) ingested by the ruminants from the BNRP following the regression between enamel (i.e. structurally bound carbonate in the bioapatite) and ingested water of Iacumin et al. (1996):

$$\delta^{18}O_{enamel} = 0.998 \times \delta^{18}O_{ew} + 33.63$$

We also consider the niche breadth B_A (Levins, 1968) and the ecological overlapping O_{Bauges} (Pianka, 1973), based on both $\delta^{18}O_{ew}$ and $\delta^{13}C_{diet}$ (see also Dantas et al., 2017). These two ecological indexes are computed with the relative proportions of individuals plotting within pre-defined isotopic bins (Table 2). Here, the full range of $\delta^{18}O_{ew}$ and $\delta^{13}C_{diet}$ based on intra tooth ranges of M_3 (we exclude M_2 data as these might potentially represent a mix of post- and pre-weaning information) are used to define the range of isotopic bins. Seven one-per-mil-intervals from –25.0 ‰ to –32.0 ‰ are then defined for the carbon isotope composition of the diet. Here, we did not consider the single unexpected high enamel $\delta^{13}C$ value of -6.9‰ on mouflons M_2 (MO8843), which might reflect either an undetected analytical error or a significant fraction of C_4 plant in the diet ($\delta^{13}C_{diet}$ = –19.29 ‰), most likely maize from cultivated fields at low altitudes. We consider this value as non-representative of the mouflon

ecology in an Alpine native ecosystem in Europe. In addition, seven one-per-mil-intervals from −16.0 ‰ to −9.0‰ are defined for the oxygen isotope composition of the environmental water (Table 2).

2.3 Estimating oxygen isotope seasonality through inverse modeling

Lastly, we use Bayesian inference inverse modeling to better infer potential seasonal variations in environmental $\delta^{18}O$ values that contribute to measured spatial variations in tooth $\delta^{18}O$. As described previously (Green et al., 2018b), we combine our chamois, mouflons, roe and red deer tooth $\delta^{18}O$ measurements with a synchrotron-based empirical model of ruminant molar enamel formation, originally derived from a population of domesticated sheep. Through forward modeling, these measurements and model predict tooth isotope compositions for any hypothetical history of seasonal $\delta^{18}O$ ingestion (see Passey and Cerling, 2002; Passey et al., 2005). We iteratively propose seasonal drinking water histories, comparing resulting forward modeled enamel $\delta^{18}O$ compositions with actual $\delta^{18}O$ data, until differences between modeled and real enamel $\delta^{18}O$ compositions are minimized (Green et al., 2018b).

Sequential isotopic measurements from enamel are generally intended to reconstruct past seasonal patterns related to an animal's behavior, physiology and environmental chemistry. This is possible because teeth form incrementally, and during formation, enamel increments mineralize at equilibrium with body chemistry, which itself fluctuates over time with changes in diet, physiology or the environment. Sequential samples measured from a tooth do not however directly record either environmental or body chemistry. First, environmental signals are altered as they enter the blood stream on the basis of physiological and molecular discrimination. Because the body has one or several reservoirs with unique turnover times for each ingested constituent, environmental signals tend to be prolonged and dampened. Second, enamel mineralizes in multiple stages with timing and geometry that changes across the tooth crown. For this reason, changes in body chemistry over time, already an indirect reflection of environmental chemistry, are further attenuated and distorted when reflected as spatial variations in enamel chemistry across the length of a tooth.

We attempt to use enamel isotopic measurements made from ruminants in the Bauges Regional Natural Park, to reconstruct their original seasonal ingested drinking waters through inverse modeling. To do this we must first propose forward models that estimate how body chemistry changes over time given changes in environmental chemistry, and then use forward

models that estimate how enamel chemistry is determined given these estimates of body water chemistry (Passey and Cerling, 2002; Passey et al., 2005). Here, we use equations adapted by Gretebeck et al. (1997) to estimate blood water $\delta^{18}O$ compositions from air ($\delta^{18}O$ = 23.5 ‰ globally), drinking water, and feed, which we here treat as pure carbohydrate for simplicity (Podlesak et al., 2008), and to which we give an invariant value of $\delta^{18}O$ = 25 ‰, comparable to other measured northern hemisphere feed $\delta^{18}O$ compositions ranging from 23–26.1 ‰ (Gretebeck et al., 1997; Podlesak et al., 2008; Green et al., 2018a). We assume a single body oxygen turnover pool (Cerling et al., 2007) in ruminants of seven days, given measured water turnover rates ranging from 3–13 days in living ruminants, and recognizing that the highest and lowest values in this range are found among either physiological specialists or domesticated animals, respectively (Macfarlane et al., 1971). We set the ratio of oxygen ingested as drinking water compared to that consumed as both feed and air to 1:1, within the range of values observed in humans, rodents and sheep (Gretebeck et al., 1997; Podlesak et al., 2008; Green et al., 2018a), and set the amount of water lost evaporatively to 40 %. Under this rubric we assume that half of animal body water is derived from water ingested directly from streams and snow, or contained within vegetation; we model the remainder of body water as deriving from metabolic water production from atmospheric oxygen ($\delta^{18}O$ = 23.5 ‰) and plant carbohydrate ($\delta^{18}O$ estimated at 25 ‰). While we recognize that carbohydrate, protein and fat resources within plants all contribute to ruminant metabolic water production, for the sake of simplicity we here consider only carbohydrate metabolism, and treat carbohydrate $\delta^{18}O$ compositions as seasonally invariant (Podlesak et al., 2008).

Given these estimates of the behavioral, environmental and physiological values and processes, from a given proposed history of seasonal drinking water $\delta^{18}O$ over time, derived either from snow, liquid water or from water within plant tissues, we can estimate body water $\delta^{18}O$ compositions over time. These compositions are then used to calculate modeled tooth enamel $\delta^{18}O$ values. Given a model of ruminant enamel formation (Green et al., 2017), we estimate that the value of any given location xy in a tooth on day d of formation, is equal to the sum of blood $\delta^{18}O$ compositions for all of i days from the initiation (init) of enamel formation until day d, multiplied by the fractional daily mineral density increases $\rho\Delta i$ relative to cumulative mineral densities ρtd at that location for all of i days until day d: $\delta^{18}Oxy,d = \Sigma id\ \delta^{18}Oi \times \rho\Delta\iota / \rho\Delta i$. A value of 19.1 ‰ taken from Pucéat et al. (2010) is added to account for the offset between blood water and mineral phosphate.

Following Green et al. (2018b), inverse seasonal blood and water $\delta^{18}O$ modeling was conducted using Python 2.7, and with the aid of optimization algorithms hosted by the python non-linear optimization module (NLopt, Johnson, 2017). For each optimization, water $\delta^{18}O$ parameter values were proposed at 14-day intervals. Local searches were conducted using constrained optimization by linear approximation (COBYLA; Powell, 1998), and global searches were conducted using the quasi-Monte Carlo multi-level single linkage algorithm (MLSL) (Rinnooy Kan and Timmer, 1987; Kucherenko and Sytsko, 2005). Parameter goodness of fit was evaluated using a likelihood framework comparing modeled tooth $\delta^{18}O$ values resulting from hypothetical drinking water $\delta^{18}O$ parameters to measured enamel $\delta^{18}O$ values. In addition to accounting for measurement error, modeled enamel $\delta^{18}O$ uncertainty incorporates 10 estimates of within-population variation in mineralization trajectory per sampled location within the enamel, and three estimates of potential between-population or between-species variation in enamel formation rates (Green et al., 2018b). Each optimization trial shown is the result of 24,000 trials, with increasingly relaxed d_{rate} priors used to increase both accuracy and precision of the result.

During modelling, we assume that 50 % of tooth crown height has been lost in second molars (M_2s), and 25 % of tooth crown height lost in third molars (M_3s), prior to sampling. Sensitivity testing indicates that altering the total estimated crown wear does not dramatically shift reconstructed drinking water $\delta^{18}O$ values. Because most chamois, mouflons and red deer M_2s and M_3s appear to form over a period of up to or beyond one year, we model their extension (growth along the cuspal-cervical axis) as equivalent to measured rates in a domesticated sheep second molar, completing within 14 months. For the roe deer, we estimate that extension completes more quickly: within 7 months, though mineralization may continue briefly afterwards (Milhaud and Nezit, 1991; Kierdorf and Kierdorf, 2000; Green et al., 2017; Witzel et al., 2018). Measured enamel carbonate $\delta^{18}O$ values in VPDB (Vienna PeeDee Belemnite) scale were converted to VSMOW (Vienna Standard Mean Ocean Water) using the equation $\delta^{18}O_{VSMOW} = 1.030911 \times \delta^{18}O_{VPDB} + 30.91$. Estimated equivalent enamel phosphate $\delta^{18}O$ values in teeth were estimated by subtracting 8 ‰ from each carbonate measurement.

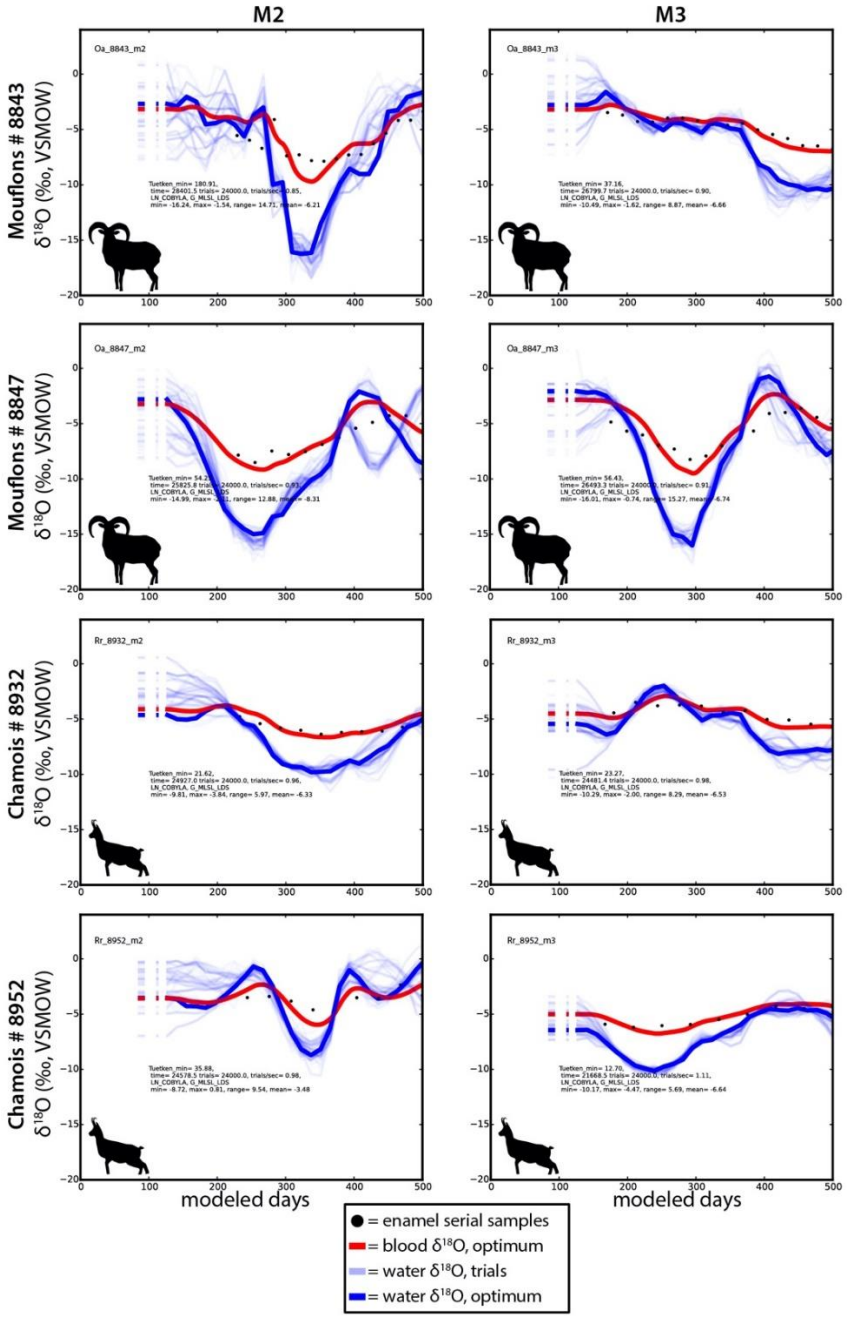

341

342 **Figure S1**. Inverse oxygen isotope input reconstructions for mouflons and chamois
343 specimens. Measurements of enamel oxygen isotope compositions ($\delta^{18}O$ ‰, here shown as
344 phosphate $\delta^{18}O$-equivalent on the VSMOW scale, with an estimated PO_4-water offset of 19.1
345 ‰ subtracted from each measurement) are made serially down the tooth crown (black
346 circles). These measurements are combined with a model of tooth formation to infer likely
347 (light blue) and best guess (dark blue) histories of ingested seasonal $\delta^{18}O$ compositions in
348 environmental and plant water. The $\delta^{18}O$ of blood water over time (red) is also estimated.
349 Periods of uncertainty resulting from significant tooth wear or limitations in the synchrotron-
350 based model of enamel formation are affect the earliest and latest days of reconstruction.
351 Uncertainty also increases towards the end of the tooth, when enamel growth slows and
352 incorporates ever greater periods of time into smaller spatial increments. Details of inverse
353 model outcomes including minimum, maximum, and mean oxygen isotope compositions are
354 listed as text on each reconstruction plot.

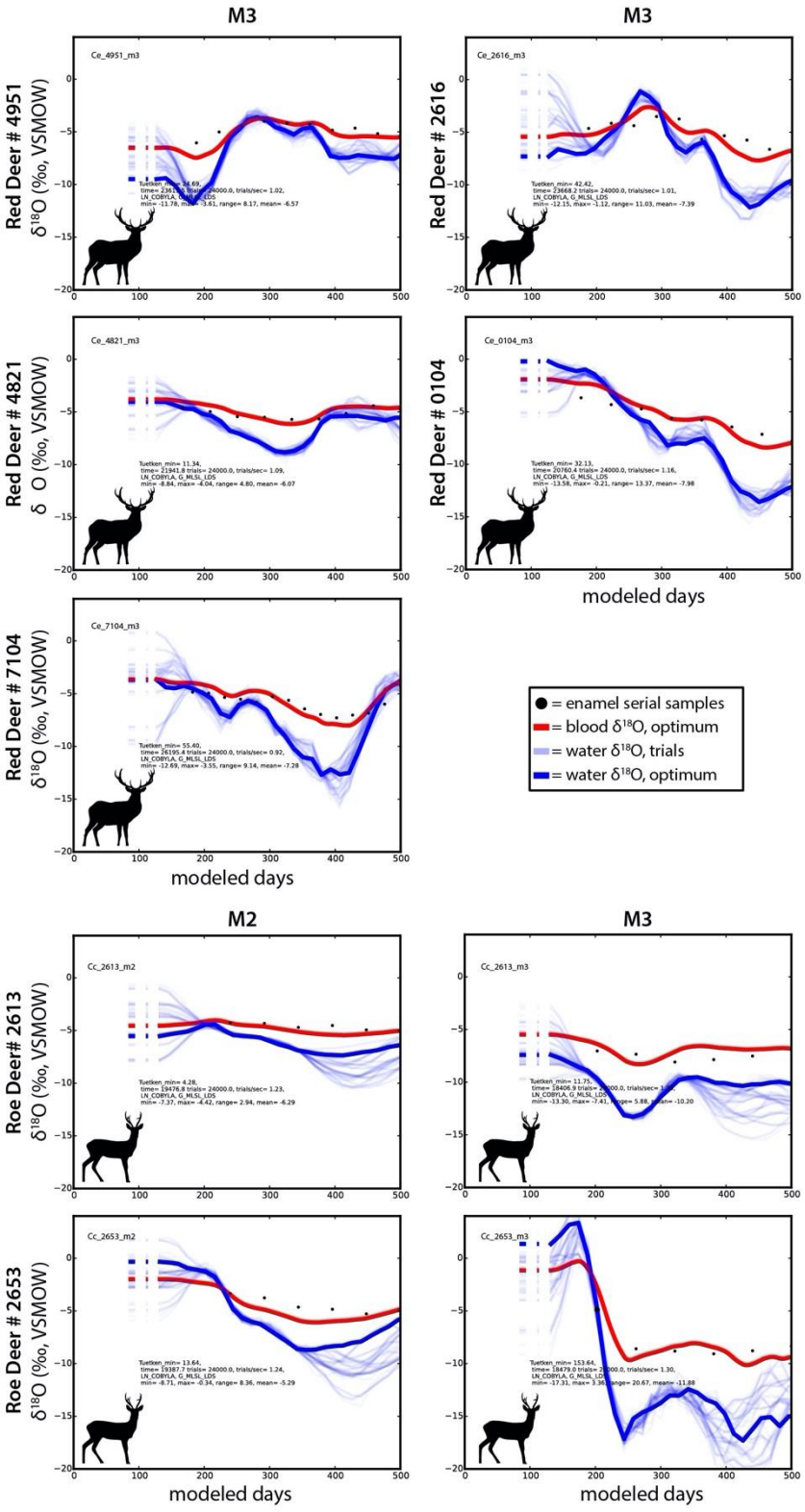

Figure S2. Inverse oxygen isotope input reconstructions for red deer and roe deer specimens. Further details are as described above for Figure S1.

2. 4. Dental microwear texture analysis

The analysis was performed on second lower molars of adult specimens with erupted and worn last third molar and thus the second molar being fully operational. This strict selection of specimens allows us to target adult individuals. Following standard procedures, replicas of the dental facet (disto-buccal facet of the protoconid) were produced with a silicone (medium consistency) polyvinylsiloxane (Coltène Whaledent, President Regular Body, ISO 4823). Scans (320×280 μm) were produced on replicas using the surface profilometer confocal DCM8 Leica Microsystems "TRIDENT" with a 100× lens (Leica Microsystems; Numerical Aperture=0.90; working distance=0.9 mm) at the Palevoprim lab, CNRS and University of Poitiers, France (see details in Merceron et al., 2016). Lateral resolution is 0.129 μm and vertical spacing is 0.002 μm. A 200×200 μm was cropped from the original scans and saved as .Plμ files (Appendix 3 provides photosimulations and false color altitudinal maps for every scan analyzed in the present study).

After treating surfaces (see supplementary information in Merceron et al., 2016), the Dental Microwear Texture Analysis (DMTA) was performed using the Scale-Sensitive Fractal Analysis using Toothfrax and Sfrax software (Surfract, http://www.surfract. com) following Scott et al. (2006). Four variables were extracted from the surface: complexity (Asfc), anisotropy (epLsar), heterogeneity of complexity (HAsfc calculated with a 9-cell mesh) and Textural fill volume (Tfv; Table 3; Appendix 2). Complexity (Asfc or Area-scale fractal complexity) is a measure of the roughness at a given scale. Anisotropy (epLsar or exact proportion of length-scale anisotropy of relief) measures the orientation concentration of surface roughness. Heterogeneity of complexity (HAsfc or heterogeneity of area-scale fractal complexity), quantifies the variation of complexity of the scanned surface area. These textural parameters are dimensionless. Textural fill volume (Tfv) measures the volume of surface roughness and is expressed in μm^3. Dispersion of the values are calculated following Plavcan and Cope (2001) Levene equations as follows:

$$\text{Disp-X} = \sum(\left| \ln(Xi) - (\text{Med}_{1 \to n} (\ln(Xi)) \right|)$$

where X*i* is the value *i* of the variable X; Med is the median.

Table S3. Analyses of variances on the box-cox transformed variables and pairwise differences for microwear texture parameters (disp-Asfc, epLsar and $HAsfc_{9\text{-cells}}$) between species of ruminants from the Bauges NRP.

Asfc	dof	SS	MS	F	p
Intercept	1	34.19026	34.19026	1648.236	0.000000
Taxa	3	0.11929	0.03976	1.917	0.133718
Residuals	78	1.61800	0.02074		
Total	81	1.73728			
epLsar		SS	MS	F	p
Intercept	1	49715.15	49715.15	527.8888	0.000000
Taxa	3	1420.54	473.51	5.0279	***0.003079***
Residuals	78	7345.83	94.18		
Total	81	8766.37			
$HAsfc_{9\text{-cells}}$		SS	MS	F	p
Intercept	1	3.348500	3.348500	1590.020	0.000000
Taxa	3	0.018368	0.006123	2.907	***0.039842***
Residuals	78	0.164264	0.002106		
Total	81	0.182632			
Tfv		SS	MS	F	p
Intercept	1	3.888671E+11	3.888671E+11	472.1923	0.000000
Taxa	3	3.281385E+08	1.093795E+08	0.1328	0.940249
Residuals	78	6.423576E+10	8.235354E+08		
Total	81	6.456390E+10			
disp-Asfc		SS	MS	F	p
Intercept	1	1.944057	1.944057	247.0138	0.000000
Taxa	3	0.065820	0.021940	2.7877	***0.046121***
Residuals	78	0.613878	0.007870		
Total	81	0.679698			
disp epLsar		SS	MS	F	p
Intercept	1	3.407464	3.407464	156.4401	0.000000
Taxa	3	0.051163	0.017054	0.7830	0.506987
Residuals	78	1.698939	0.021781		
Total	81	1.750102			
$disp\text{-}HAsfc_{9\text{-cells}}$		SS	MS	F	p
Intercept	1	0.286799	0.286799	158.8392	0.000000
Taxa	3	0.003448	0.001149	0.6366	0.593660
Residuals	78	0.140836	0.001806		
Total	81	0.144285			
disp Tfv		SS	MS	F	p
Intercept	1	1.823465	1.823465	163.1278	0.000000
Taxa	3	0.027674	0.009225	0.8252	0.483894
Residuals	78	0.871894	0.011178		
Total	81	0.899568			

dof: degree of freedom. SS: sum of squares. MS: mean of squares; F: statistic F; p: probability p.

	C. capreolus	*C. elaphus*	*O. gmelini*	*R. rupicapra*
C. capreolus		disp-Asfc (+)	epLsar(+)	
C. elaphus	HAsfc (+), disp-Asfc (-)		epLsar (+), HAsfc (+)	
O. gmelini	epLsar (-)	epLsar (-), HAsfc (-)		
R. rupicapra	epLsar (-), disp-Asfc (-)	epLsar (-), HAsfc (-)		

Significance at $p<.05$ is indicated below the diagonal for Fisher's LSD tests and above the diagonal for both Tukey's HSD and Fisher's LSD tests (+ and – indicate how is the value found for the species in row compared to the one in column)

After box-cox transformations, one-way analyses of variance (ANOVAs) were performed for each texture parameter (Table S3). For each significant parameter, pairwise comparisons were performed using the combination of Tukey's HSD (Honest Significant Difference) and the less conservative Fisher's LSD test (Least Significant Difference; Figure 6; Table S3). Furthermore, seasonal variations in DMTA are explored on the mouflons as 10 of them were sampled in late summer/early fall 2015 and 12 others during winter 2009. Seasonal variations cannot be assessed for the other species as they were not seasonally-balanced sampled. Values were also box-cox transformed before applying a t-test of Student (Table S4).

Table S4. T test on the box-cox transformed variables from the Dental Microwear Textural Analysis on the mouflon samples from the Bauges NRP comparing the samples with specimens sampled at different seasons.

	Group #1: late summer/early fall 2015 Group #2: early winter 2009 & late fall 2009										
Variable	Mean (# 1)	Mean (# 2)	*t*	dof	p	n (# 1)	n (# 2)	sd (# 1)	sd (# 2)	F-ratio Variances	p Variances
Asfc	1.20	1.22	-0.13	20	0.896	10	12	0.45	0.32	2.04	0.26
epLsar	4.76	4.41	0.69	20	0.494	10	12	1.28	1.09	1.38	0.60
HAsfc	0.27	0.31	-1.16	20	0.258	10	12	0.08	0.08	1.09	0.90
Tfv	87236.3	53578.7	2.97	20	0.007	10	12	21811.7	29626.5	1.84	0.36

dof: degree of freedom, t: Statistic t, sd: standard deviation, n: number of individuals, F: Statistic F, p: probability p, n: sample size.

References

Azorit, C., Tellado, S., Oya, A., Moro, J., 2012. Seasonal and specific diet variations in sympatric red and fallow deer of southern Spain: a preliminary approach to feeding behaviour. Anim. Prod. Sci. 52, 720–727.

Bonafini, M., Pellegrini, M., Ditchfield, P., Pollard, A.M., 2013. Investigation of the 'canopy effect'in the isotope ecology of temperate woodlands. J. Archaeol. Sci. 40, 3926–3935.

Bowen, G.J., 2010. Isoscapes: spatial pattern in isotopic biogeochemistry. Annu. Rev. Earth Planet. Sci. 38, 161–187.

Breitenbach, S.F.M., Bernasconi, S.M., 2011. Carbon and oxygen isotope analysis of small carbonate samples (20 to 100 µg) with a GasBench II preparation device. Rapid Commun. Mass Spectrom. 25, 1910–1914. https://doi.org/10.1002/rcm.5052

Bugalho, M.N., Milne, J.A., 2003. The composition of the diet of red deer (*Cervus elaphus*) in a Mediterranean environment: a case of summer nutritional constraint? For. Ecol. Manag. 181, 23–29.

Cerling, T.E., Ayliffe, L.K., Dearing, M.D., Ehleringer, J.R., Passey, B.H., Podlesak, D.W., Torregrossa, A.-M., West, A.G., 2007. Determining biological tissue turnover using stable isotopes: the reaction progress variable. Oecologia 151, 175–189.

Cibien, C., 1984. Variations saisonnières de l'utilisation de l'espace en fonction des disponibilités alimentaires chez le chevreuil (*Capreolus capreolus* L.). Université François Rabelais, Académie de Tours-Orléans, Tours.

Cornelis, J., Casaer, J., Hermy, M., 1999. Impact of season, habitat and research techniques on diet composition of roe deer (*Capreolus capreolus*): a review. J. Zool. 248, 195–207.

Cransac, N., Cibien, C., Angibault, J.-M., Morrelet, N., Vincent, J.-P., Hewison, A.J.M., 2001. Variations saisonnières du régime alimentaire du chevreuil (*Capreolus capreolus*) selon le sexe en milieu forestier à forte densité (forêt domaniale de Dourdan). Mammalia 65, 1–12.

Dansgaard, W., 1964. Stable isotopes in precipitation. Tellus 16, 436–468.

Dantas, M.A.T., Cherkinsky, A., Bocherens, H., Drefahl, M., Bernardes, C., França, L. de M., 2017. Isotopic paleoecology of the Pleistocene megamammals from the Brazilian Intertropical Region: Feeding ecology ($\delta^{13}C$), niche breadth and overlap. Quat. Sci. Rev. 170, 152–163. https://doi.org/10.1016/j.quascirev.2017.06.030

Darmon, G., Bourgoin, G., Marchand, P., Garel, M., Dubray, D., Jullien, J.-M., Loison, A. 2014. Do ecologically close species shift their daily activities when in sympatry? A test on chamois in the presence of mouflon. Biol. J. Linnean Soc. 111, 621–626

Demény, A., Gugora, A.D., Kesjár, D., Lécuyer, C., Fourel, F., 2019. Stable isotope analyses of the carbonate component of bones and teeth: The need for method standardization. J. Archaeol. Sci. 109, 104979.

Drucker, D.G., Bocherens, H., 2009. Carbon stable isotopes of mammal bones as tracers of canopy development and habitat use in temperate and boreal contexts. For. Canopies For. Prod. Ecosyst. Health Clim. Cond. U. S. Am. Nova Sci. Publ. Inc 2–8.

Espunyes, J., Bartolomé, J., Garel, M., Gálvez-Cerón, A., Aguilar, X.F., Colom-Cadena, A., Calleja, J.A., Gassó, D., Jarque, L., Lavín, S., 2019. Seasonal diet composition of Pyrenean chamois is mainly shaped by primary production waves. PloS One 14, e0210819.

Farquhar, G.D., Gan, K.S., 2003. On the progressive enrichment of the oxygen isotopic composition of water along a leaf. Plant Cell Environ. 26, 1579–1597.

Farquhar, G.D., Lloyd, J., 1993. Carbon and oxygen isotope effects in the exchange of carbon dioxide between terrestrial plants and the atmosphere, in: Stable Isotopes and Plant Carbon-Water Relations. Elsevier, pp. 47–70.
Fiebig, J., Schöne, B.R., Oschmann, W., 2005. High-precision oxygen and carbon isotope analysis of very small (10–30 μg) amounts of carbonates using continuous flow isotope ratio mass spectrometry. Rapid Commun. Mass Spectrom. Int. J. Devoted Rapid Dissem. ---Minute Res. Mass Spectrom. 19, 2355–2358.
Gat, J.R., 1996. Oxygen and hydrogen isotopes in the hydrologic cycle. Annu. Rev. Earth Planet. Sci. 24, 225–262.
Gebert, C., Verheyden-Tixier, H., 2001. Variations of diet composition of red deer (*Cervus elaphus* L.) in Europe. Mammal Rev. 31, 189–201.
Green, D.R., Green, G.M., Colman, A.S., Bidlack, F.B., Tafforeau, P., Smith, T.M., 2017. Synchrotron imaging and Markov chain Monte Carlo reveal tooth mineralization patterns. PloS One 12.
Green, D.R., Olack, G., Colman, A.S., 2018a. Determinants of blood water δ18O variation in a population of experimental sheep: Implications for paleoclimate reconstruction. Chem. Geol. 485, 32–43.
Green, D.R., Smith, T.M., Green, G.M., Bidlack, F.B., Tafforeau, P., Colman, A.S., 2018b. Quantitative reconstruction of seasonality from stable isotopes in teeth. Geochim. Cosmochim. Acta 235, 483–504.
Gretebeck, R.J., Schoeller, D.A., Socki, R.A., Davis-Street, J., Gibson, E.K., Schulz, L.O., Lane, H.W., 1997. Adaptation of the doubly labeled water method for subjects consuming isotopically enriched water. J. Appl. Physiol. 82, 563–570.
Iacumin, P., Bocherens, H., Mariotti, A., Longinelli, A., 1996. Oxygen isotope analyses of co-existing carbonate and phosphate in biogenic apatite: a way to monitor diagenetic alteration of bone phosphate? Earth Planet. Sci. Lett. 142, 1–6.
Kierdorf, H., Witzel, C., Upex, B., Dobney, K., Kierdorf, U., 2012. Enamel hypoplasia in molars of sheep and goats, and its relationship to the pattern of tooth crown growth. J. Anat. 220, 484–495.
Kierdorf, U., Kierdorf, H., 2000. Comparative analysis of dental fluorosis in roe deer (Capreolus capreolus) and red deer (*Cervus elaphus*): interdental variation and species differences. J. Zool. 250, 87–93.
Kohn, M.J., Schoeninger, M.J., Valley, J.W., 1996. Herbivore tooth oxygen isotope compositions: Effects of diet and physiology. Geochim. Cosmochim. Acta 60, 3889–3896.
Kucherenko, S., Sytsko, Y., 2005. Application of deterministic low-discrepancy sequences in global optimization. Comput. Optim. Appl. 30, 297–318.
Levins, R., 1968. Evolution in changing environments: some theoretical explorations. Princeton University Press.
Macfarlane, W.V., Howard, B., Haines, H., Kennedy, P.J., Sharpe, C.M., 1971. Hierarchy of water and energy turnover of desert mammals. Nature 234, 483–484.
Marchand, P., Redjadj, C., Garel, M., Cugnasse, J.-M., Maillard, D., Loison, A., 2013. Are mouflon *Ovis gmelini musimon* really grazers? A review of variation in diet composition. Mammal Rev. 43, 275–291.
Merceron, G., Ramdarshan, A., Blondel, C., Boisserie, J.-R., Brunetiere, N., Francisco, A., Gautier, D., Milhet, X., Novello, A., Pret, D., 2016. Untangling the environmental from the dietary: dust does not matter. Proceeding R. Soc. Lond. B 283, 20161032.
Milhaud, G., Nezit, J., 1991. Développement des molaires chez le mouton. Etude morphologique, radiographique et microdurométrique. Recl. Médecine Vét. 167, 121–127.

Osmond, C.B., Ziegler, H., Stichler, W., Trimborn, P., 1975. Carbon isotope discrimination in alpine succulent plants supposed to be capable of crassulacean acid metabolism (CAM). Oecologia 18, 209–217.

Passey, B.H., Cerling, T.E., 2002. Tooth enamel mineralization in ungulates: Implications for recovering a primary isotopic time-series. Geochim. Cosmochim. Acta 81, 3225–3234.

Passey, B.H., Robinson, T.F., Ayliffe, L.K., Cerling, T.E., Sponheimer, M., Dearing, M.D., Roeder, B.L., Ehleringer, J.R., 2005. Carbon isotope fractionation between diet, breath CO_2, and bioapatite in different mammals. J. Archaeol. Sci. 32, 1459–1470.

Pérez-Barberia, F.J., Olivan, M., Osoro, K., Nores, C., 1997. Sex, seasonal and spatial differences in the diet of Cantabrian chamois *Rupicapra pyrenaica parva*. Acta Theriol. (Warsz.) 42, 37–46.

Pianka, E.R., 1973. The structure of lizard communities. Annu. Rev. Ecol. Syst. 4, 53–74.

Plavcan, J.M., Cope, D.A., 2001. Metric variation and species recognition in the fossil record. Evol. Anthropol. Issues News Rev. Issues News Rev. 10, 204–222.

Podlesak, D.W., Torregrossa, A.-M., Ehleringer, J.R., Dearing, M.D., Passey, B.H., Cerling, T.E., 2008. Turnover of oxygen and hydrogen isotopes in the body water, CO_2, hair, and enamel of a small mammal. Geochim. Cosmochim. Acta 72, 19–35.

Powell, M.J., 1998. Direct search algorithms for optimization calculations. Acta Numer. 7, 287–336.

Pucéat, E., Joachimski, M.M., Bouilloux, A., Monna, F., Bonin, A., Motreuil, S., Morinière, P., Hénard, S., Mourin, J., Dera, G., Quesne, D., 2010. Revised phosphate–water fractionation equation reassessing paleotemperatures derived from biogenic apatite. Earth Planet. Sci. Lett. 298, 135–142. https://doi.org/10.1016/j.epsl.2010.07.034

Pyankov, V.I., Ziegler, H., Akhani, H., Deigele, C., Lüttge, U., 2010. European plants with C4 photosynthesis: geographical and taxonomic distribution and relations to climate parameters: European Plants with C_4 Photosynthesis. Bot. J. Linn. Soc. 163, 283–304. https://doi.org/10.1111/j.1095-8339.2010.01062.x

Redjadj, C., Darmon, G., Maillard, D., Chevrier, T., Bastianelli, D., Verheyden, H., Loison, A., Saïd, S., 2014. Intra- and interspecific differences in diet quality and composition in a large herbivore community. PLoS ONE 9, e84756. https://doi.org/10.1371/journal.pone.0084756

Rinnooy Kan, A.H., Timmer, G.T., 1987. Stochastic global optimization methods part II: Multi level methods. Math. Program. Ser. B 39, 57–78.

Rozanski, K., Araguás-Araguás, L., Gonfiantini, R., 1993. Isotopic patterns in modern global precipitation. Geophys. Monogr. 78, 1–36.

Scott, R.S., Ungar, P., Bergstrom, T.S., Brown, C.A.; Childs, B.E.; Teaford, M.F., Walker, A. 2006. Dental microwear texture analysis: technical considerations. J. Hum. Evol. 51, 339–49.

Song, X.I.N., Barbour, M.M., Farquhar, G.D., Vann, D.R., Helliker, B.R., 2013. Transpiration rate relates to within-and across-species variations in effective path length in a leaf water model of oxygen isotope enrichment. Plant Cell Environ. 36, 1338–1351.

Spötl, C., Vennemann, T.W., 2003. Continuous-flow isotope ratio mass spectrometric analysis of carbonate minerals: Letter to the Editor. Rapid Commun. Mass Spectrom. 17, 1004–1006. https://doi.org/10.1002/rcm.1010

Storms, D., Aubry, Ph., Hamann, J.-L., Saïd, S., Fritz, H., Saint-Andrieux, Ch., Klein, F., 2008. Seasonal variation in diet composition and similarity of sympatric red deer *Cervus elaphus* and roe deer *Capreolus capreolus*. Wildl. Biol. 14, 237–250.

Suter, W., Suter, U., Kriisi, B., Schütz, M., 2004. Spatial variation of summer diet of red deer *Cervus elaphus* in the eastern Swiss Alps. Wildl. Biol. 10, 43–50. https://doi.org/10.2981/wlb.2004.008

Teaford, M.F., Oyen, O.J., 1989. In vivo and in vitro turnover in dental microwear. Am. J. Phys. Anthropol. 80, 447–460. https://doi.org/10.1002/ajpa.1330800405

Teaford, M.F., ungar, P.S., Taylor, A.B., Ross, C.F., Vinyard, C.J., 2017. In vivo rates of dental microwear formation in laboratory primates fed different food items. Biosurface Biotribology. https://doi.org/10.1016/j.bsbt.2017.11.005

Tejada-Lara, J.V., MacFadden, B.J., Bermudez, L., Rojas, G., Salas-Gismondi, R., Flynn, J.J., 2018. Body mass predicts isotope enrichment in herbivorous mammals. Proc. R. Soc. B Biol. Sci. 285, 20181020.

Thuiller, W., Guéguen, M., Bison, M., Duparc, A., Garel, M., Loison, A., Renaud, J., Poggiato, G., 2018. Combining point-process and landscape vegetation models to predict large herbivore distributions in space and time-A case study of *Rupicapra rupicapra*. Divers. Distrib. 24, 352–362. https://doi.org/10.1111/ddi.12684

Tixier, H., Duncan, P., 1996. Are European roe deer browsers? A review of variations in the composition of their diets. Rev. Ecol. Terre Vie 51, 3–17.

Tixier, H., Duncan, P., Scehovic, J., Yani, A., Gleizes, M., Lila, M., 1997. Food selection by a roe deer (*Capreolus capreolus*): effects of plant chemistry, and consequences for the nutritional value of their diet. J. Zool. 242, 229–245.

Witzel, C., Kierdorf, U., Frölich, K., Kierdorf, H., 2018. The pay-off of hypsodonty-timing and dynamics of crown growth and wear in molars of Soay sheep. BMC Evol. Biol. 18, 207.

Appendix 1. Intra-tooth carbon and oxygen stable isotope compositions of analyzed specimens.

Taxon	specimen	tooth	sample position on tooth	crown height (mm)	distance from apex (mm)	$\delta^{13}C$	$\delta^{18}O$
Cervus elaphus	CEM2616	M3	1	27.4	1.2	-16.33	-7.90
			2		3.5	-15.98	-7.43
			3		5.5	-16.37	-7.66
			4		7.7	-15.78	-6.81
			5		9.7	-15.82	-7.04
			6		12.9	-15.45	-8.91
			7		15.8	-15.98	-8.59
			8		18.8	-16.46	-8.99
			9		21.5	-16.24	-9.84
			10		24.0	-16.67	-10.11
	CE0104	M3	1	24.3	1.0	-16.40	-6.98
			2		2.9	-16.27	-7.61
			3		5.6	-16.22	-8.00
			4		9.3	-15.97	-8.88
			5		11.9	-16.09	-9.03
			6		15.3	-16.58	-9.66
			7		18.7	-16.48	-10.35
			8		21.6	-16.89	-10.95
	CE4951	M3	1	21.4	0.0	-16.20	-9.27
			2		1.8	-15.93	-8.27
			3		3.6	-15.36	-7.74
			4		5.7	-15.62	-7.30
			5		8.0	-15.75	-7.46
			6		10.2	-15.50	-7.57
			7		12.5	-15.47	-8.10
			8		14.8	-15.45	-7.91
			9		17.1	-15.74	-8.42
			10		19.3	-16.00	-8.67
	CEF7104	M3	1	28.0	0.8	-16.22	-8.11
			2		2.7	-16.64	-8.22
			3		4.7	-16.22	-8.60
			4		6.6	-16.18	-8.77
			5		8.8	-16.46	-9.05
			6		10.6	-15.77	-8.54
			7		12.6	-15.60	-8.87
			8		14.5	-15.53	-9.66
			9		16.5	-15.91	-10.17
			10		18.7	-15.68	-10.48
			11		20.6	-15.95	-10.23
			12		22.8	-15.71	-10.05
			13		24.7	-16.03	-9.21
			14		26.7	-15.83	-7.54
	CE4821	M3	1	23.5	0.9	-15.74	-7.87
			2		3.0	-15.98	-8.23
			3		5.3	-16.14	-8.70
			4		7.9	-15.89	-8.75
			5		10.4	-15.75	-8.95
			6		13.0	-16.19	-8.91
			7		15.7	-16.20	-8.40
			8		18.6	-15.71	-7.69
			9		20.5	-15.57	-8.05

Appendix 1. *continued*

Taxon	specimen	tooth	sample position on tooth	crown height (mm)	distance from apex (mm)	$\delta^{13}C$	$\delta^{18}O$
Ovis amon	15MO8847	M3	1	40.3	0.6	-15.38	-8.12
			2		2.8	-15.72	-8.92
			3		4.6	-16.05	-9.26
			4		6.7	-16.69	-10.16
			6		11.5	-16.23	-10.49
			8		15.9	-16.48	-11.40
			9		18.0	-17.13	-11.10
			10		20.5	-16.79	-10.22
			11		23.1	-16.28	-9.69
			12		25.4	-16.07	-8.91
			13		28.0	-15.30	-7.37
			14		30.7	-14.99	-7.29
			15		33.4	-15.30	-6.92
			16		36.2	-15.26	-7.72
			17		38.9	-15.17	-7.91
		M2	1	32.6	1.2	-17.34	-11.02
			2		3.1	-17.53	-11.67
			3		5.4	-17.47	-10.67
			4		8.0	-17.32	-10.97
			5		10.5	-17.14	-10.72
			6		12.7	-16.57	-10.10
			7		15.6	-16.10	-9.48
			8		17.9	-15.28	-8.67
			9		20.7	-15.44	-8.15
			10		22.9	-15.30	-7.56
			11		25.5	-15.21	-7.57
			12		28.2	-15.42	-8.94
	15MO8843	M3	1	36.8	2.5	-14.70	-6.78
			2		4.4	-14.72	-7.00
			3		6.8	-15.08	-7.57
			4		8.8	-14.87	-7.62
			5		10.6	-14.83	-7.27
			6		12.4	-15.06	-7.27
			7		14.4	-15.43	-7.51
			8		16.3	-15.85	-7.83
			9		18.6	-16.06	-7.90
			10		20.4	-16.44	-7.72
			11		22.6	-16.49	-8.30
			12		24.9	-16.53	-8.71
			13		27.3	-16.59	-9.06
			14		29.4	-16.59	-9.68
			15		31.8	-16.35	-9.71
			16		34.1	-15.25	-9.96
		M2	1	36.8	0.4	-16.54	-8.80
			2		2.1	-16.63	-9.21
			3		4.3	-16.59	-9.92
			4		6.8	-6.85	-7.39
			5		9.3	-16.96	-10.58
			6		11.9	-16.43	-10.49
			7		14.2	-17.09	-10.99
			8		16.4	-17.16	-11.05
			9		18.9	-16.64	-10.82
			10		20.8	-16.45	-10.50
			11		23.3	-16.70	-10.46
			12		25.3	-16.54	-9.51
			13		27.5	-16.15	-8.59
			14		29.9	-15.90	-7.47
			15		32.2	-15.14	-7.45
			16		34.7	-14.54	-6.68

Appendix 1. *continued*

Taxon	specimen	tooth	sample position on tooth	crown height (mm)	distance from apex (mm)	$\delta^{13}C$	$\delta^{18}O$
Rupicapra rupicapra	15IS8952	M3	1	22.8	1.2	-13.91	-9.15
			2		4.3	-14.54	-9.42
			3		6.6	-14.63	-9.27
			4		8.7	-14.73	-9.17
			5		10.9	-14.63	-8.74
			6		12.9	-14.57	-8.28
			7		15.2	-14.31	-7.58
			8		17.9	-13.84	-7.76
			9		20.4	-14.02	-7.50
		M2	1	20.3	1.0	-14.38	-6.81
			2		3.3	-14.47	-6.72
			3		5.2	-13.95	-7.12
			4		7.5	-14.42	-7.88
			5		9.9	-14.76	-7.92
			6		12.2	-14.42	-6.82
			7		14.3	-14.39	-6.86
			8		16.3	-14.21	-5.71
			9		18.7	-14.62	-6.62
	15IS8932	M3	1	26.6	0.5	-13.68	-7.72
			2		2.5	-13.79	-6.81
			3		4.9	-14.00	-7.10
			4		7.2	-14.00	-7.03
			5		9.7	-14.25	-7.12
			6		12.0	-14.46	-7.66
			7		14.5	-14.39	-7.51
			8		16.7	-14.69	-8.29
			9		19.2	-14.60	-8.35
			10		21.3	-14.70	-8.72
			11		23.6	-14.40	-8.91
		M2	1	26.0	1.5	-14.13	-8.05
			2		3.7	-14.77	-8.65
			3		6.2	-14.72	-9.03
			4		8.7	-14.97	-9.24
			5		10.9	-15.17	-9.59
			6		13.3	-14.90	-9.42
			7		15.3	-15.24	-9.36
			8		17.8	-15.23	-9.30
			9		19.7	-14.96	-8.96
			10		22.2	-14.44	-7.98

Appendix 1. *continued*

Taxon	specimen	tooth	sample position on tooth	crown height (mm)	distance from apex (mm)	$\delta^{13}C$	$\delta^{18}O$
Capreolus capreolus	CC2653	M3	1	12.0	0.8	-14.69	-8.17
			2		2.2	-18.69	-11.74
			3		3.8	-18.69	-11.96
			4		5.2	-18.71	-12.21
			5		6.9	-18.63	-11.92
			6		8.7	-18.77	-11.49
		M2	1	11.3	1.1	-18.49	-6.66
			2		2.9	-18.27	-7.06
			3		4.7	-18.10	-7.91
			4		6.5	-18.25	-8.10
			5		8.2	-18.37	-8.53
			6		9.8	-18.70	-9.00
	CC2613	M3	1	10.4	0.7	-17.63	-10.24
			2		2.0	-18.12	-10.54
			3		3.7	-18.65	-11.26
			4		5.3	-18.22	-11.03
			5		6.8	-18.91	-10.70
			6		8.7	-18.70	-10.15
		M2	1	10.4	0.5	-17.04	-7.56
			2		1.7	-16.95	-7.61
			3		3.2	-16.57	-7.98
			4		5.4	-16.31	-7.80
			5		7.3	-16.18	-8.21
			6		9.0	-16.31	-8.31

Appendix 2. List of 82 specimens with individuals values of the dental microwear texture parameters. All analyses were associated with $r^2 > 0.97$, which guarantees the robustness of the complexity calculation. M: male; F: female. DMTA was done on disto-buccal enamel facet of protoconid or hypoconid if the former facet was damaged.

Taxa	Specimen	Sex	Date (d/m/y)	Asfc	epLsar	HAsfc	Tfv	disp Asfc	disp epLsar	disp HAsfc	disp-Tfv2
C. capreolus	CC2611	F	19/9/15	7.58	0.00053	0.41	65541.5	1.15	2.48	0.02	0.56
	CC2183	F	23/9/15	1.74	0.00459	0.57	44994.0	0.01	0.32	0.12	0.18
	CC2637	M	27/9/15	0.90	0.00738	0.53	45588.3	0.35	0.15	0.10	0.19
	CC8624	F	27/9/15	1.67	0.00735	0.50	64059.5	0.01	0.15	0.08	0.53
	CC8640	M	27/9/15	3.49	0.00346	0.44	33042.4	0.51	0.60	0.04	0.13
	CC2184	F	30/9/15	2.23	0.00619	0.30	3624.0	0.17	0.02	0.06	2.34
	CC7122	M	3/10/15	0.41	0.00540	0.32	0.0	0.65	0.16	0.05	10.53
	CC2613	M	4/10/15	2.75	0.00519	0.54	37524.2	0.33	0.20	0.11	0.00
	CC0741	M	11/10/15	9.47	0.00282	0.17	52070.3	1.35	0.81	0.16	0.33
	CC2538	M	18/10/14	1.97	0.00648	0.07	26758.6	0.09	0.02	0.25	0.34
	CC0642	M	20/10/15	1.27	0.00723	0.42	46146.8	0.18	0.13	0.02	0.21
	CC0742	M	24/10/15	1.06	0.00897	0.36	33255.6	0.27	0.35	0.02	0.12
	CC7124	F	31/10/15	1.45	0.00511	0.43	43440.8	0.10	0.21	0.03	0.15
	CC0259	F	22/11/15	1.09	0.00738	0.41	1598.8	0.26	0.15	0.02	3.16
	CC0017	M	29/11/15	5.32	0.00776	0.24	40779.0	0.85	0.20	0.11	0.08
	CC0258	F	16/1/16	0.45	0.00750	0.19	37402.9	0.63	0.17	0.15	0.00
	CC0262	M	17/1/16	0.95	0.01055	0.36	26035.5	0.33	0.51	0.02	0.37
	CC0001	M	16/2/16	3.25	0.00508	0.17	48888.4	0.45	0.22	0.17	0.26
C. elaphus	CE4525	F	4/10/15	1.21	0.00574	0.39	28787.4	0.00	0.01	0.00	0.32
	CE4687	F	11/10/15	1.69	0.00834	0.38	42898.9	0.19	0.37	0.01	0.08
	CE3732	F	17/10/15	1.55	0.00708	0.86	47363.7	0.14	0.20	0.29	0.18
	CE0106	M	18/10/15	0.49	0.00195	0.55	27926.2	0.39	1.09	0.11	0.35
	CE4691	F	22/10/15	1.54	0.00989	0.65	42382.8	0.14	0.54	0.17	0.07
	CE4820	F	22/10/15	1.24	0.00782	0.52	53617.2	0.01	0.30	0.08	0.30
	CE4821	F	22/10/15	1.21	0.00465	0.62	39634.9	0.00	0.22	0.15	0.00
	CE4825	F	22/10/15	0.90	0.00586	0.68	34551.1	0.15	0.01	0.19	0.14
	CE4929	F	22/10/15	1.02	0.00573	0.37	52437.9	0.09	0.01	0.02	0.28
	CE2655	M	24/10/15	0.94	0.00806	0.28	24835.1	0.13	0.33	0.09	0.47
	CE2616	M	26/10/15	2.04	0.00292	0.23	38476.6	0.32	0.68	0.13	0.03
	CE0104	F	31/10/15	0.89	0.00537	0.40	30946.8	0.16	0.07	0.00	0.25
	CE7104	F	31/10/15	1.62	0.00238	2.54	30463.3	0.17	0.89	0.93	0.26
	CE5002	F	5/11/15	2.71	0.00848	0.42	45048.0	0.52	0.38	0.02	0.13
	CE4526	F	8/11/15	1.03	0.00257	0.39	26323.7	0.09	0.81	0.00	0.41
	CE5616	M	12/11/15	1.96	0.00554	0.33	42387.0	0.29	0.04	0.05	0.07
	CE5837	M	15/11/15	0.87	0.00915	0.36	42479.9	0.17	0.46	0.02	0.07
	CE2620	M	22/11/15	1.35	0.00826	0.22	41100.1	0.06	0.36	0.13	0.04
	CE4951	F	22/11/15	2.56	0.00110	0.56	42542.5	0.48	1.66	0.11	0.07
	CE0141	F	5/12/15	0.85	0.00578	0.54	13323.6	0.18	0.00	0.10	1.09
	CE4819	F	1/10/15	0.99	0.00920	0.28	27184.6	0.10	0.47	0.09	0.38
O. gmelini	MO8837	M	11/9/15	2.82	0.00280	0.35	31520.0	0.28	0.02	0.01	0.09
	MO8832	M	21/9/15	2.50	0.00223	0.26	52733.6	0.19	0.25	0.05	0.43
	MO8841	M	21/9/15	1.75	0.00549	0.50	43273.9	0.05	0.65	0.12	0.23
	MO8847	M	22/9/15	3.20	0.00286	0.38	49720.7	0.37	0.00	0.04	0.37
	MO8857	F	25/9/15	1.13	0.00505	0.33	34747.8	0.31	0.57	0.00	0.01
	MO8845	F	9/10/15	1.02	0.00878	0.18	41925.9	0.36	1.12	0.12	0.20
	MO8851	F	9/10/15	0.72	0.00279	0.27	33061.6	0.52	0.02	0.05	0.04
	MO8849	F	28/10/15	1.01	0.00994	0.15	62871.9	0.37	1.25	0.14	0.60
	MO8833	M	30/10/15	3.77	0.00218	0.30	45893.7	0.50	0.27	0.03	0.29
	MO8843	M	30/10/15	2.36	0.00065	0.30	35142.6	0.15	1.48	0.03	0.02

Taxa	Specimen	Sex	Date (d/m/y)	Asfc	epLsar	HAsfc	Tfv	disp Asfc	disp epLsar	disp HAsfc	disp-Tfv2
O. gmelini	MO0007	M	8/1/09	2.01	0.00117	0.50	34291.8	0.04	0.89	0.12	0.00
	MO0013	F	9/2/09	1.50	0.00736	0.19	15881.7	0.14	0.95	0.12	0.77
	MO0008	F	15/1/09	3.35	0.00314	0.34	25049.6	0.41	0.10	0.00	0.32
	MO0015	M	14/2/09	2.83	0.00520	0.50	27146.2	0.28	0.60	0.12	0.24
	MO0017	F	16/2/09	2.62	0.00096	0.40	55256.3	0.22	1.09	0.05	0.47
	MO0018	M	19/2/09	2.77	0.00275	0.27	36637.5	0.26	0.04	0.05	0.06
	MO0010	M	24/1/09	1.78	0.00284	0.21	1065.9	0.04	0.01	0.10	3.47
	MO0020	F	11/3/09	1.57	0.00285	0.38	31646.3	0.12	0.00	0.04	0.08
	MO0021	F	11/3/09	2.03	0.00118	0.36	31841.6	0.05	0.88	0.02	0.08
	MO0022	F	12/3/09	1.53	0.00419	0.39	6715.1	0.13	0.38	0.05	1.63
	MO0024	F	16/3/09	1.32	0.00169	0.43	34534.7	0.22	0.52	0.07	0.00
	MO0025	F	27/3/09	0.81	0.00664	0.26	25048.3	0.47	0.84	0.05	0.32
R. rupicapra	IS8911	M	3/9/15	0.79	0.00518	0.39	38168.2	0.37	0.19	0.06	0.02
	IS8915	M	10/9/15	1.59	0.00381	0.30	33961.0	0.00	0.11	0.01	0.13
	IS8934	M	11/9/15	1.29	0.00264	0.19	41859.5	0.12	0.48	0.09	0.08
	IS8621	M	16/9/15	1.70	0.00671	0.15	38371.4	0.04	0.45	0.13	0.01
	IS8944	M	21/9/15	1.82	0.00444	0.21	10125.9	0.08	0.04	0.08	1.34
	IS8929	F	21/9/15	1.33	0.00175	0.31	38788.5	0.11	0.89	0.00	0.00
	IS8932	M	21/9/15	2.32	0.00079	0.26	38832.5	0.25	1.68	0.04	0.00
	IS8943	M	21/9/15	3.43	0.00412	0.61	43862.2	0.54	0.03	0.21	0.12
	IS8884	F	25/9/15	1.01	0.00683	0.33	47498.2	0.25	0.47	0.01	0.20
	IS8891	F	25/9/15	1.67	0.00458	0.21	47669.3	0.03	0.07	0.08	0.21
	IS8892	F	25/9/15	1.12	0.00728	0.23	52005.5	0.20	0.54	0.06	0.29
	IS8940	F	1/10/15	0.65	0.00564	1.04	26647.1	0.45	0.28	0.44	0.38
	IS8878	F	9/10/15	1.53	0.00427	0.27	45365.9	0.02	0.00	0.03	0.16
	IS8939	F	9/10/15	1.85	0.00398	0.33	8846.8	0.10	0.07	0.02	1.48
	IS8638	M	24/10/15	3.38	0.00386	0.41	35336.9	0.53	0.10	0.08	0.09
	IS8913	F	9/11/15	1.62	0.00510	0.50	49291.0	0.01	0.18	0.14	0.24
	IS8885	M	10/11/15	2.49	0.00426	0.27	37838.9	0.30	0.00	0.03	0.02
	IS8960	F	10/11/15	4.55	0.00051	0.88	39707.6	0.76	2.12	0.36	0.02
	IS2643	F	2/12/15	1.38	0.00370	0.55	52855.0	0.08	0.14	0.17	0.31
	IS2647	F	19/12/15	0.85	0.00419	0.40	32509.5	0.34	0.02	0.07	0.18
	IS0001	M	15/3/09	1.27	0.00588	0.31	10019.3	0.13	0.32	0.00	1.35

Appendix 3. Photosimulations and false color elevation map of the dental surfaces scanned on the disto-buccal facets of the protoconid or hypoconid on the second lower molars of roe deer, red deer, chamois and mouflons.

Photosimulations and false color elevation maps of scanned molar facets of the chamois (*Rupicapra rupicapra*) from the Bauges Natural Regional Park, France
scanned at the PALEVOPRIM lab by G. Merceron , CNRS and University of Poitiers, France with "TRIDENT", white light confocal microscope Leica DCM8

ANR-13-JSV7-0008-01, PI: G. Merceron

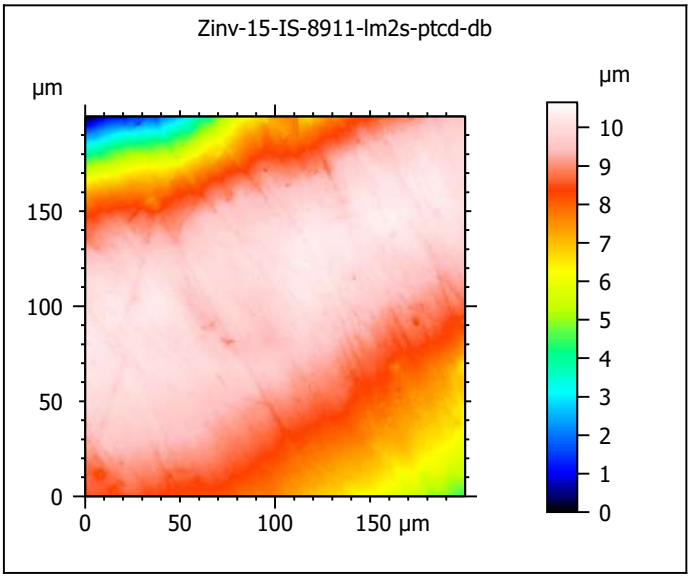

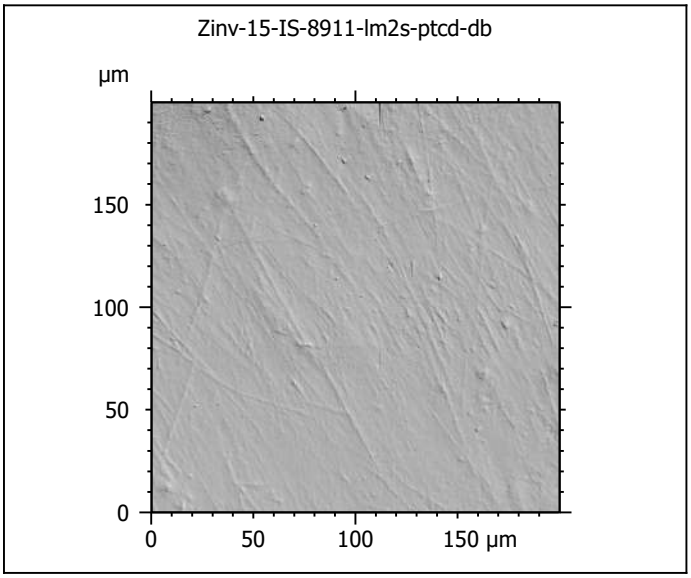

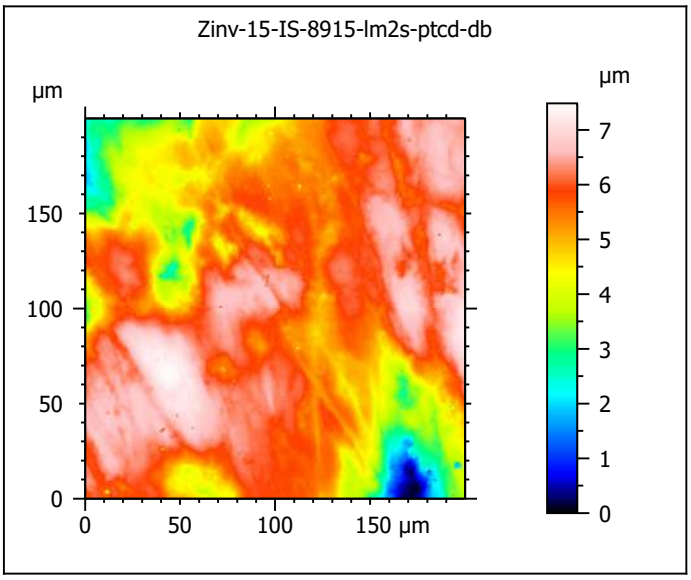

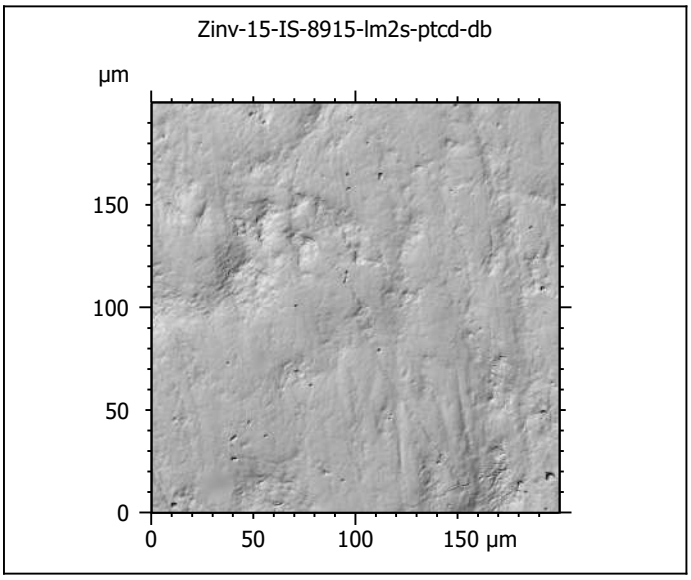

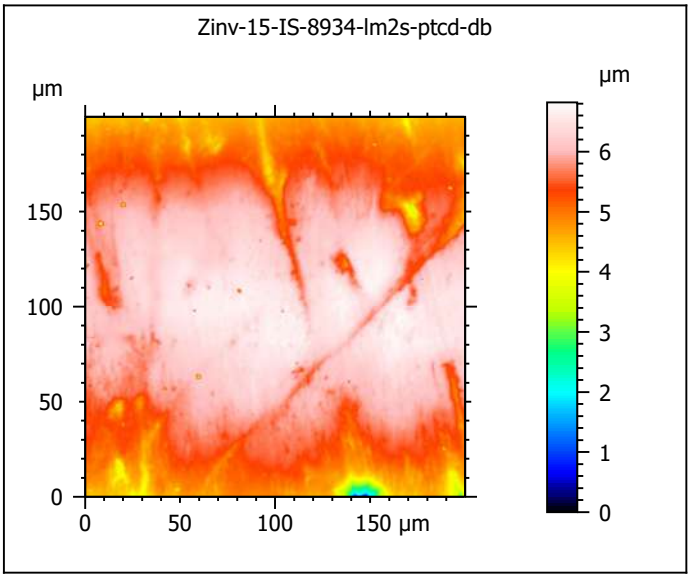

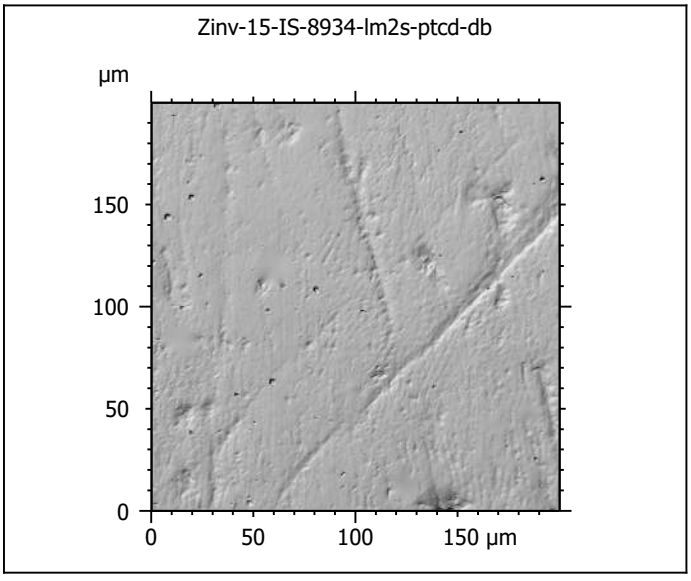

Leica Map Premium 8.0.9151

Photosimulations and false color elevation maps of scanned molar facets of the chamois (*Rupicapra rupicapra*) from the Bauges Natural Regional Park, France
scanned at the PALEVOPRIM lab by G. Merceron , CNRS and University of Poitiers, France with "TRIDENT", white light confocal microscope Leica DCM8

ANR-13-JSV7-0008-01, PI: G. Merceron

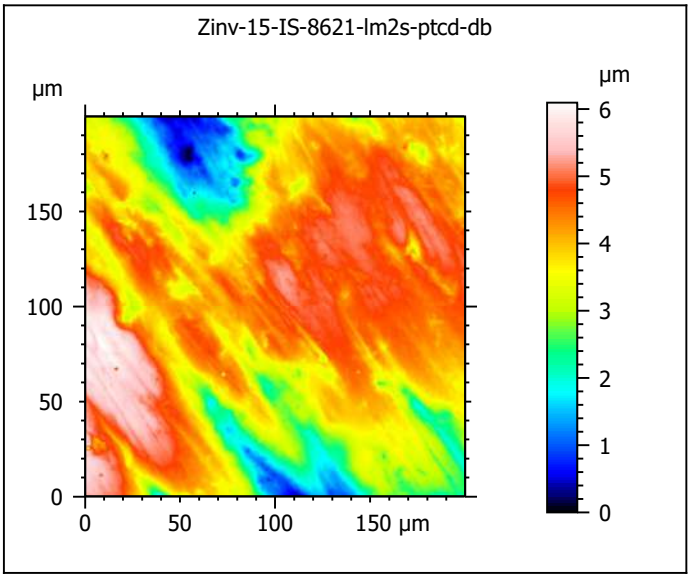

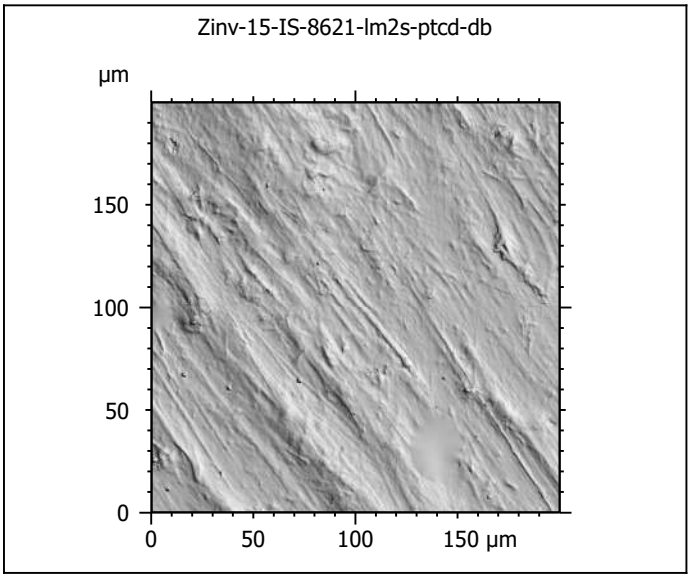

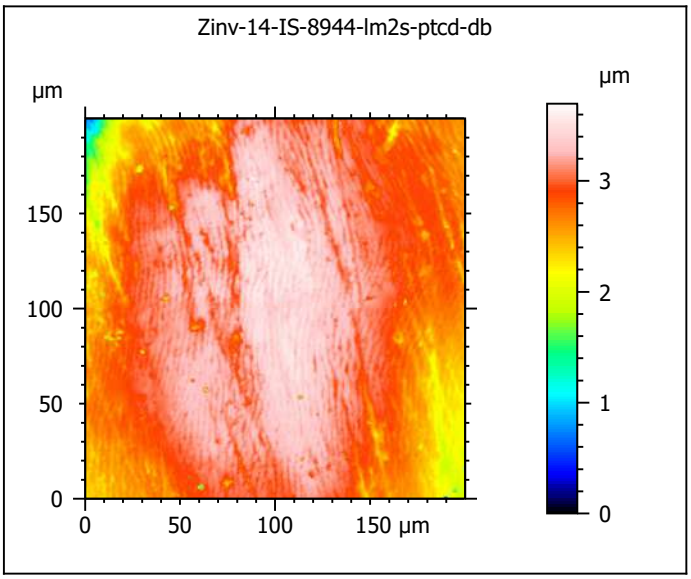

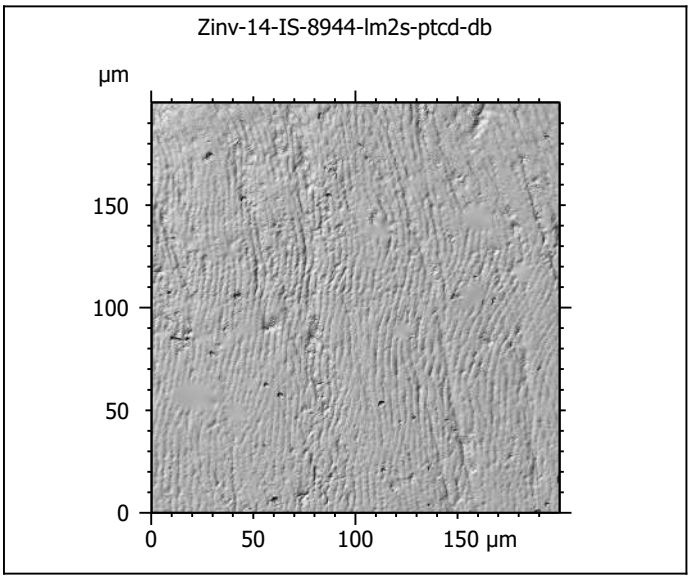

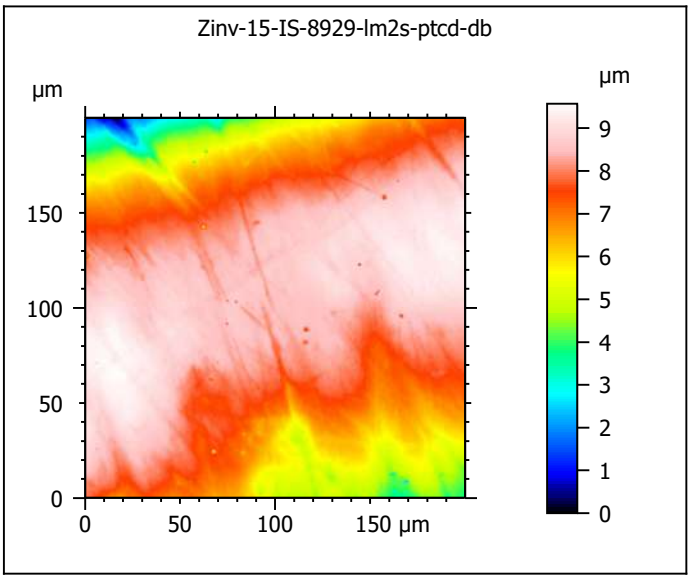

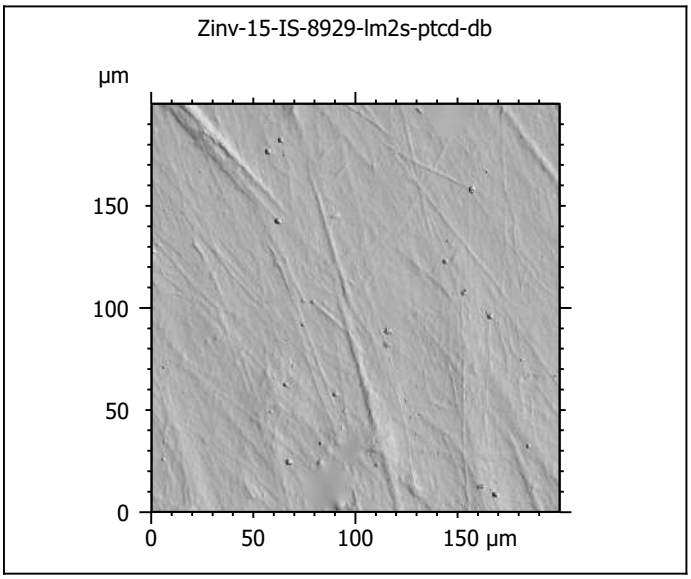

Leica Map Premium 8.0.9151

Photosimulations and false color elevation maps of scanned molar facets of the chamois (*Rupicapra rupicapra*) from the Bauges Natural Regional Park, France
scanned at the PALEVOPRIM lab by G. Merceron , CNRS and University of Poitiers, France with "TRIDENT", white light confocal microscope Leica DCM8

ANR-13-JSV7-0008-01, PI: G. Merceron

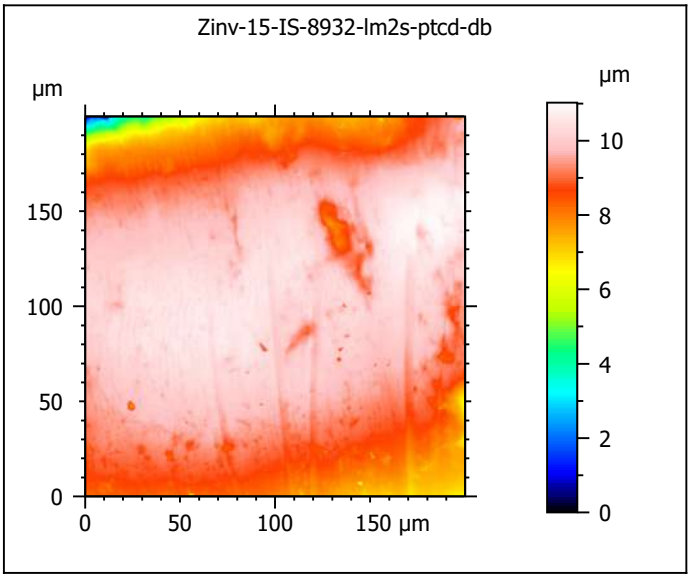

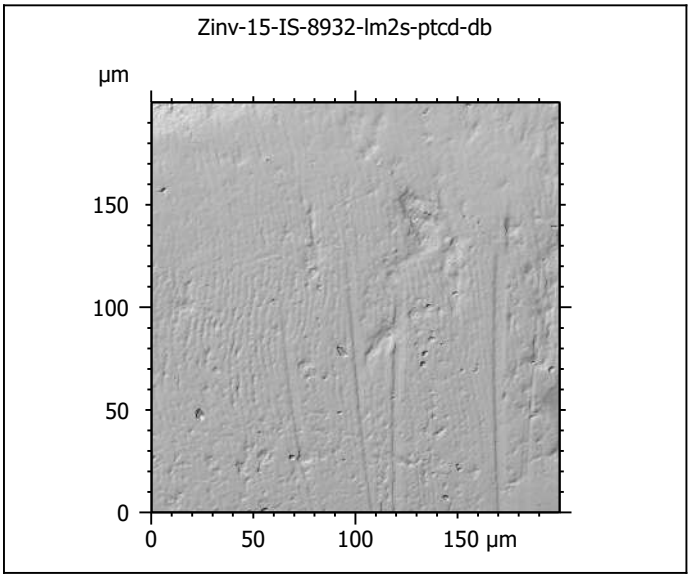

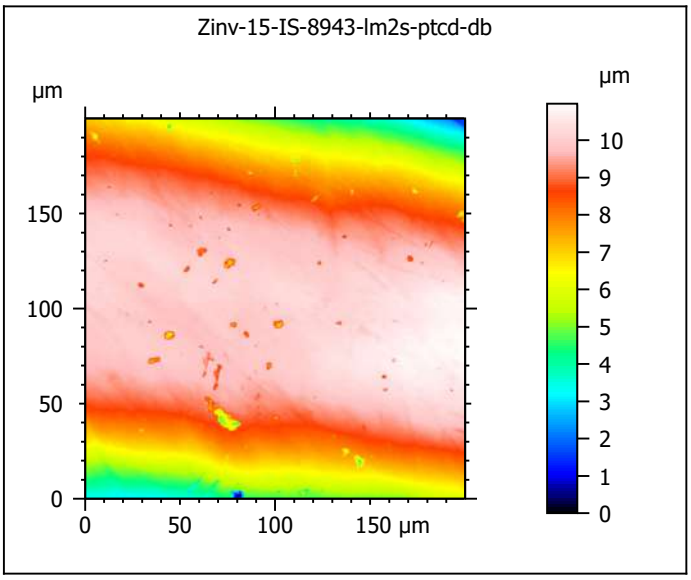

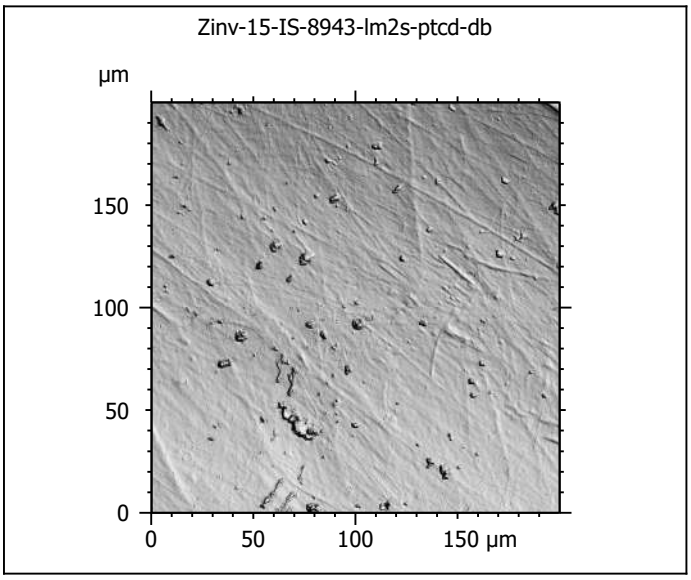

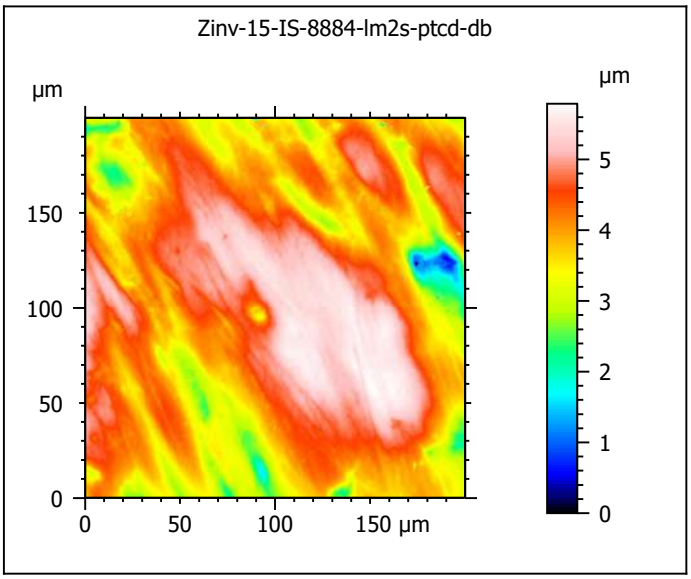

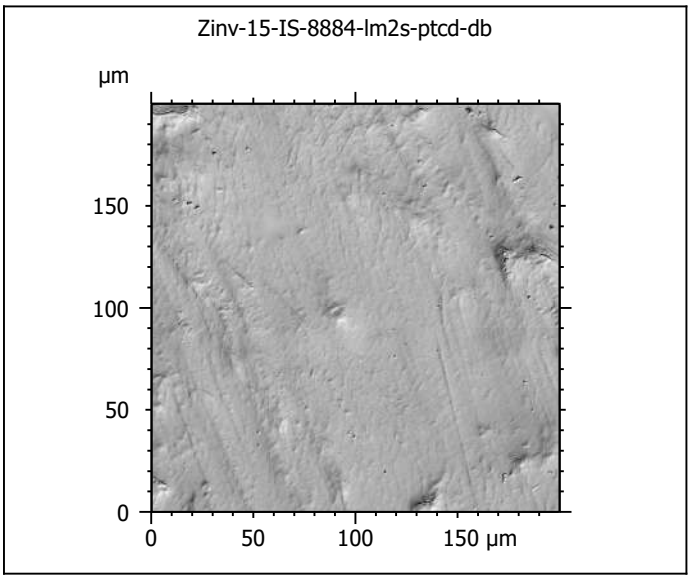

Leica Map Premium 8.0.9151

Photosimulations and false color elevation maps of scanned molar facets of the chamois (*Rupicapra rupicapra*) from the Bauges Natural Regional Park, France
scanned at the PALEVOPRIM lab by G. Merceron , CNRS and University of Poitiers, France with "TRIDENT", white light confocal microscope Leica DCM8

ANR-13-JSV7-0008-01, PI: G. Merceron

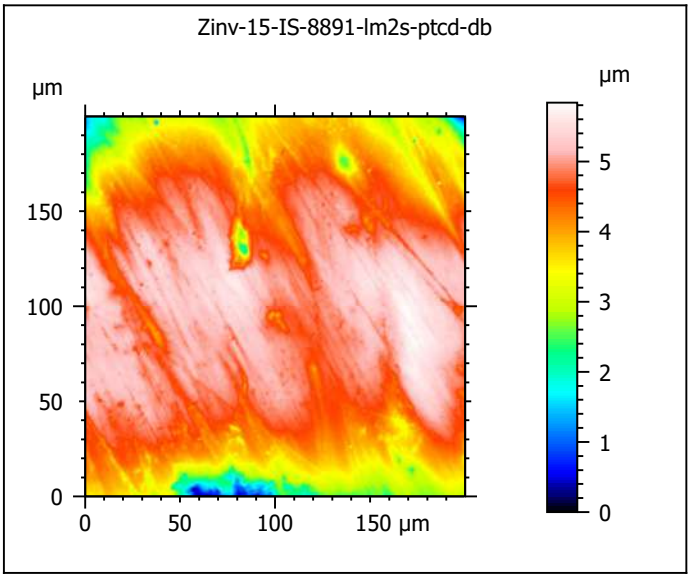

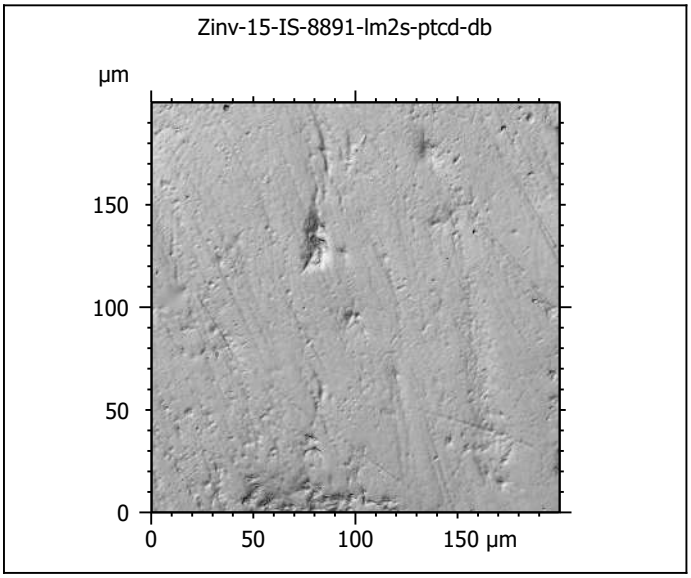

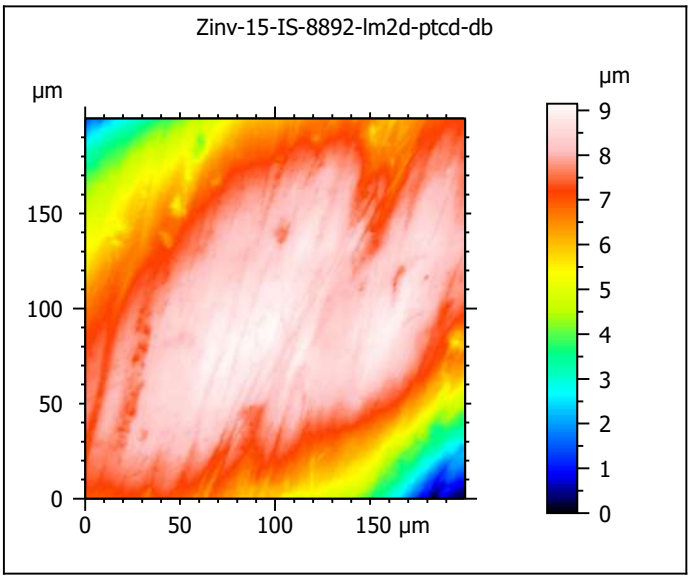

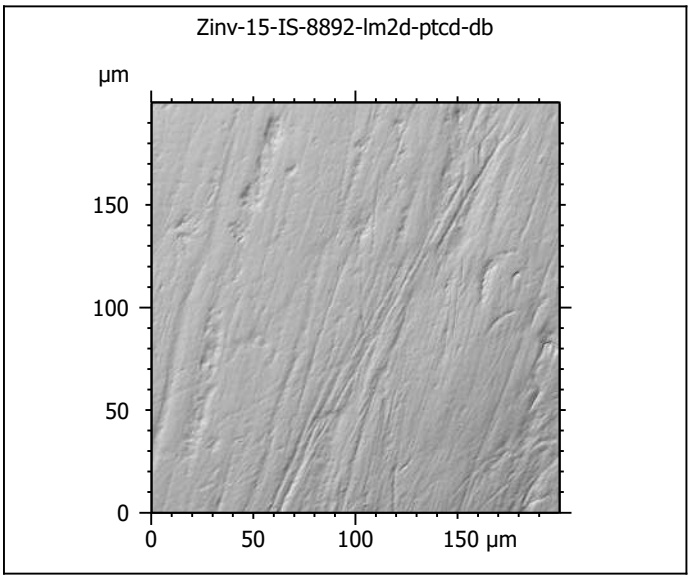

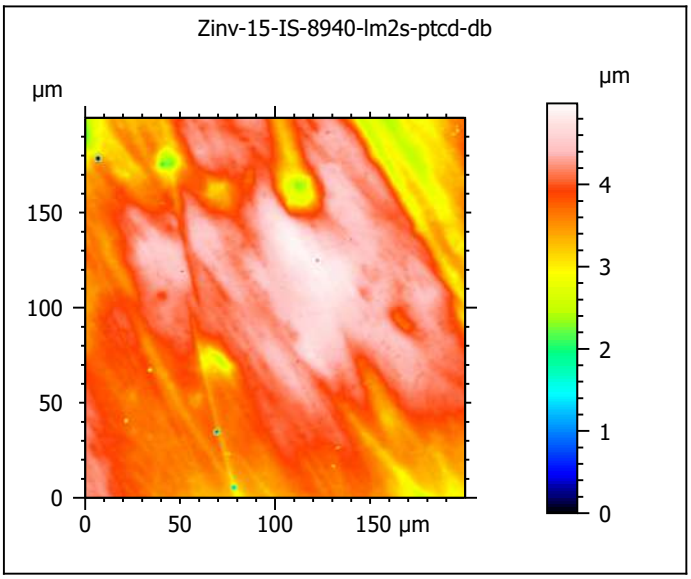

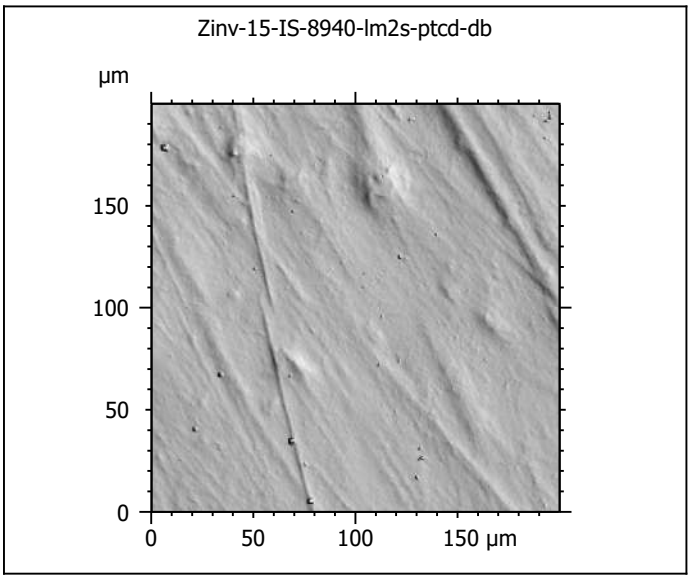

Leica Map Premium 8.0.9151

Photosimulations and false color elevation maps of scanned molar facets of the chamois (*Rupicapra rupicapra*) from the Bauges Natural Regional Park, France
scanned at the PALEVOPRIM lab by G. Merceron , CNRS and University of Poitiers, France with "TRIDENT", white light confocal microscope Leica DCM8

ANR-13-JSV7-0008-01, PI: G. Merceron

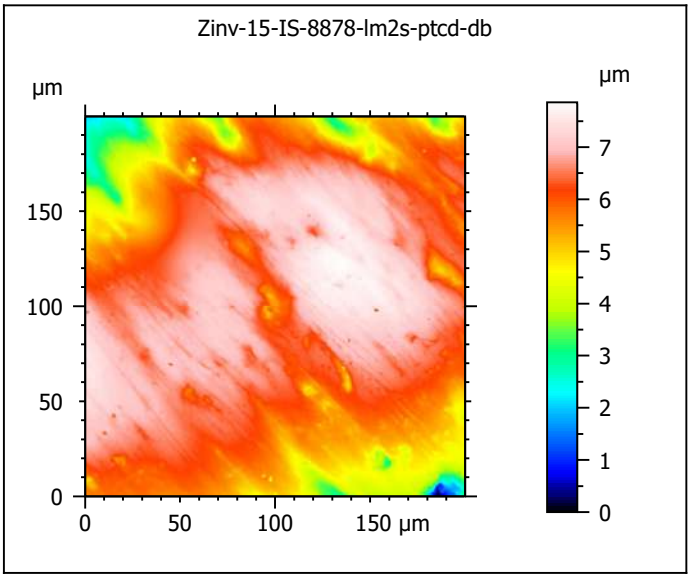

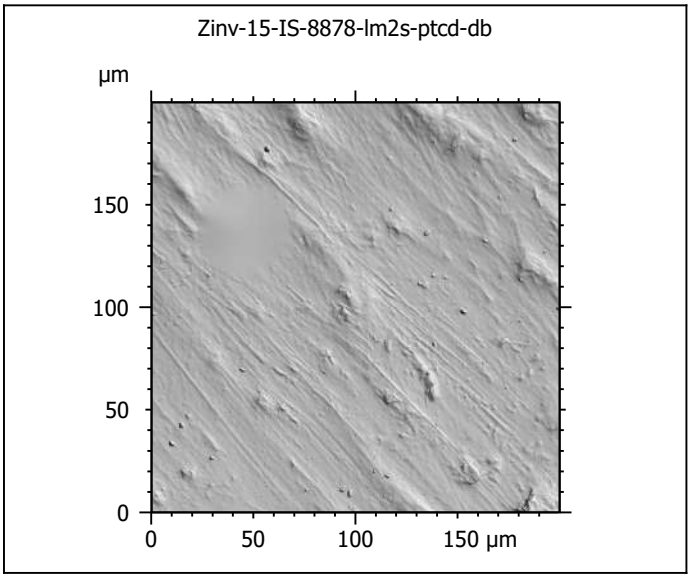

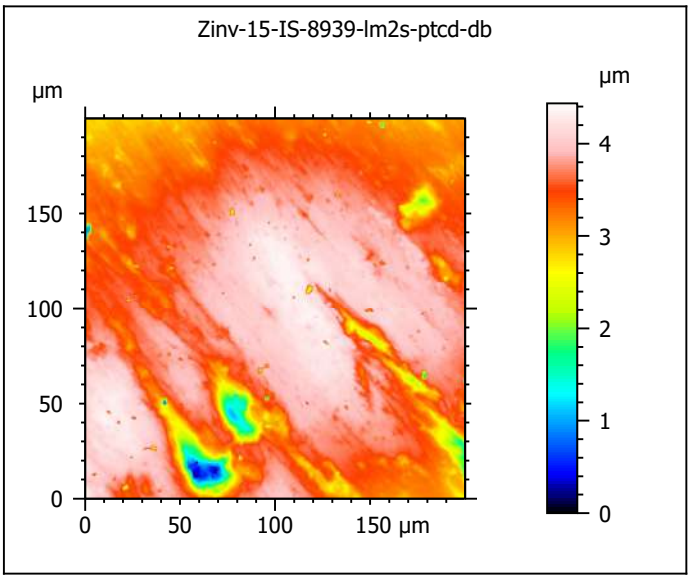

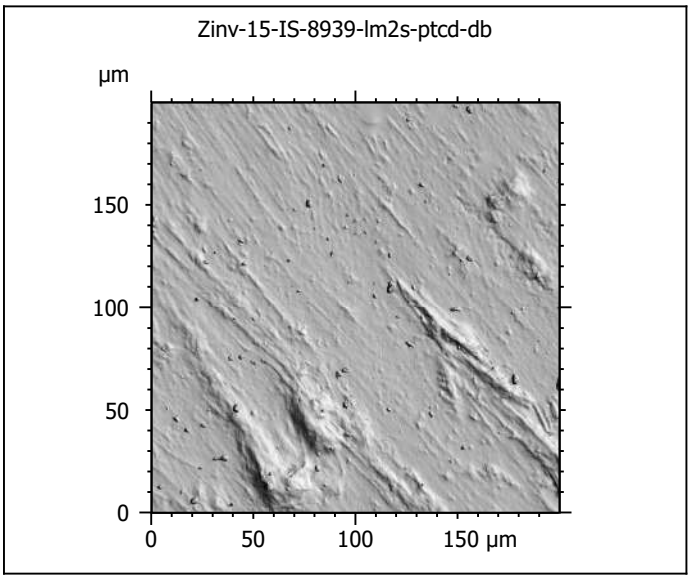

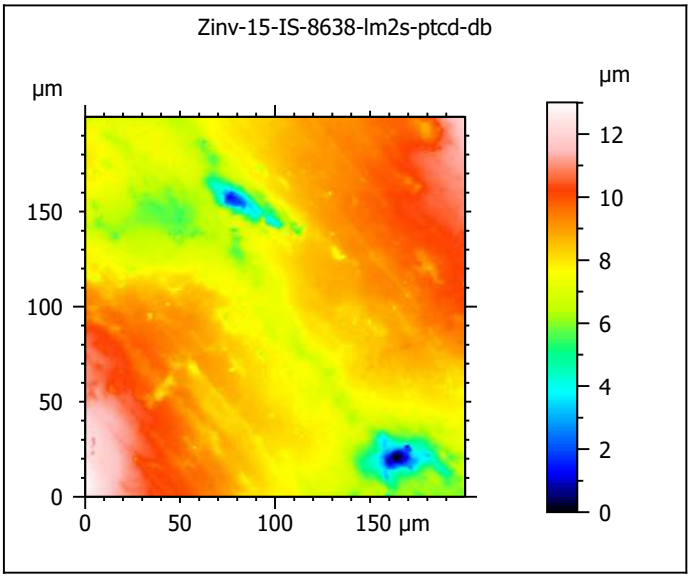

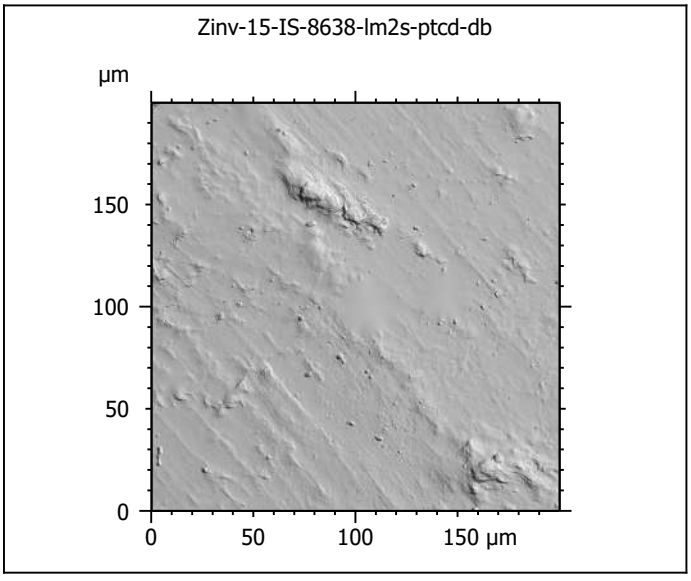

Leica Map Premium 8.0.9151

Photosimulations and false color elevation maps of scanned molar facets of the chamois (*Rupicapra rupicapra*) from the Bauges Natural Regional Park, France
scanned at the PALEVOPRIM lab by G. Merceron , CNRS and University of Poitiers, France with "TRIDENT", white light confocal microscope Leica DCM8

ANR-13-JSV7-0008-01, PI: G. Merceron

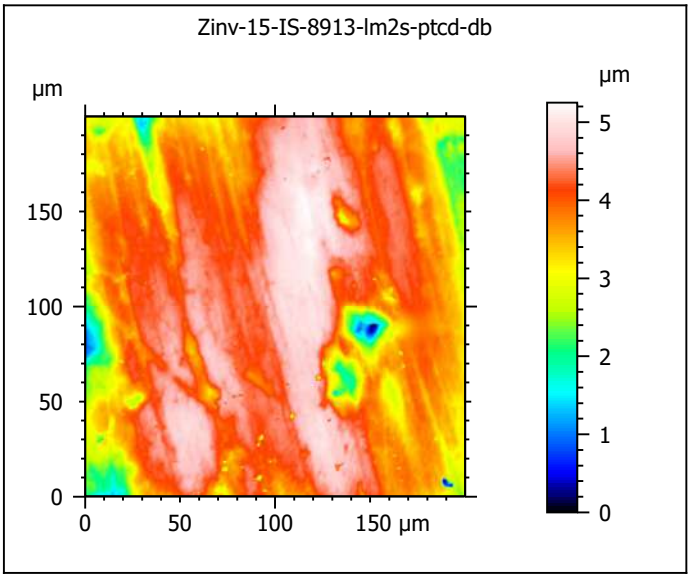

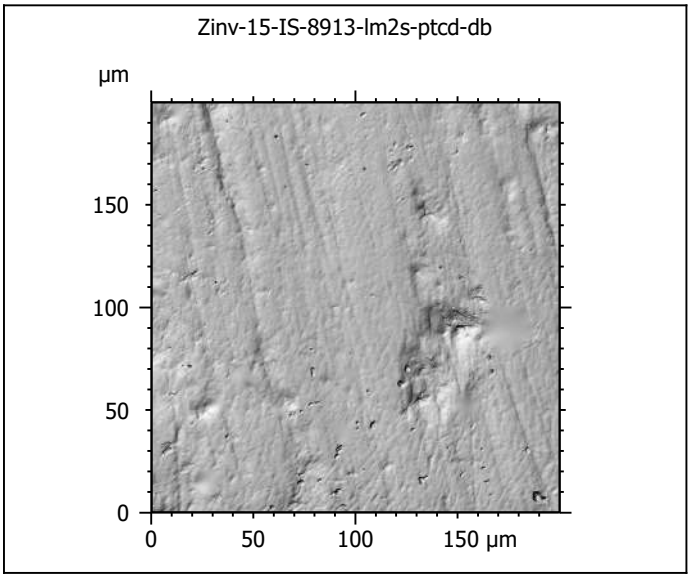

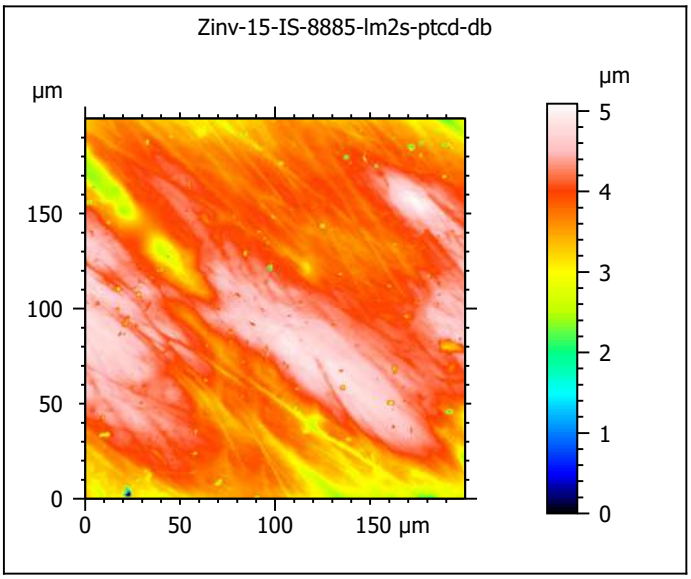

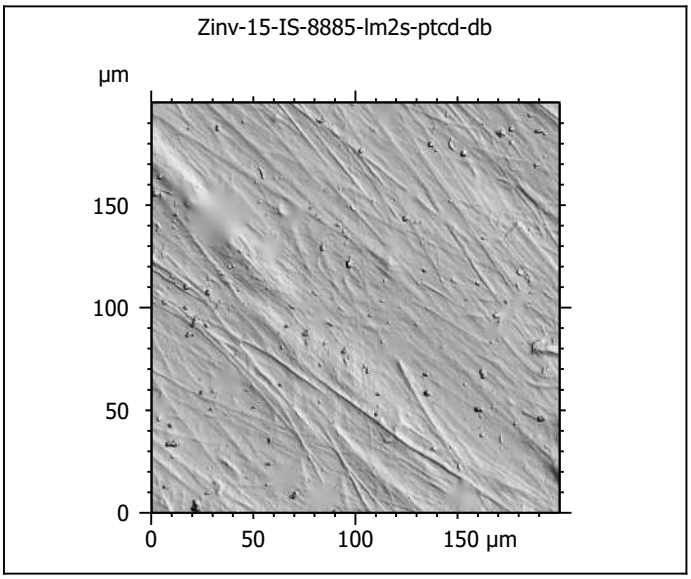

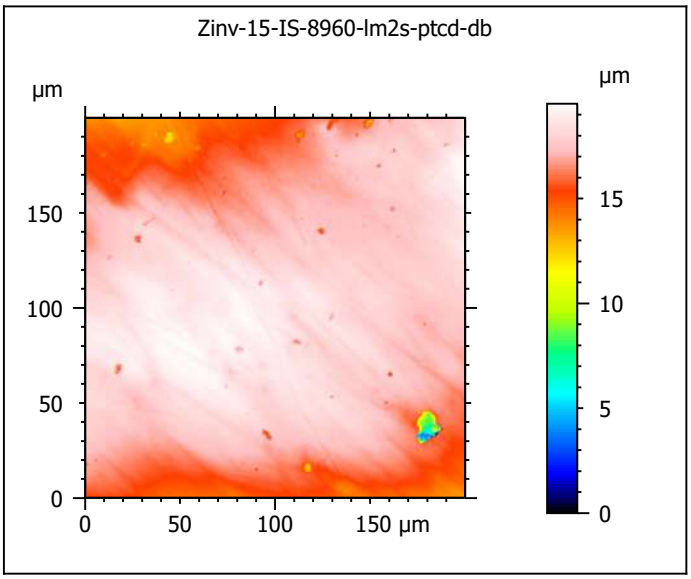

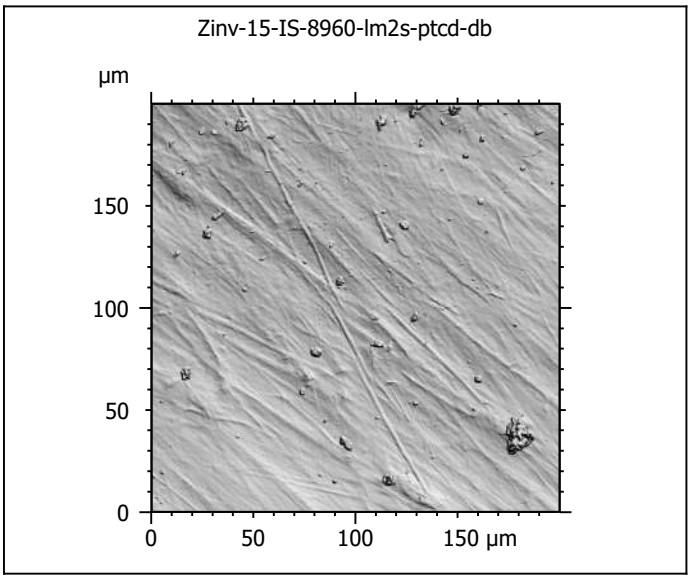

Leica Map Premium 8.0.9151

Photosimulations and false color elevation maps of scanned molar facets of the chamois (*Rupicapra rupicapra*) from the Bauges Natural Regional Park, France
scanned at the PALEVOPRIM lab by G. Merceron , CNRS and University of Poitiers, France with "TRIDENT", white light confocal microscope Leica DCM8

ANR-13-JSV7-0008-01, PI: G. Merceron

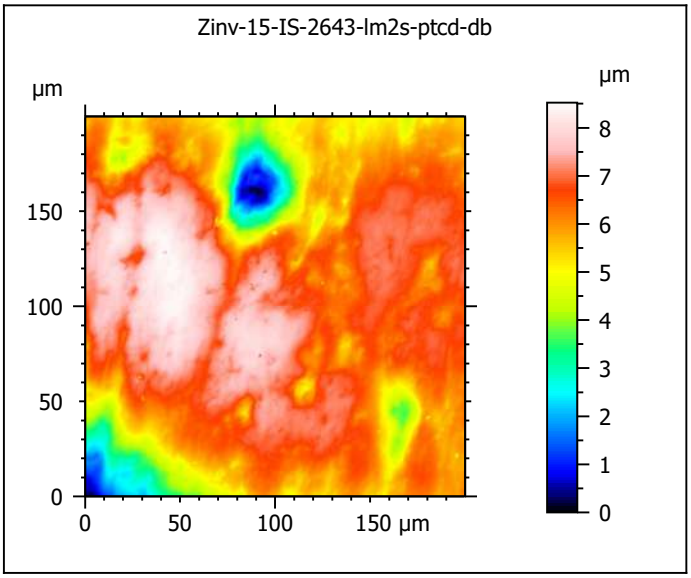

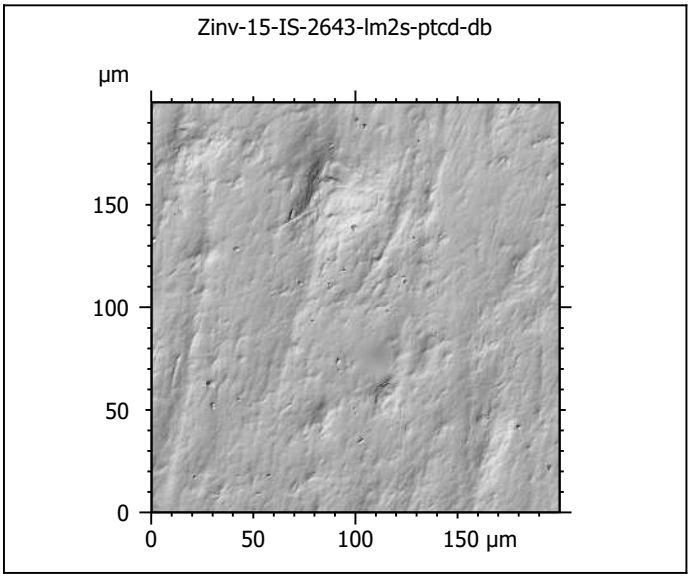

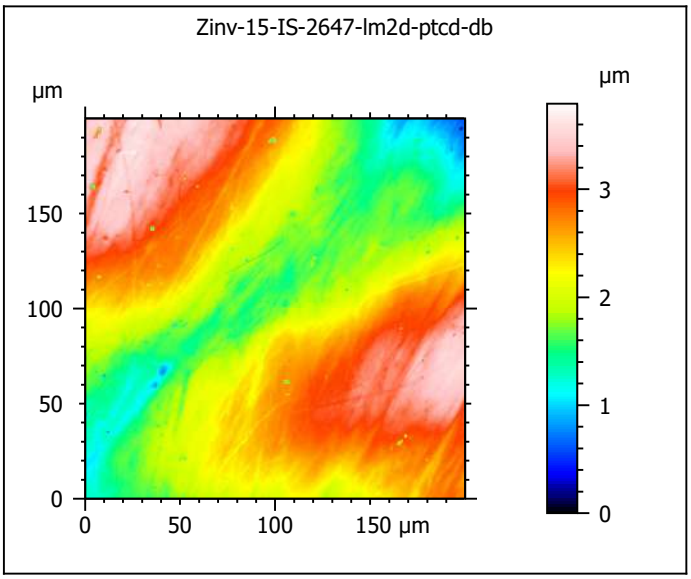

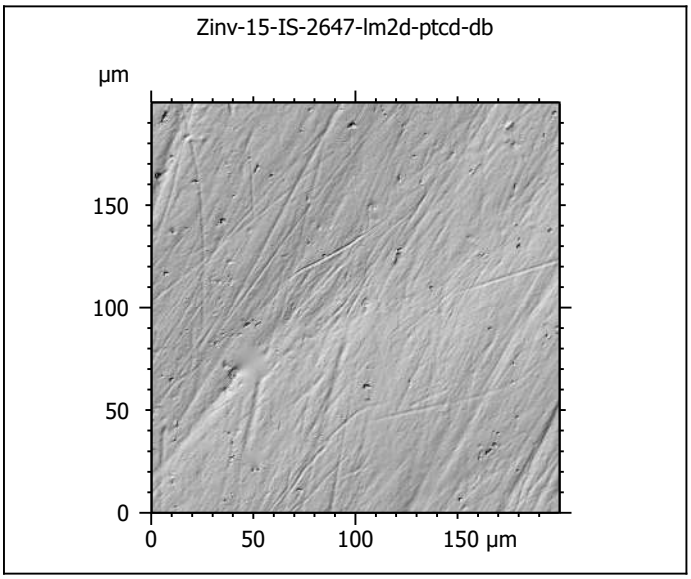

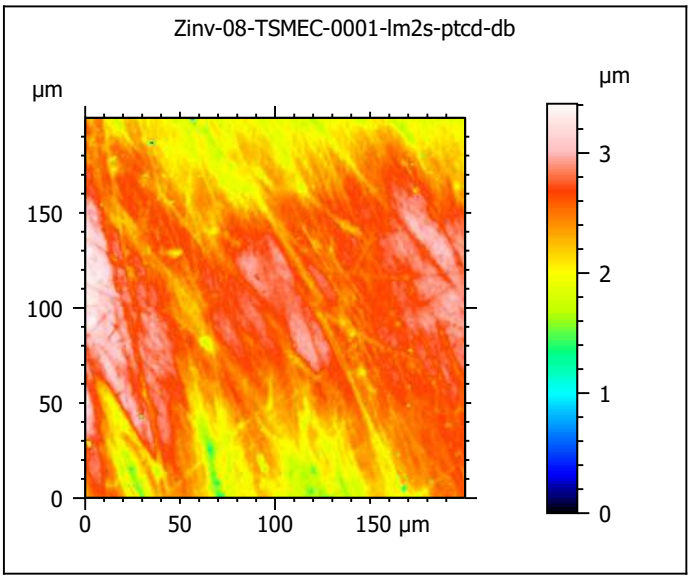

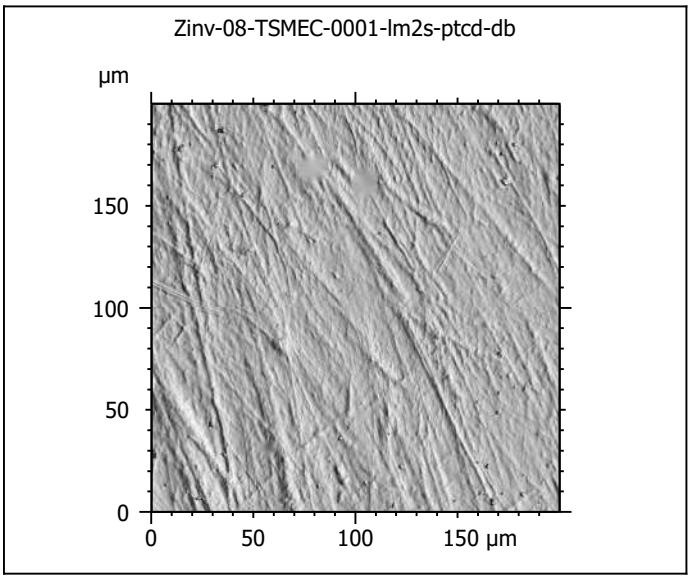

Leica Map Premium 8.0.9151

Photosimulations and false color elevation maps of scanned molar facets of the mouflon (*Ovis gmelini musimon*) from the Bauges Natural Regional Park, France
scanned at the PALEVOPRIM lab by G. Merceron , CNRS and University of Poitiers, France with "TRIDENT", white light confocal microscope Leica DCM8

ANR-13-JSV7-0008-01, PI: G. Merceron

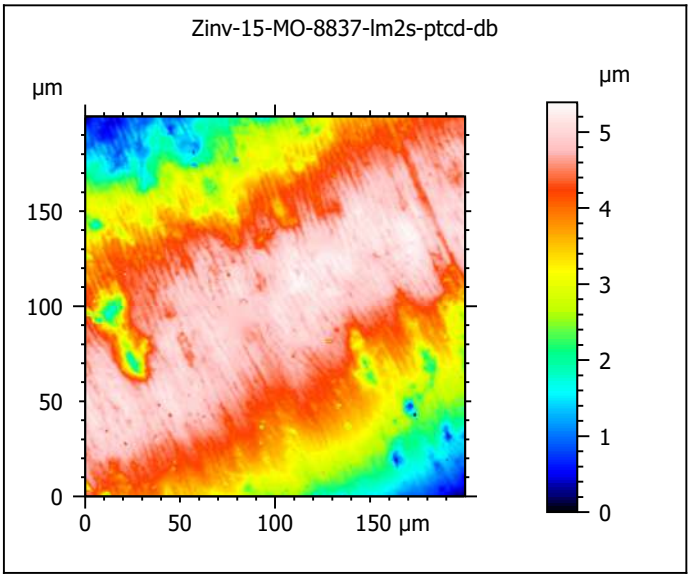

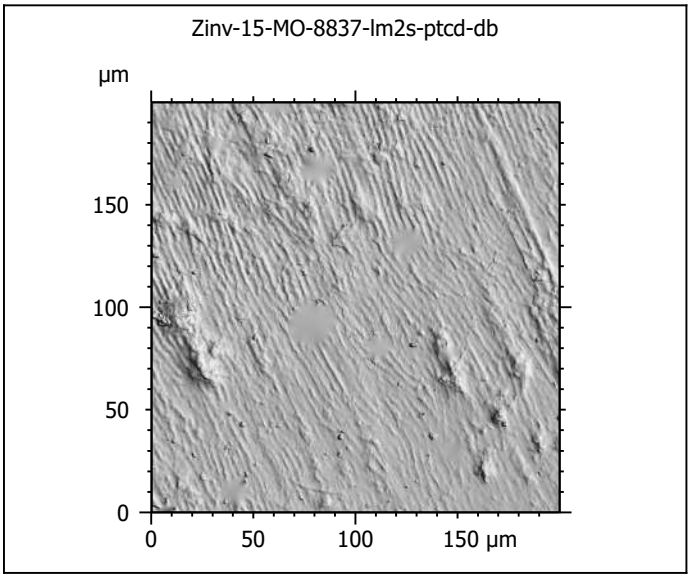

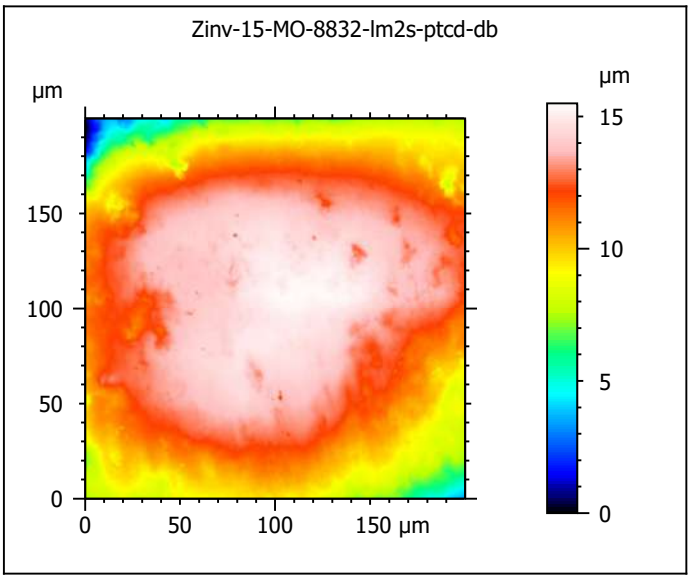

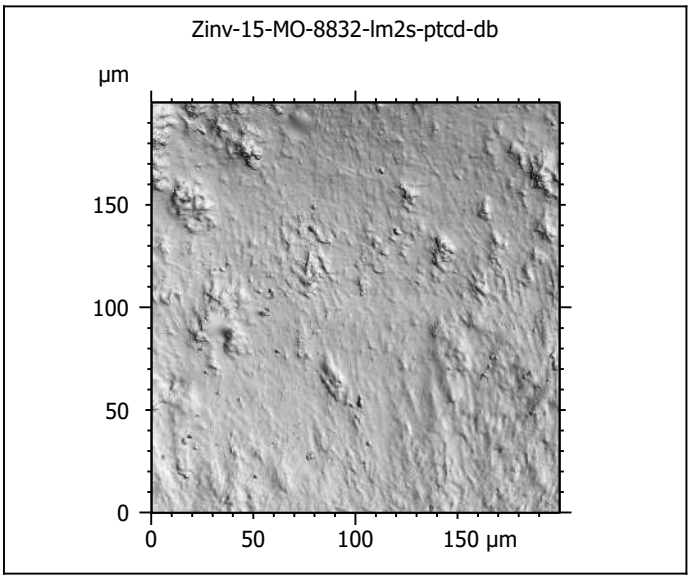

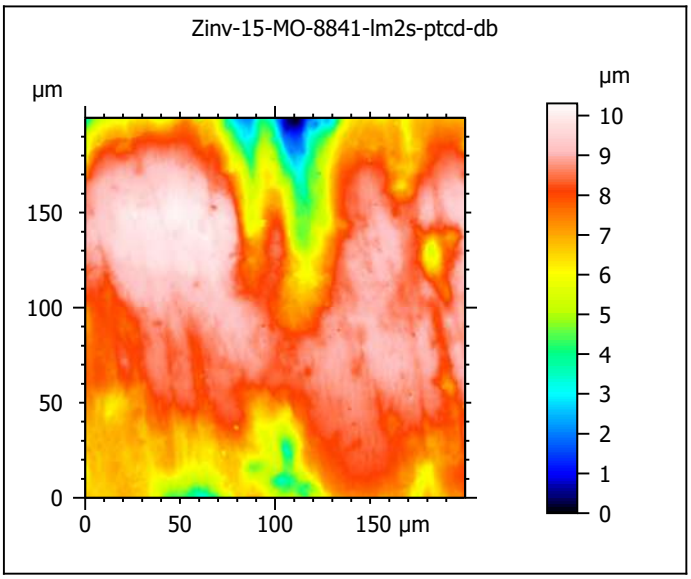

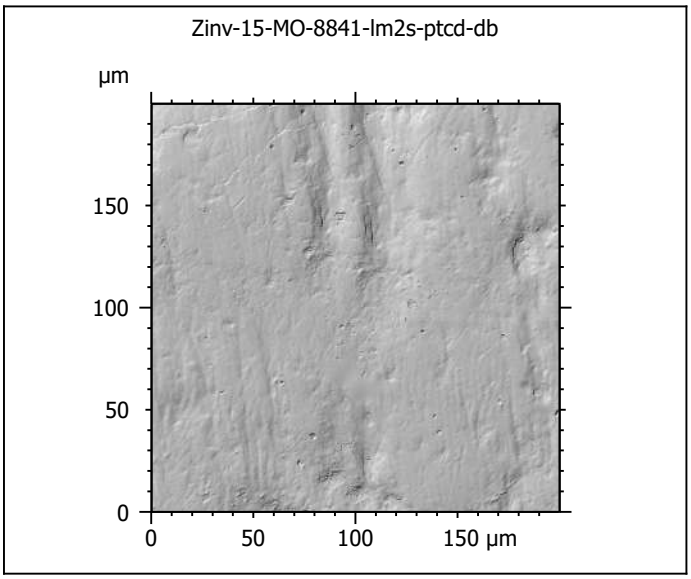

Leica Map Premium 8.0.9151

Photosimulations and false color elevation maps of scanned molar facets of the mouflon (*Ovis gmelini musimon*) from the Bauges Natural Regional Park, France
scanned at the PALEVOPRIM lab by G. Merceron , CNRS and University of Poitiers, France with "TRIDENT", white light confocal microscope Leica DCM8

ANR-13-JSV7-0008-01, PI: G. Merceron

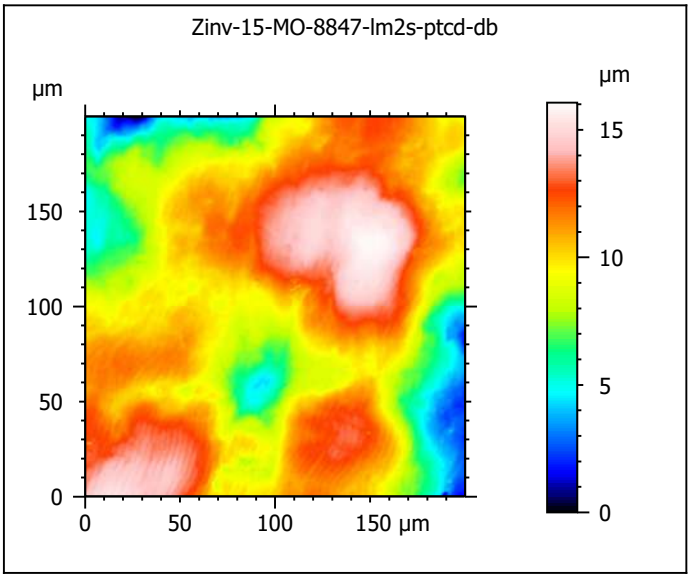

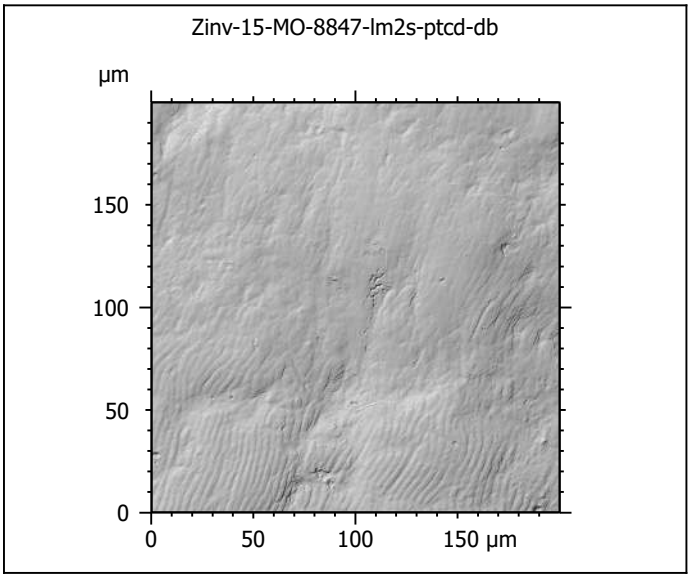

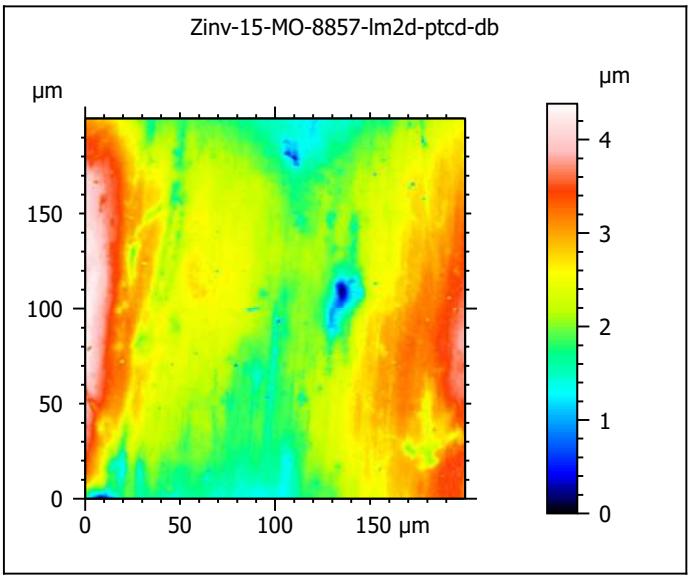

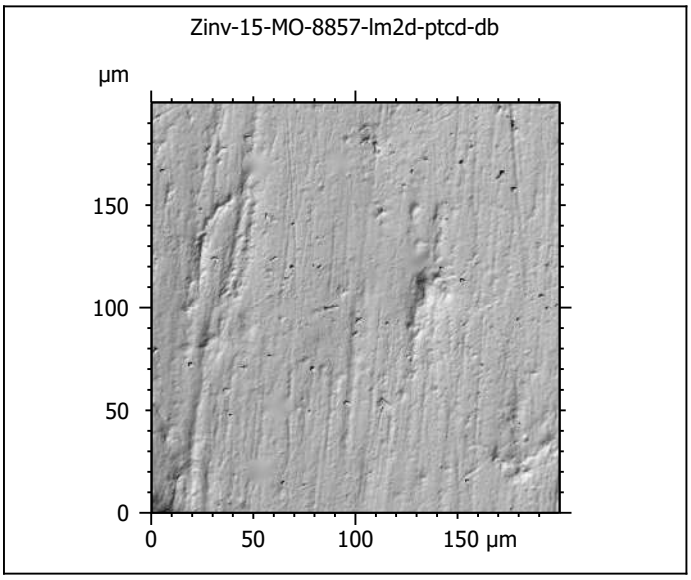

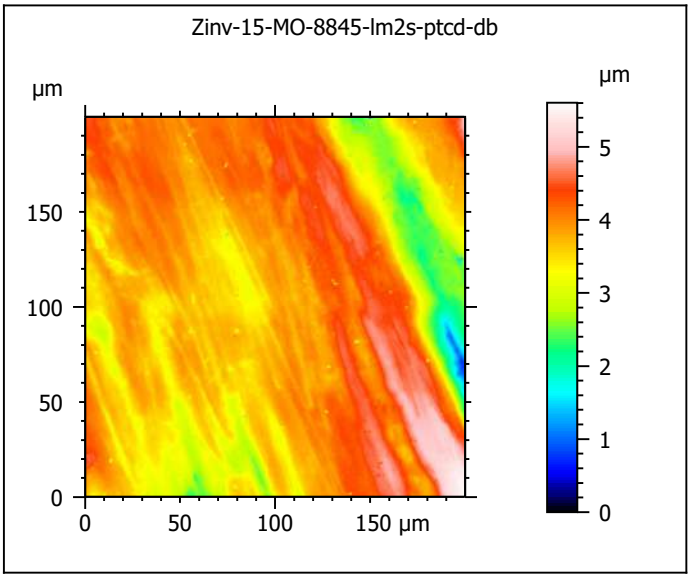

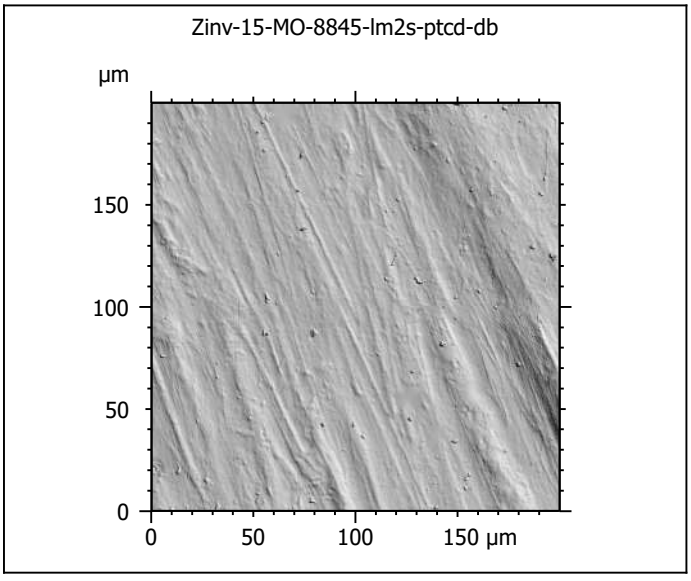

Leica Map Premium 8.0.9151

Photosimulations and false color elevation maps of scanned molar facets of the mouflon (*Ovis gmelini musimon*) from the Bauges Natural Regional Park, France
scanned at the PALEVOPRIM lab by G. Merceron , CNRS and University of Poitiers, France with "TRIDENT", white light confocal microscope Leica DCM8

ANR-13-JSV7-0008-01, PI: G. Merceron

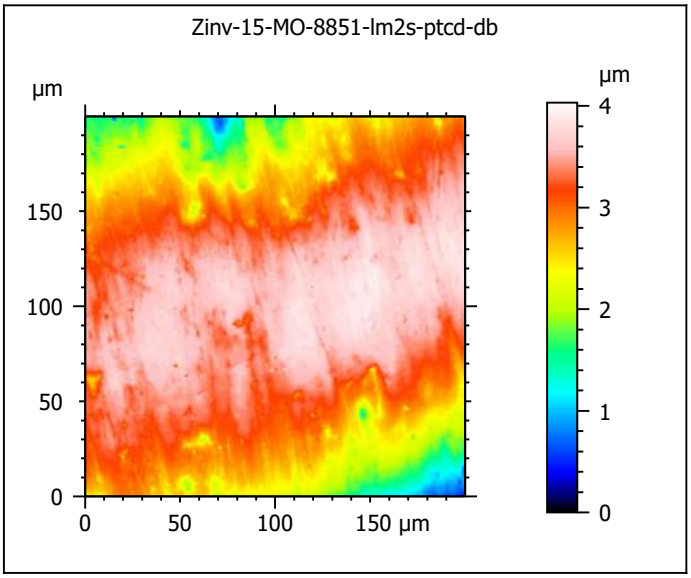

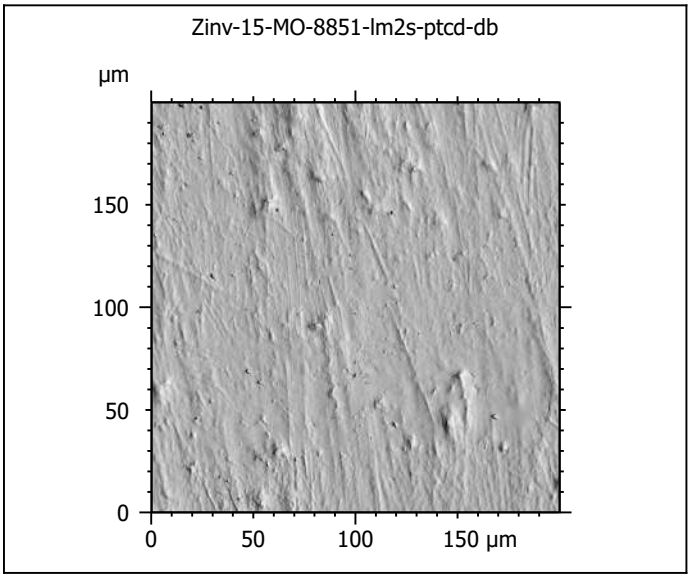

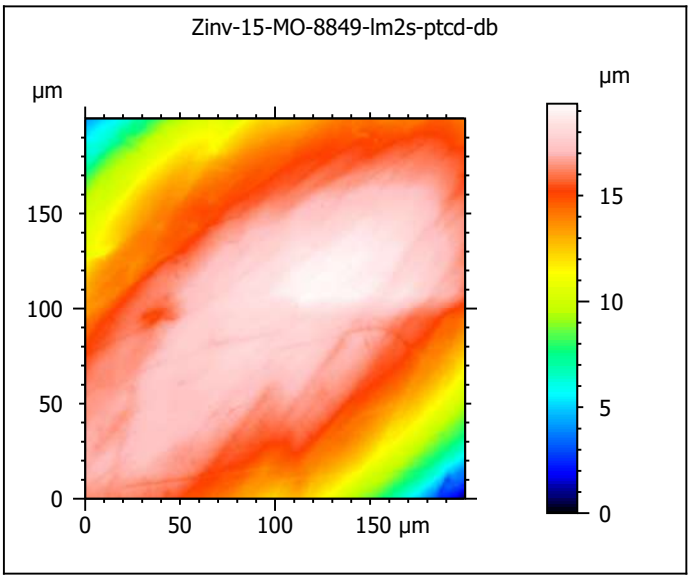

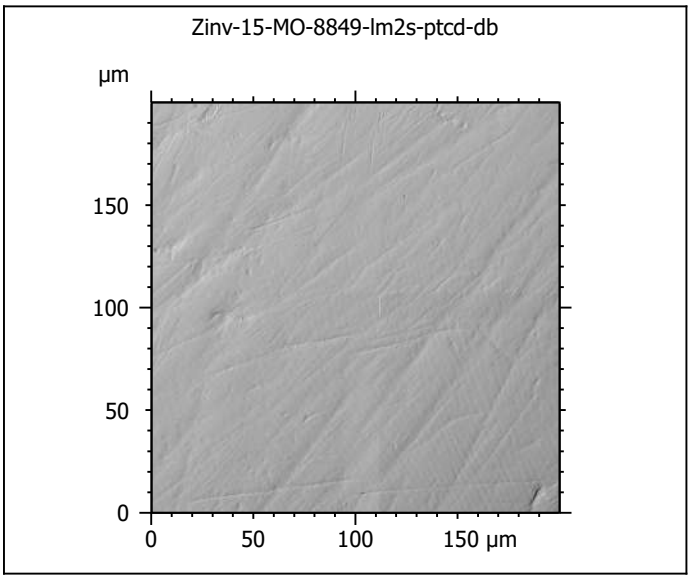

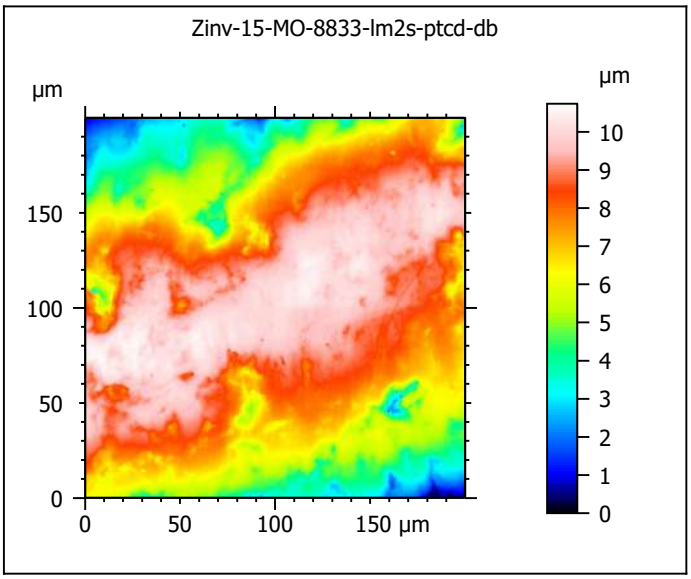

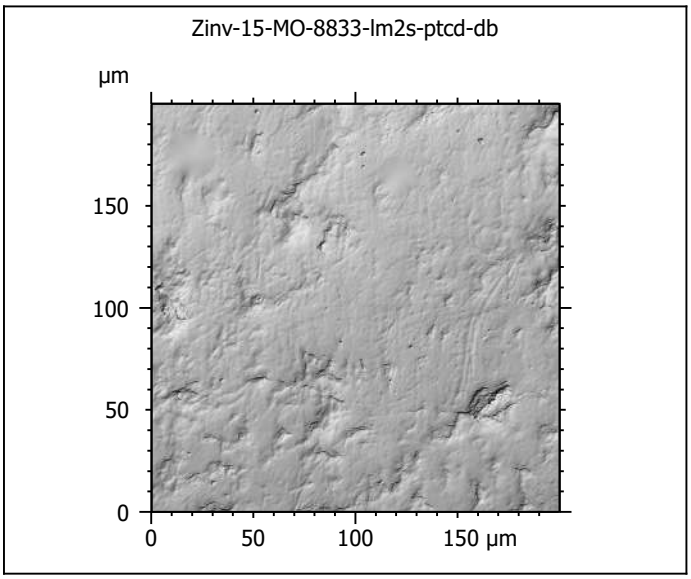

Leica Map Premium 8.0.9151

Photosimulations and false color elevation maps of scanned molar facets of the mouflon (*Ovis gmelini musimon*) from the Bauges Natural Regional Park, France
scanned at the PALEVOPRIM lab by G. Merceron , CNRS and University of Poitiers, France with "TRIDENT", white light confocal microscope Leica DCM8

ANR-13-JSV7-0008-01, PI: G. Merceron

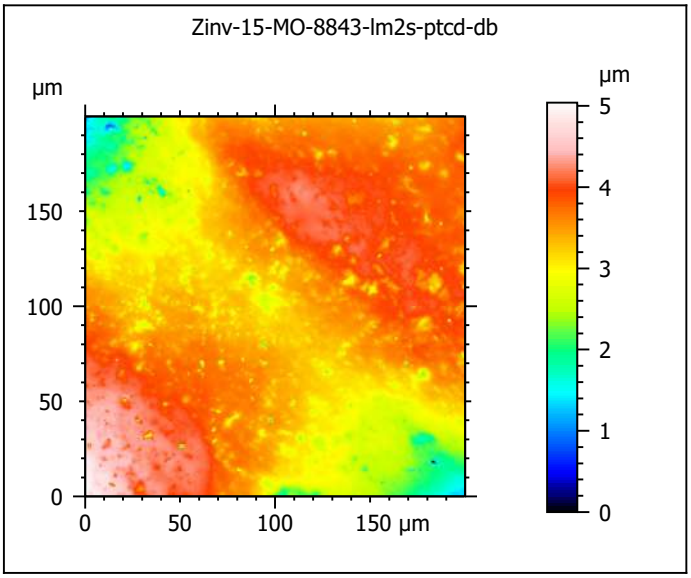

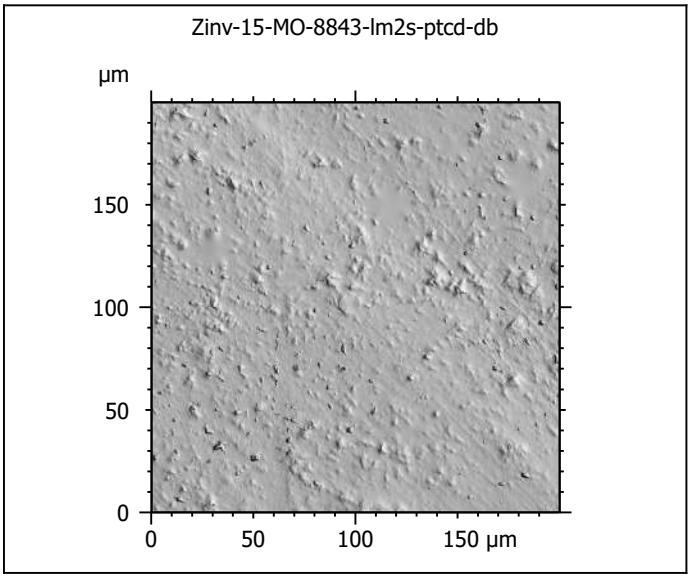

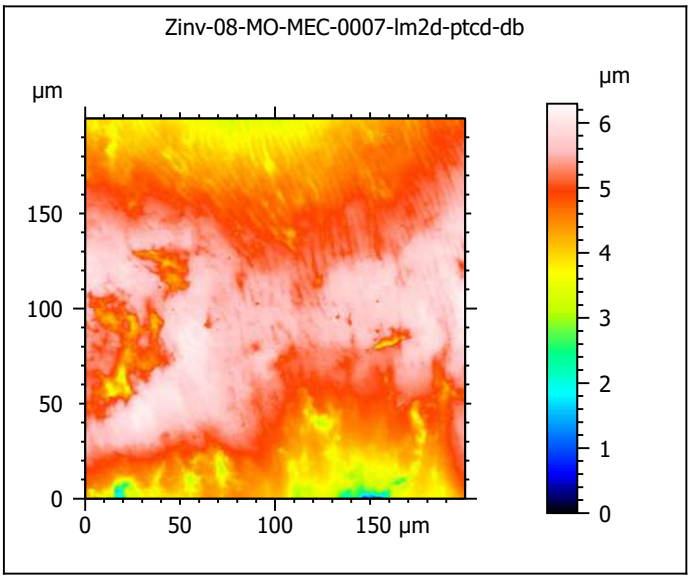

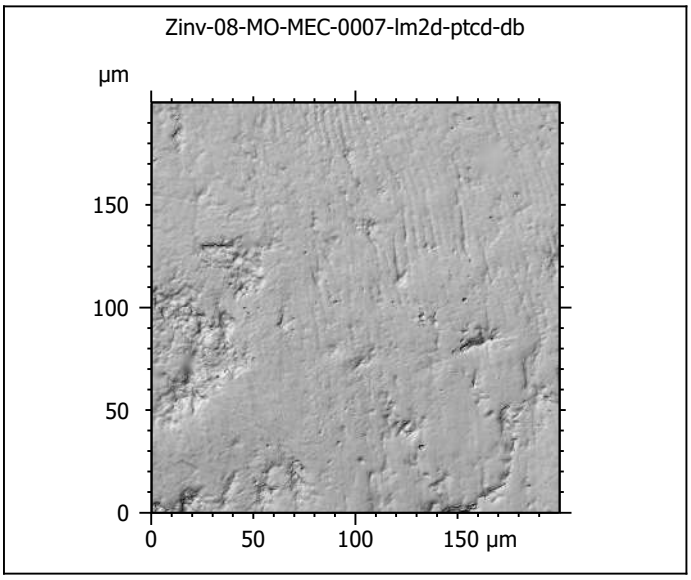

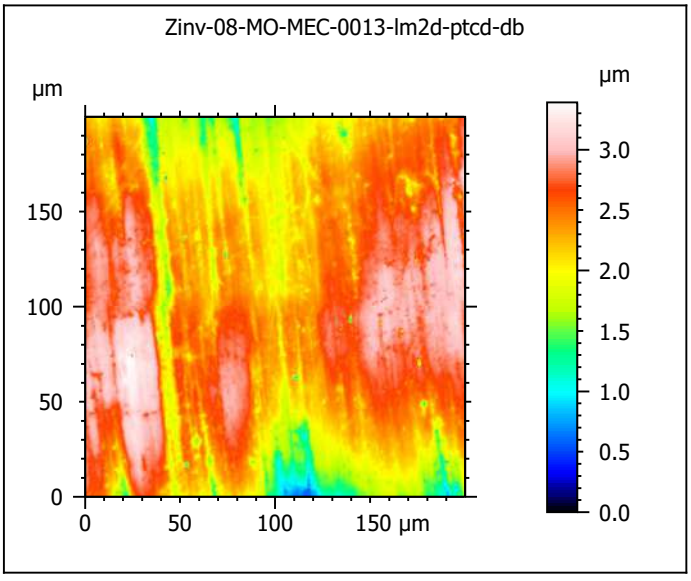

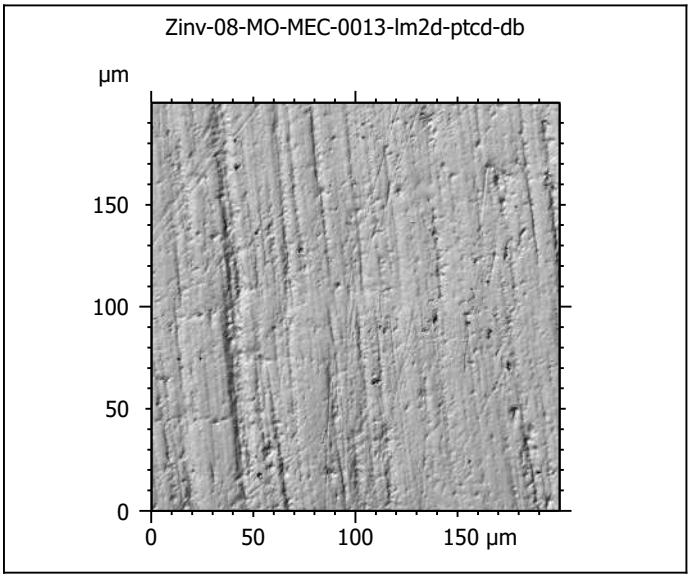

Leica Map Premium 8.0.9151

Photosimulations and false color elevation maps of scanned molar facets of the mouflon (*Ovis gmelini musimon*) from the Bauges Natural Regional Park, France
scanned at the PALEVOPRIM lab by G. Merceron , CNRS and University of Poitiers, France with "TRIDENT", white light confocal microscope Leica DCM8

ANR-13-JSV7-0008-01, PI: G. Merceron

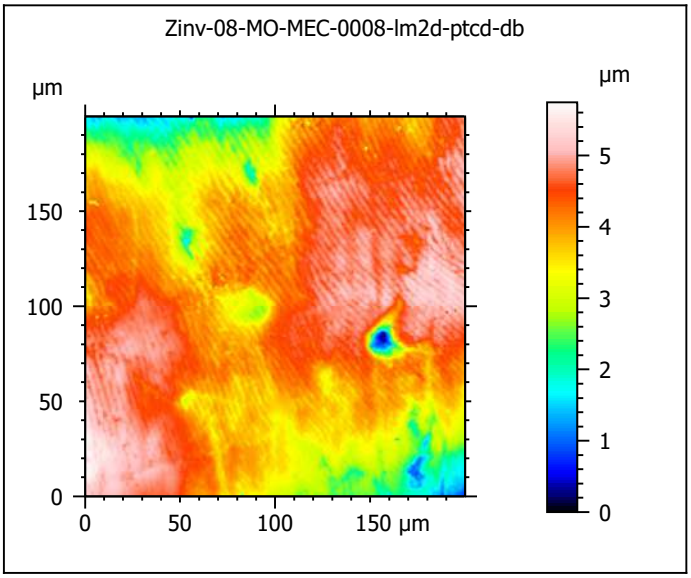

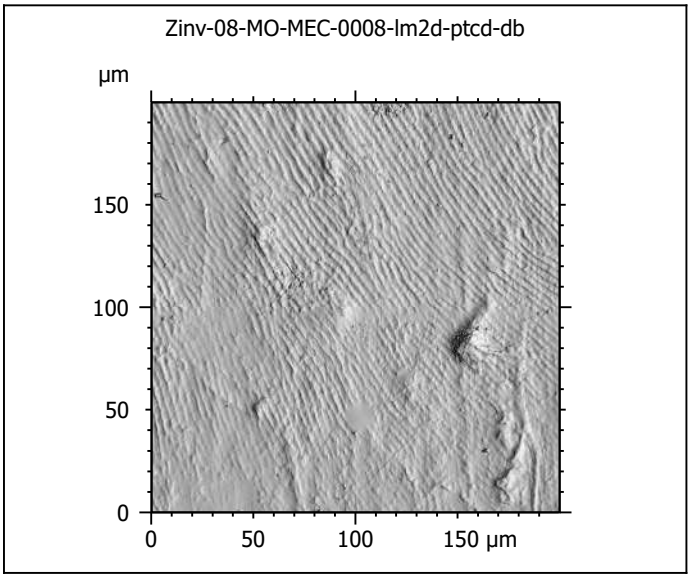

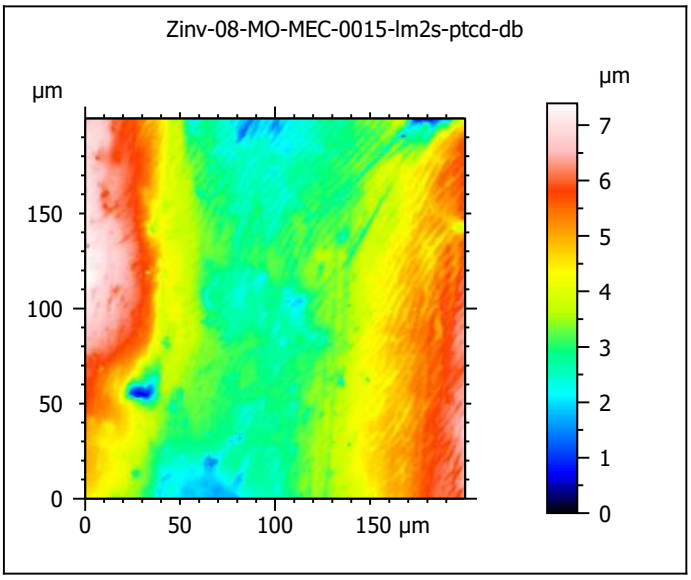

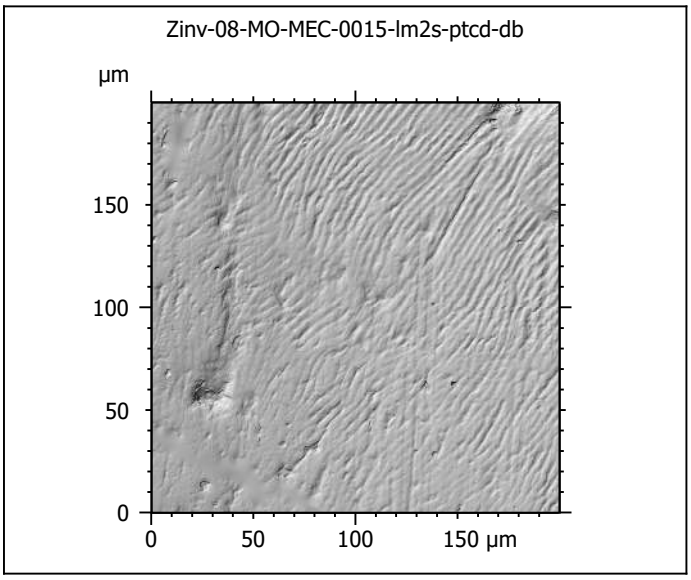

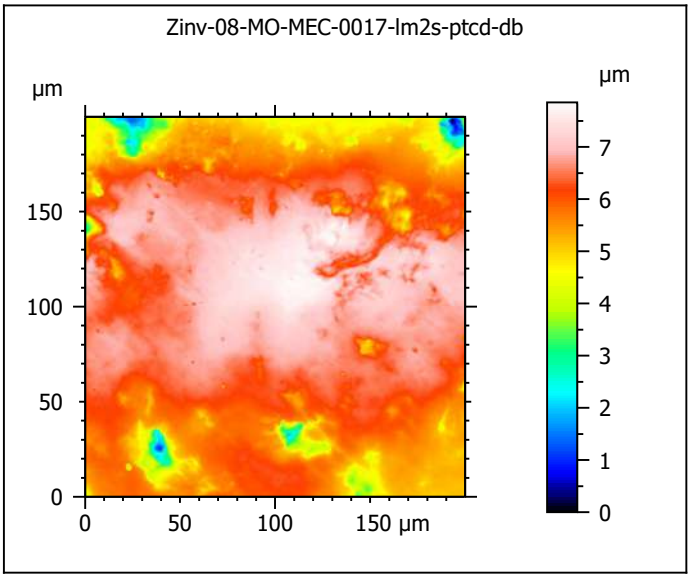

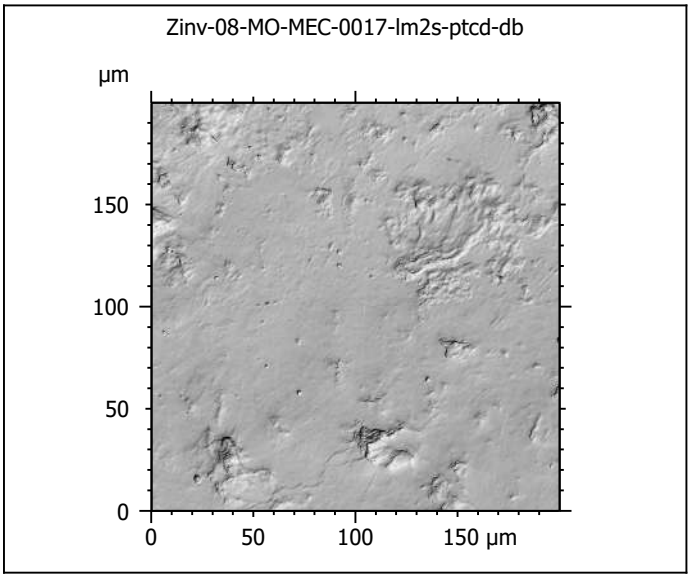

Leica Map Premium 8.0.9151

Photosimulations and false color elevation maps of scanned molar facets of the mouflon (*Ovis gmelini musimon*) from the Bauges Natural Regional Park, France
scanned at the PALEVOPRIM lab by G. Merceron , CNRS and University of Poitiers, France with "TRIDENT", white light confocal microscope Leica DCM8

ANR-13-JSV7-0008-01, PI: G. Merceron

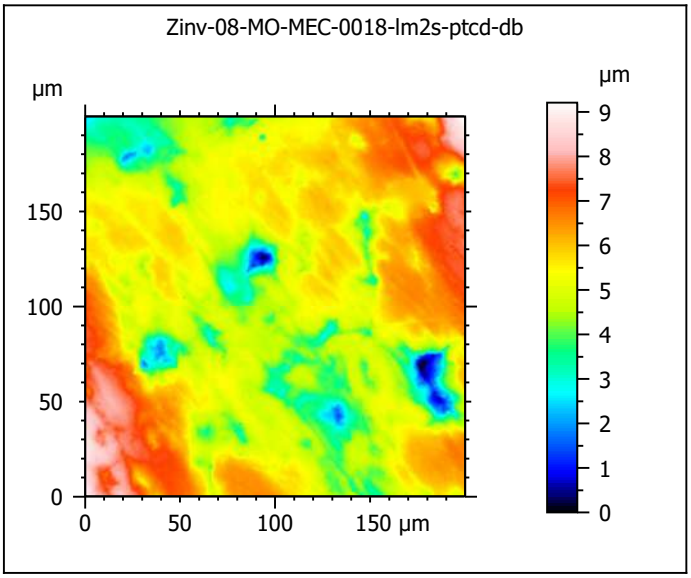

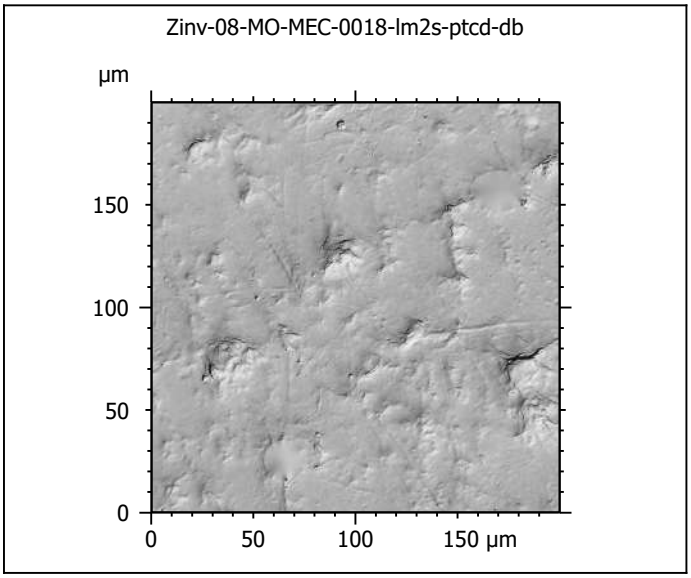

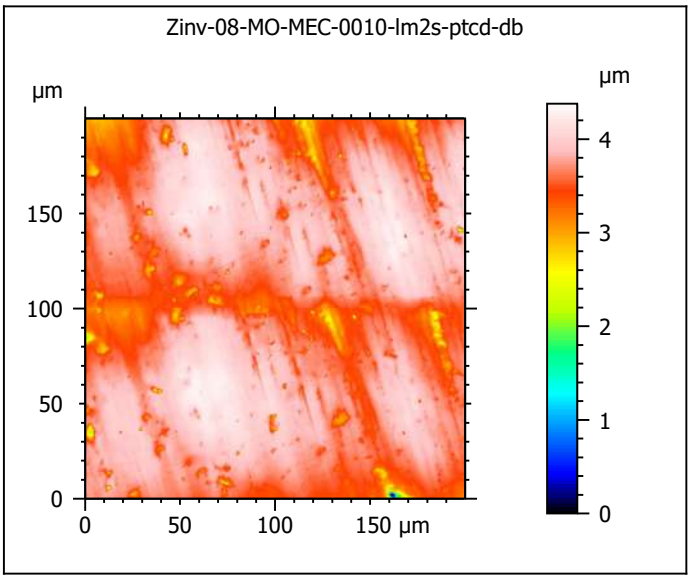

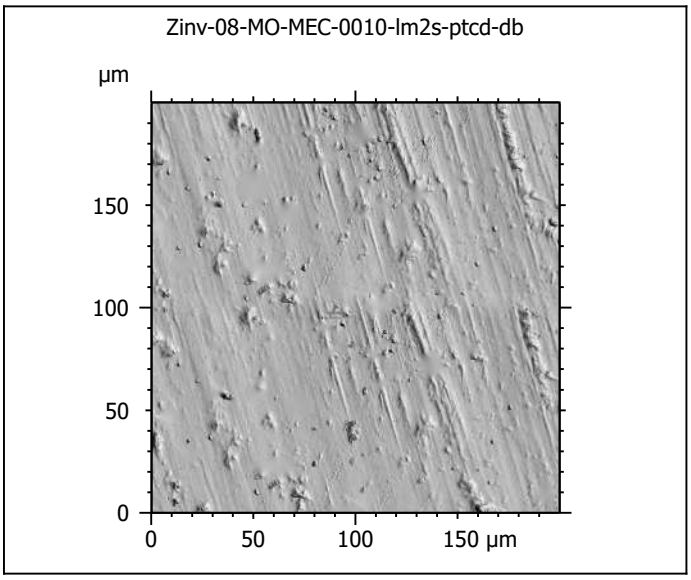

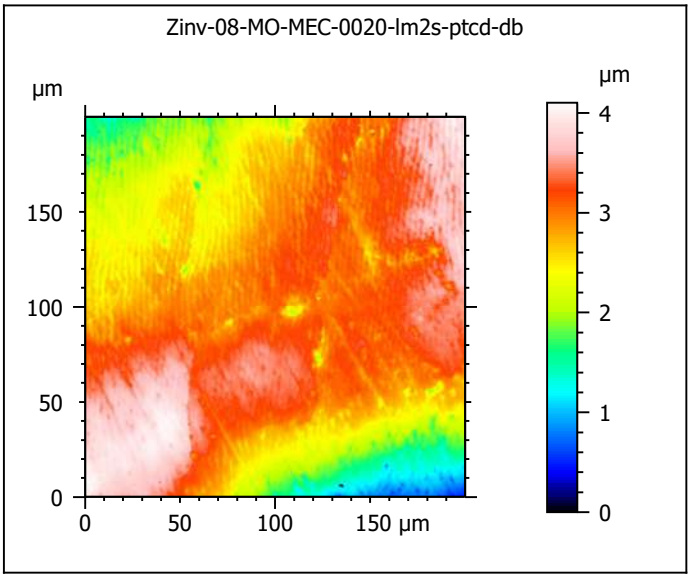

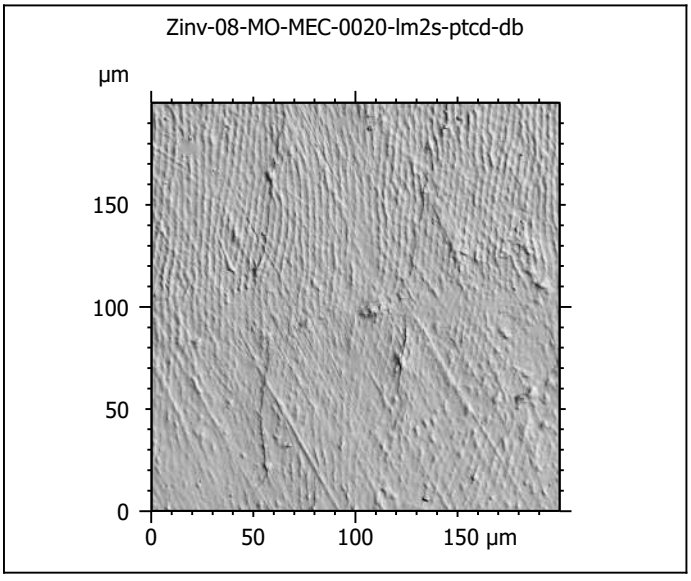

Leica Map Premium 8.0.9151

Photosimulations and false color elevation maps of scanned molar facets of the mouflon (*Ovis gmelini musimon*) from the Bauges Natural Regional Park, France
scanned at the PALEVOPRIM lab by G. Merceron , CNRS and University of Poitiers, France with "TRIDENT", white light confocal microscope Leica DCM8

ANR-13-JSV7-0008-01, PI: G. Merceron

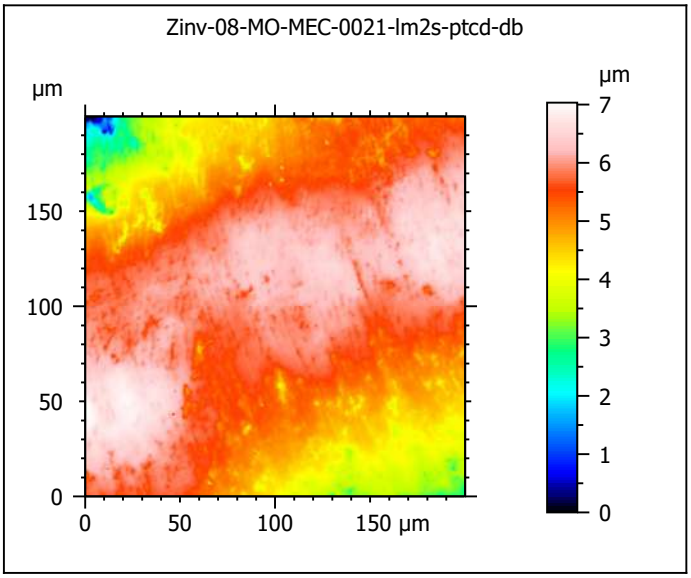

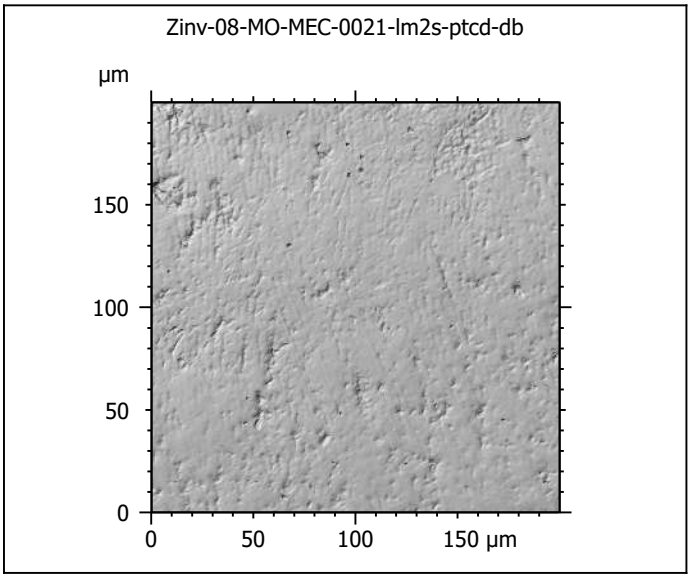

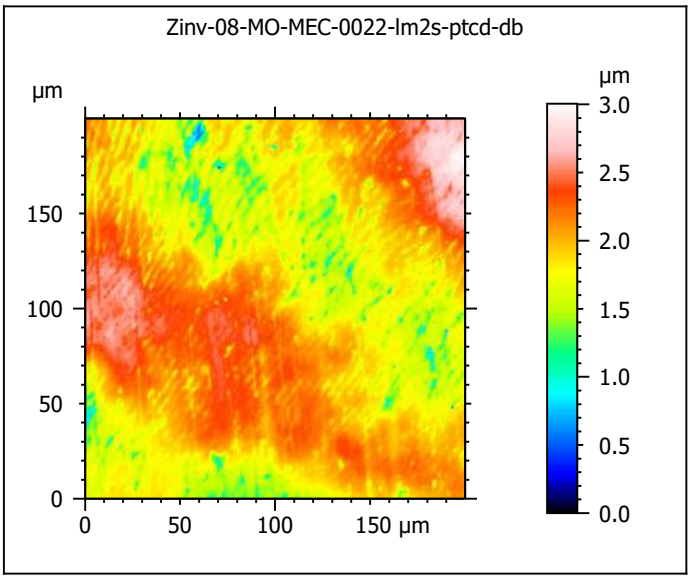

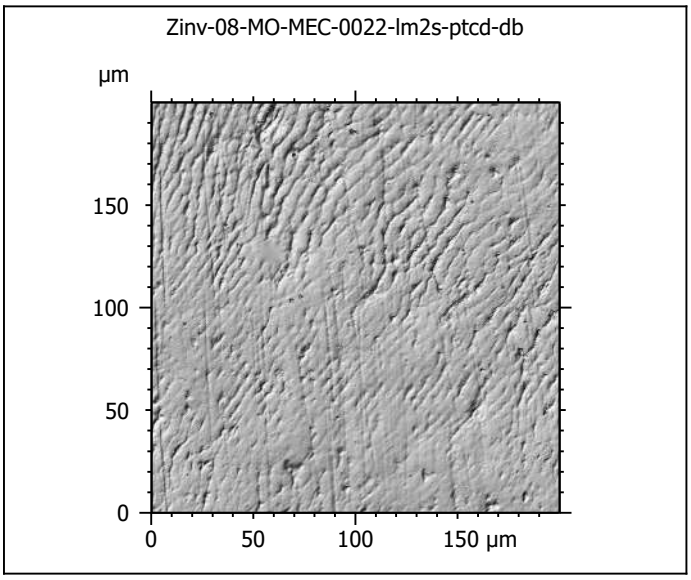

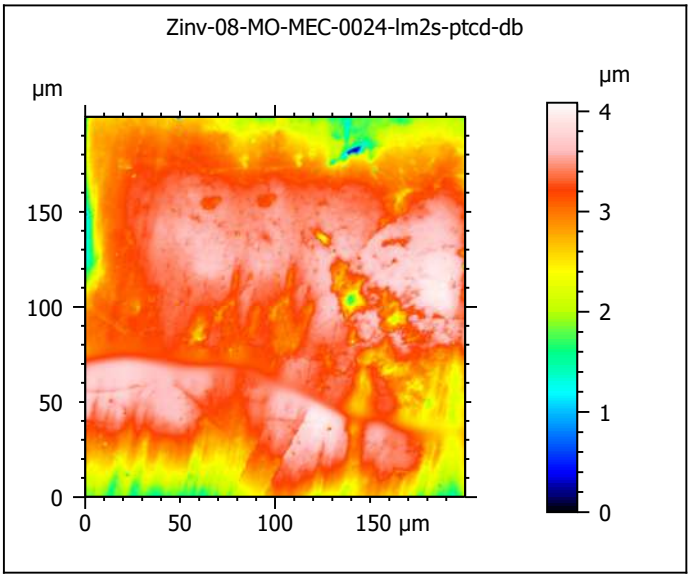

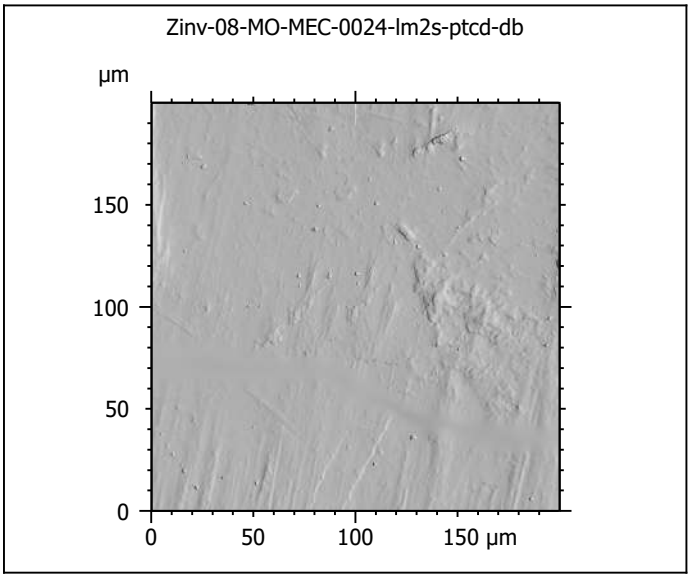

Leica Map Premium 8.0.9151

Photosimulations and false color elevation maps of scanned molar facets of the mouflon (*Ovis gmelini musimon*) from the Bauges Natural Regional Park, France
scanned at the PALEVOPRIM lab by G. Merceron , CNRS and University of Poitiers, France with "TRIDENT", white light confocal microscope Leica DCM8

ANR-13-JSV7-0008-01, PI: G. Merceron

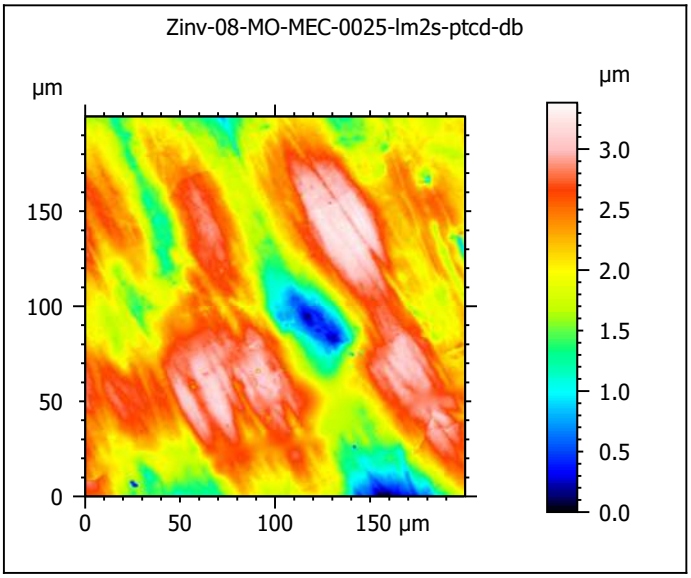

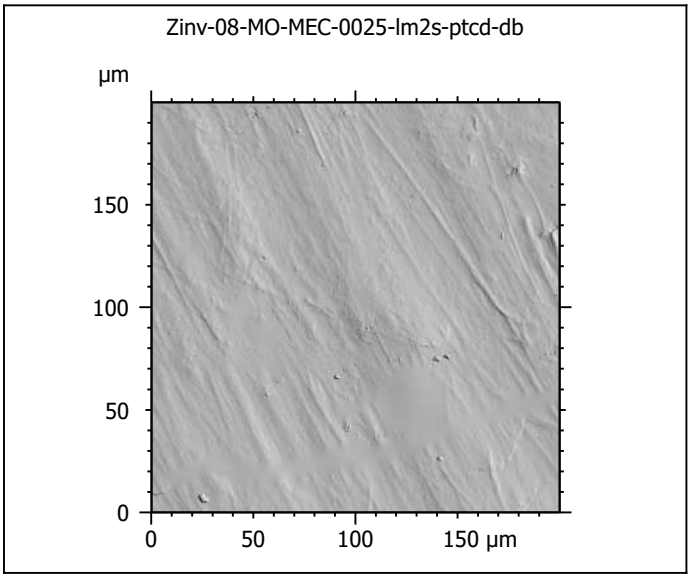

Photosimulations and false color elevation maps of scanned molar facets of the red deer (*Cervus elaphus*) from the Bauges Natural Regional Park, France scanned at the PALEVOPRIM lab by G. Merceron , CNRS and University of Poitiers, France with "TRIDENT", white light confocal microscope Leica DCM8

ANR-13-JSV7-0008-01, PI: G. Merceron

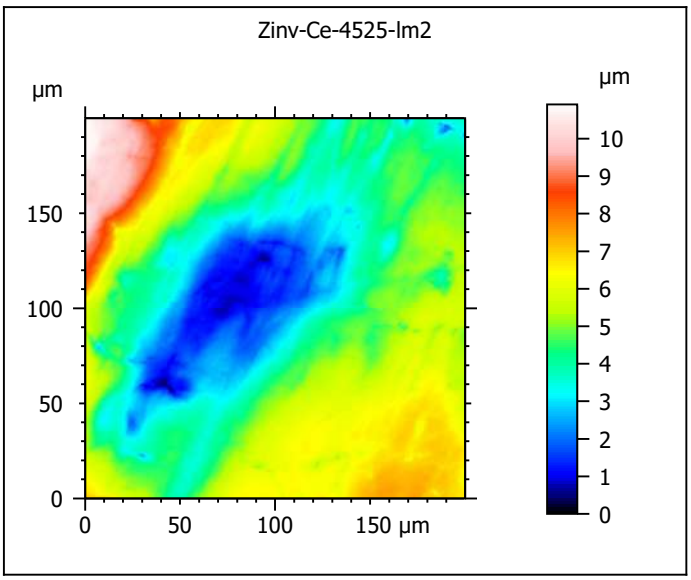

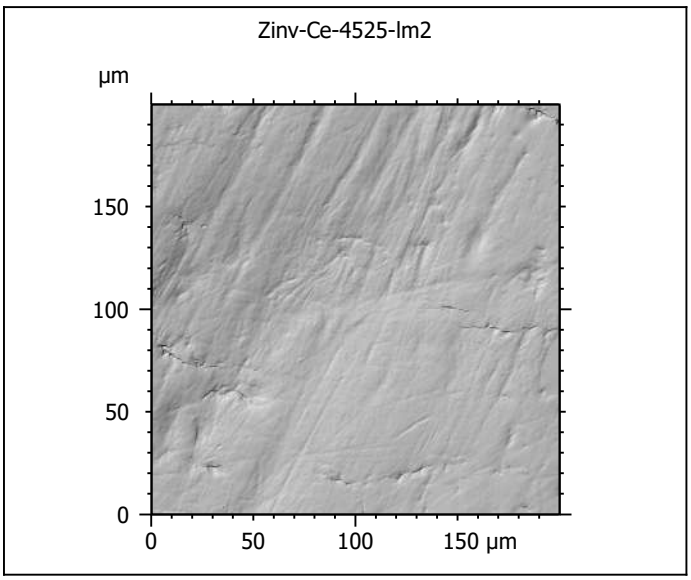

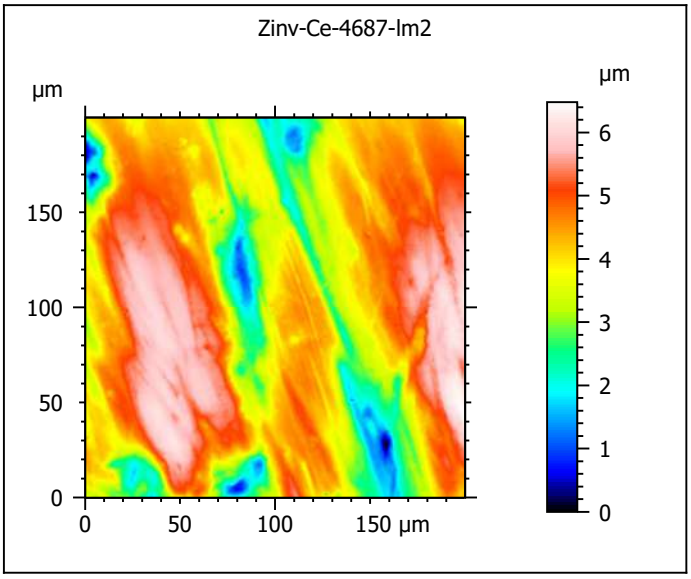

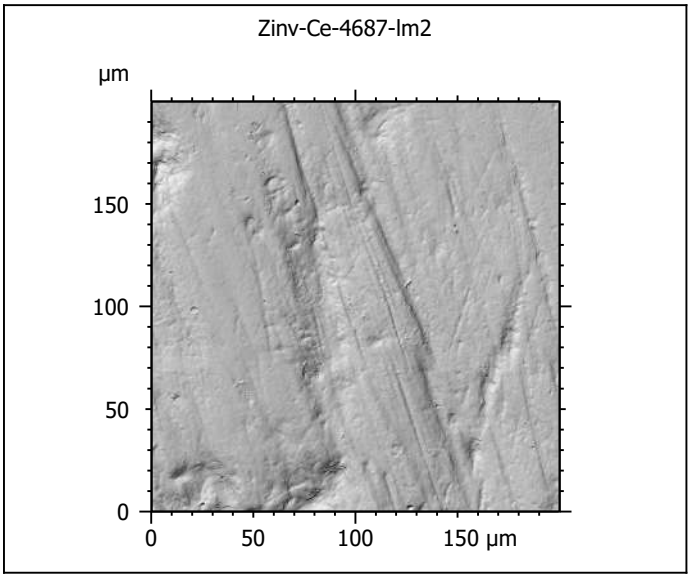

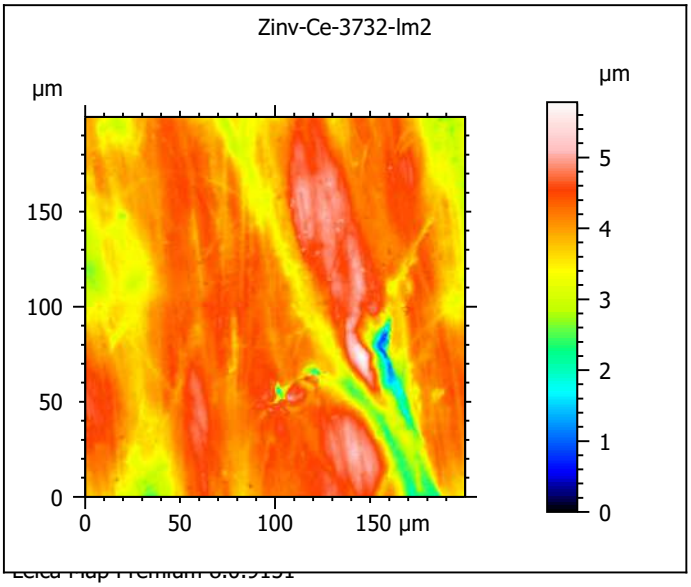

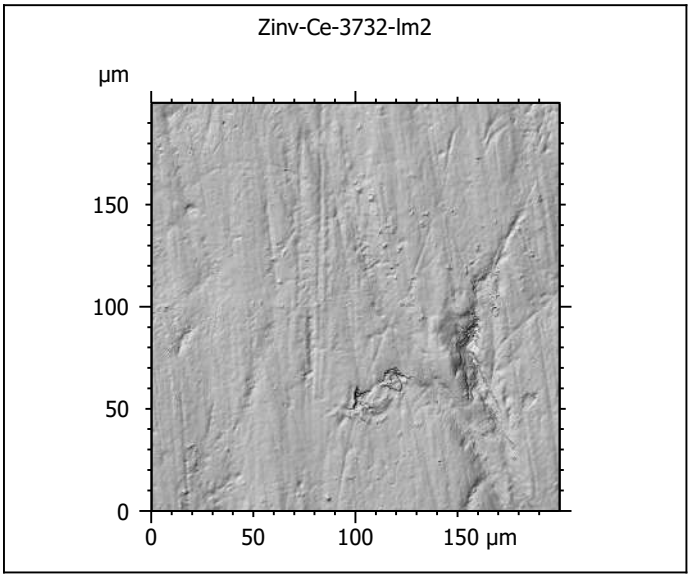

Photosimulations and false color elevation maps of scanned molar facets of the red deer (*Cervus elaphus*) from the Bauges Natural Regional Park, France scanned at the PALEVOPRIM lab by G. Merceron , CNRS and University of Poitiers, France with "TRIDENT", white light confocal microscope Leica DCM8

ANR-13-JSV7-0008-01, PI: G. Merceron

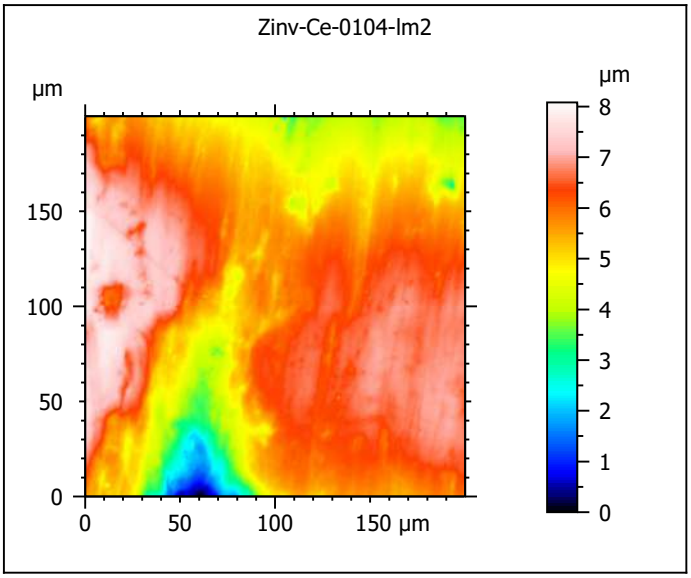

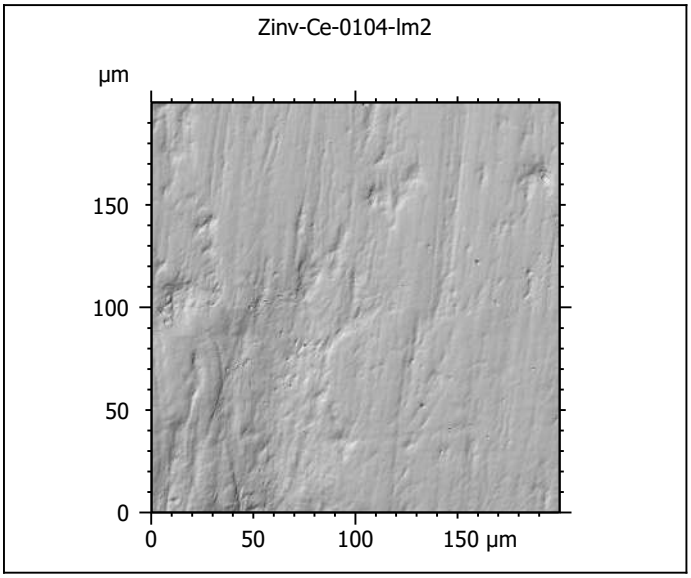

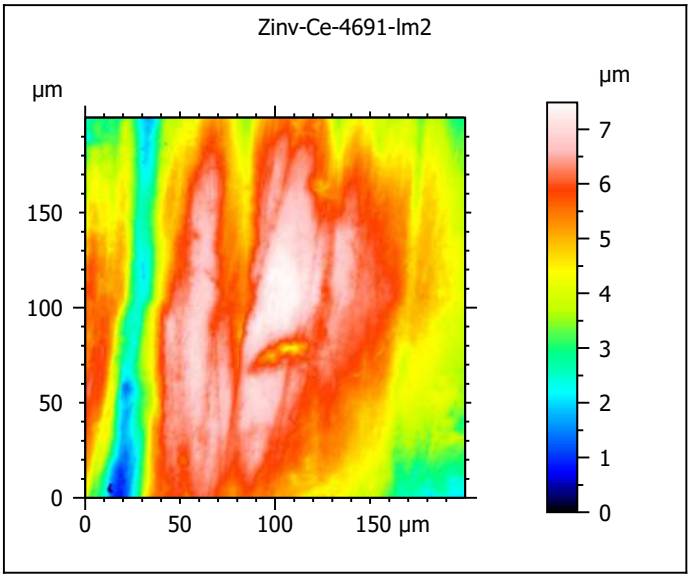

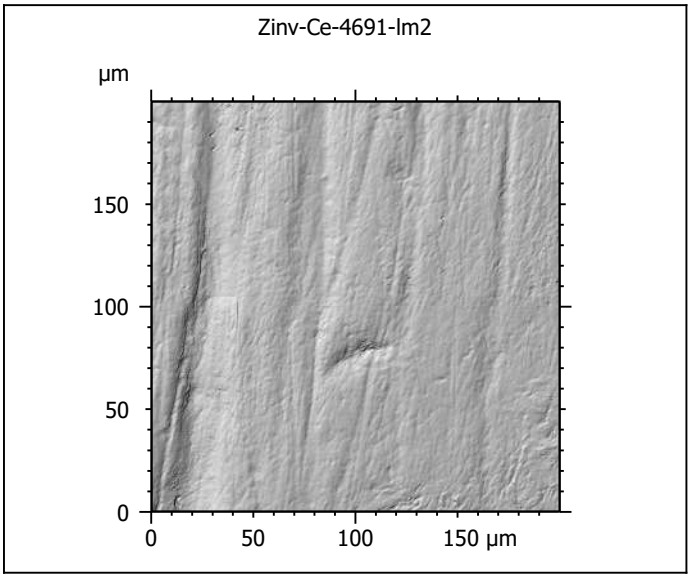

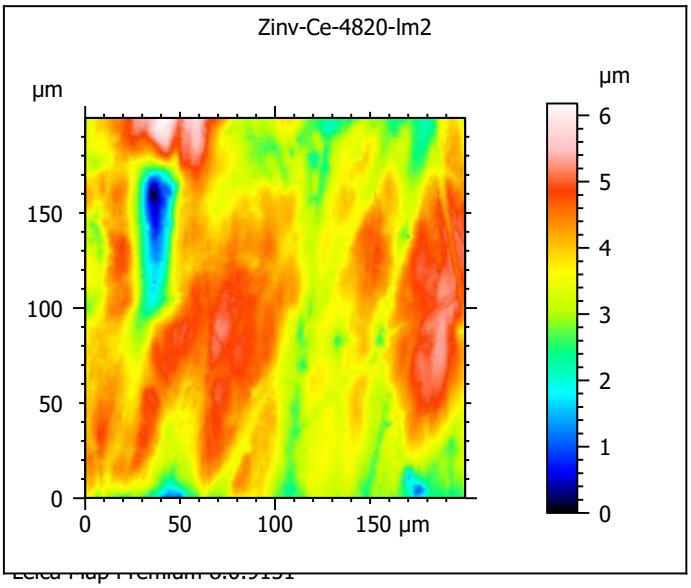

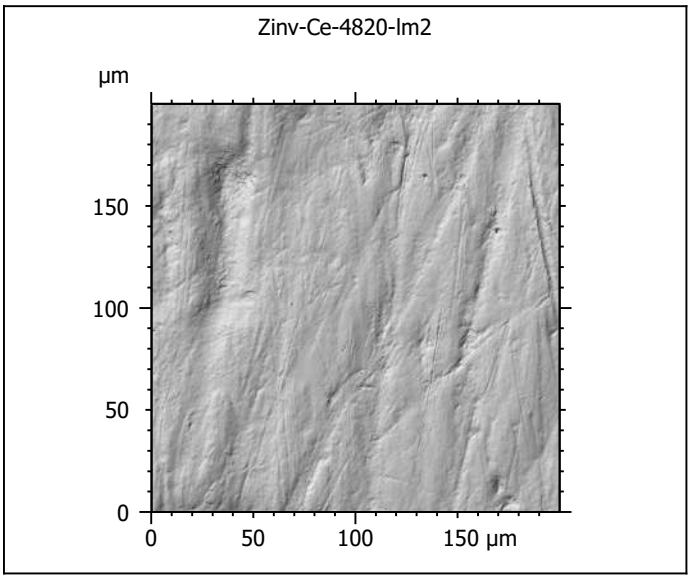

Photosimulations and false color elevation maps of scanned molar facets of the red deer (*Cervus elaphus*) from the Bauges Natural Regional Park, France scanned at the PALEVOPRIM lab by G. Merceron , CNRS and University of Poitiers, France with "TRIDENT", white light confocal microscope Leica DCM8

ANR-13-JSV7-0008-01, PI: G. Merceron

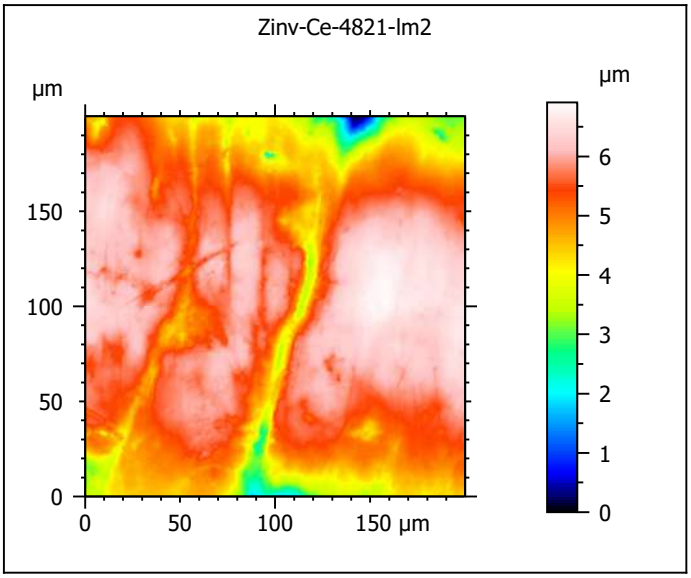

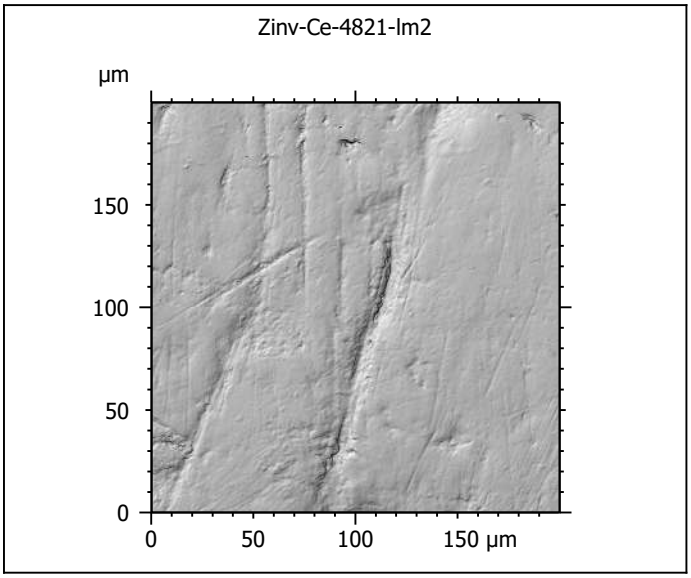

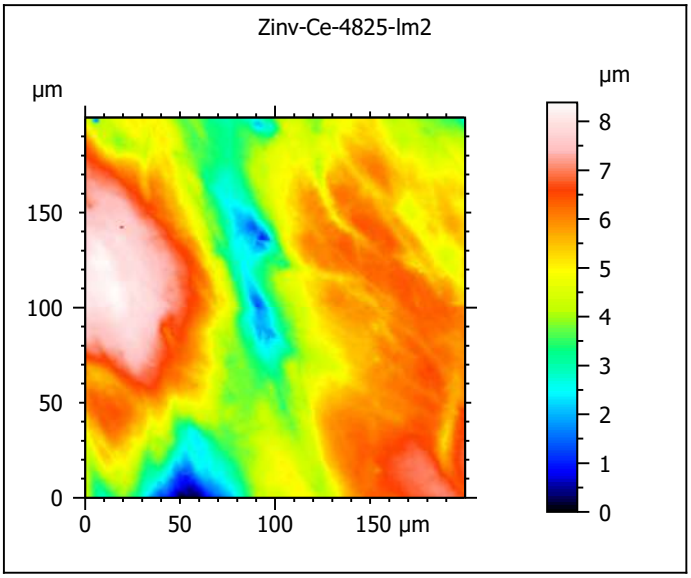

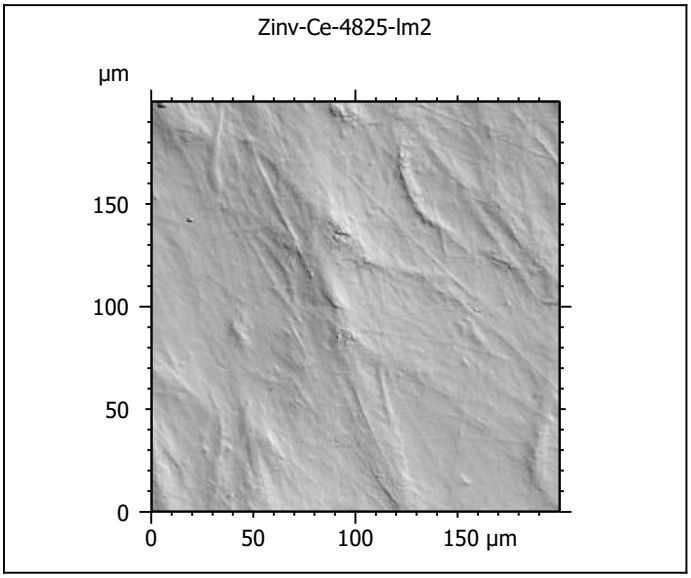

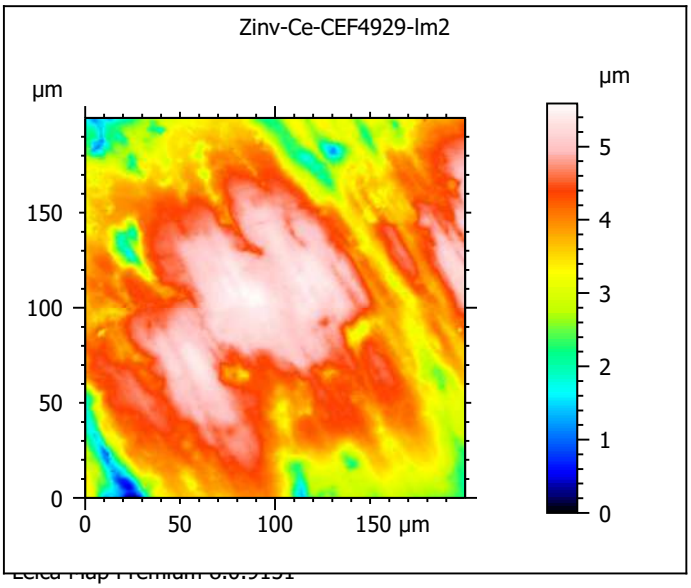

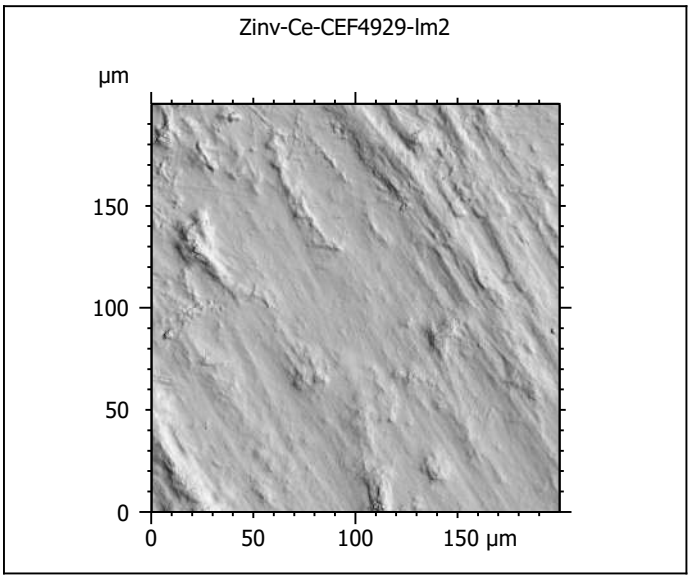

Photosimulations and false color elevation maps of scanned molar facets of the red deer (*Cervus elaphus*) from the Bauges Natural Regional Park, France scanned at the PALEVOPRIM lab by G. Merceron , CNRS and University of Poitiers, France with "TRIDENT", white light confocal microscope Leica DCM8

ANR-13-JSV7-0008-01, PI: G. Merceron

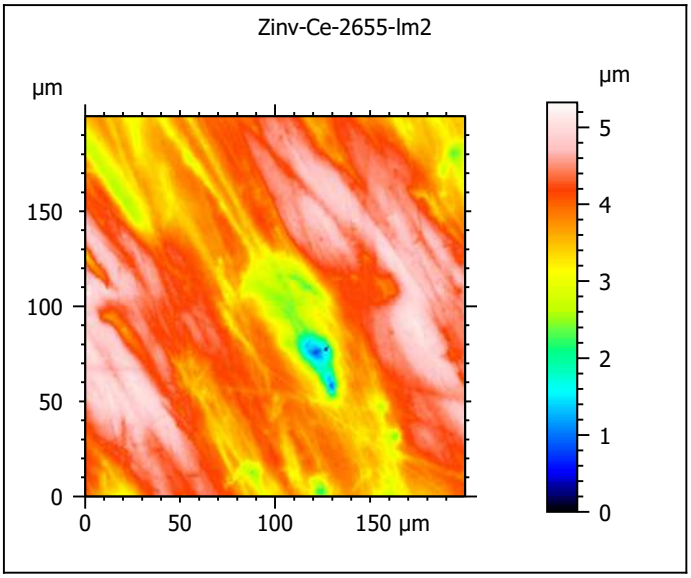

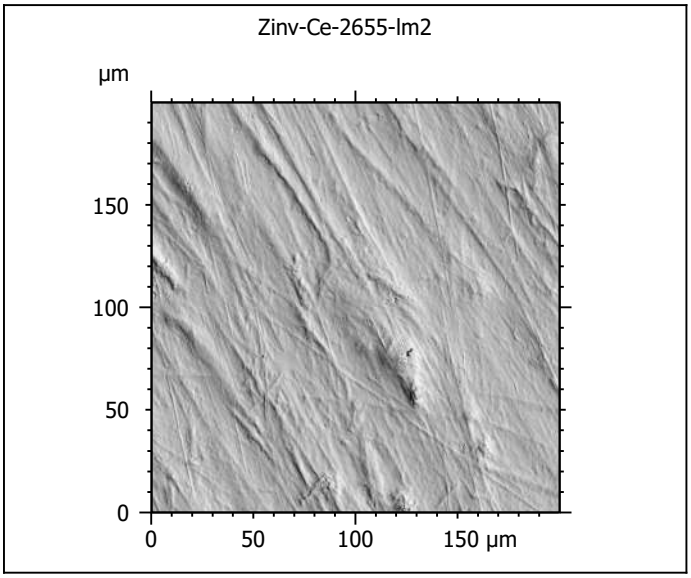

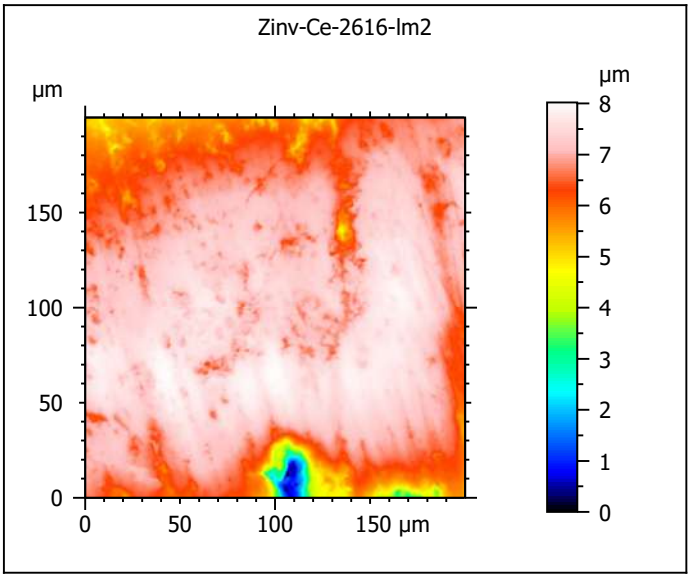

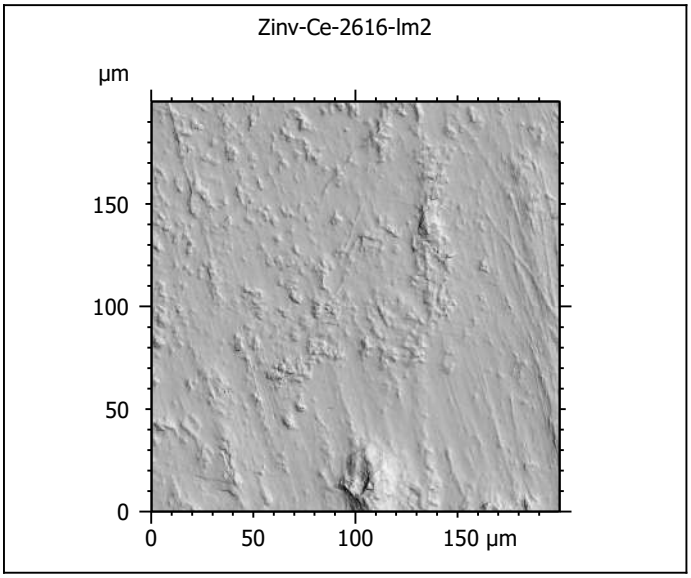

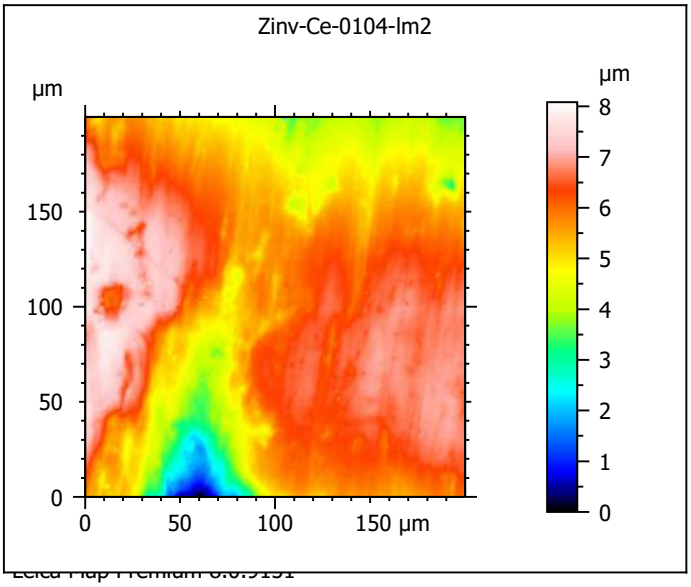

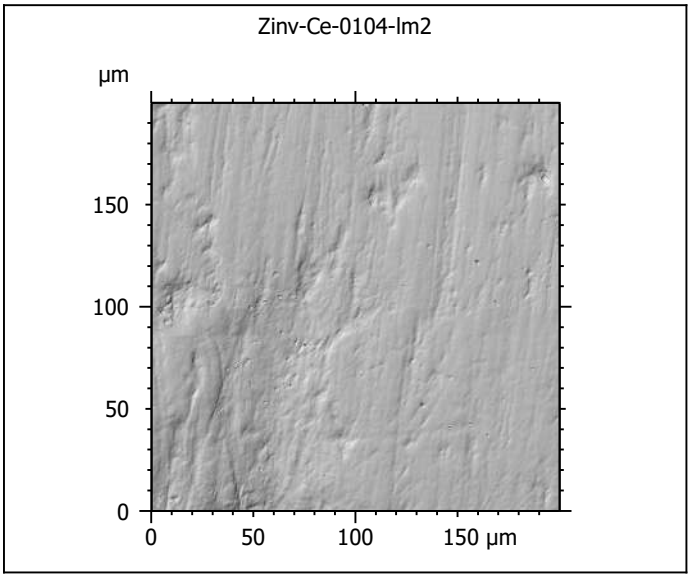

Photosimulations and false color elevation maps of scanned molar facets of the red deer (*Cervus elaphus*) from the Bauges Natural Regional Park, France scanned at the PALEVOPRIM lab by G. Merceron , CNRS and University of Poitiers, France with "TRIDENT", white light confocal microscope Leica DCM8

ANR-13-JSV7-0008-01, PI: G. Merceron

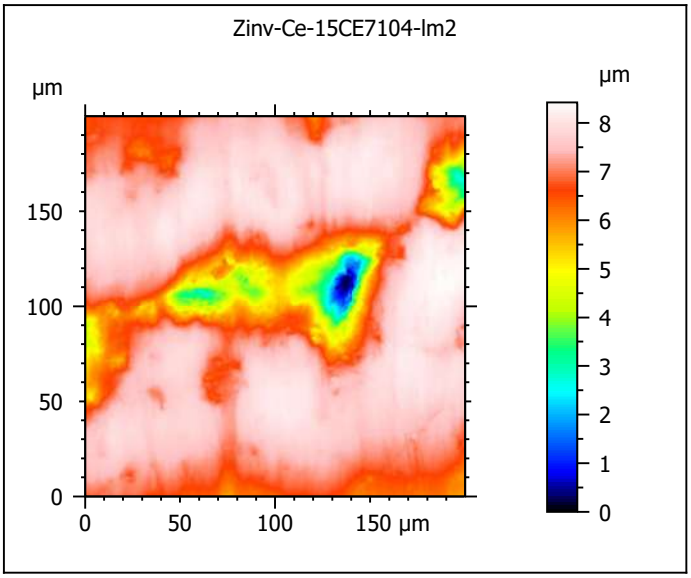

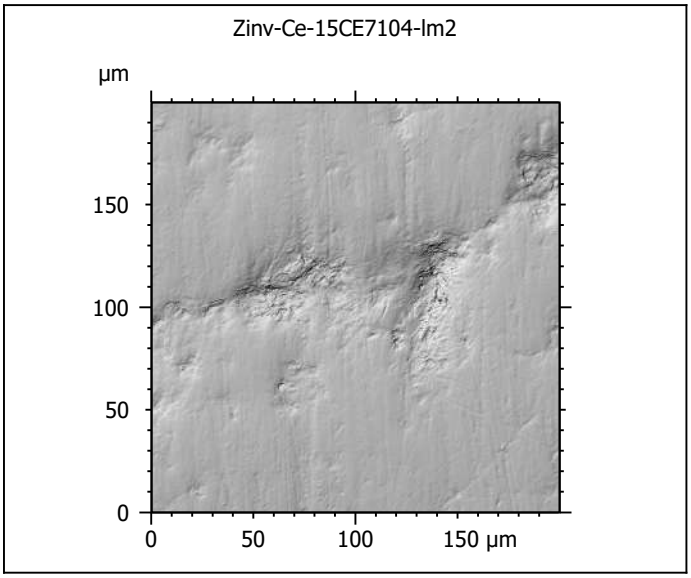

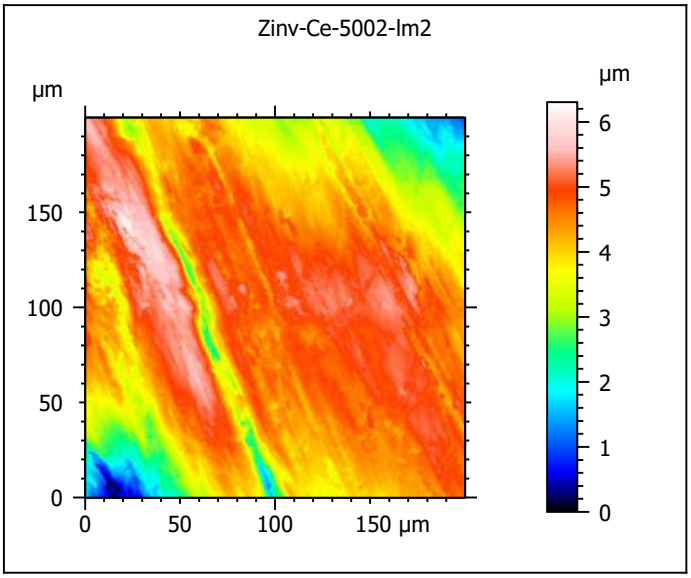

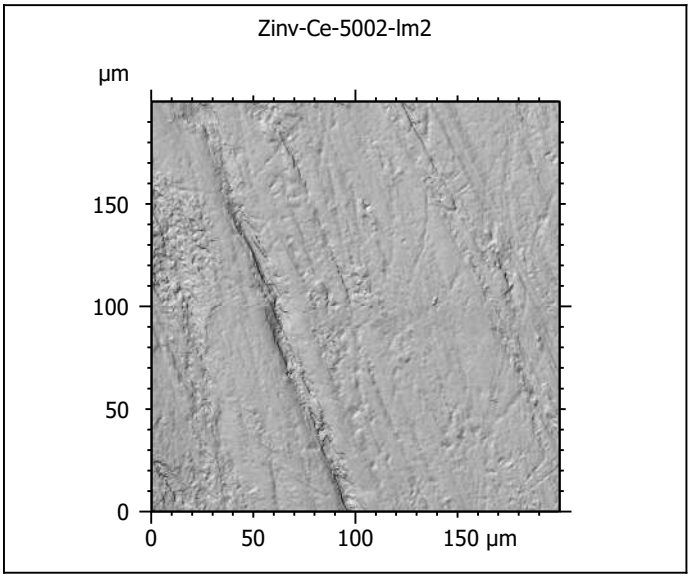

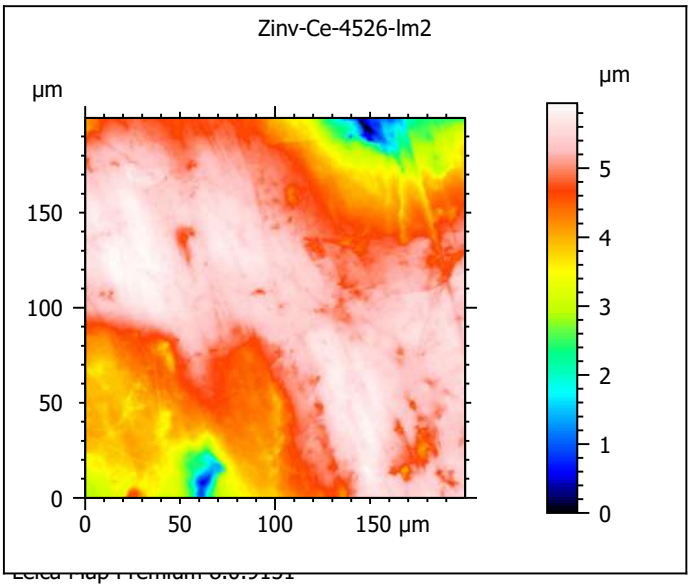

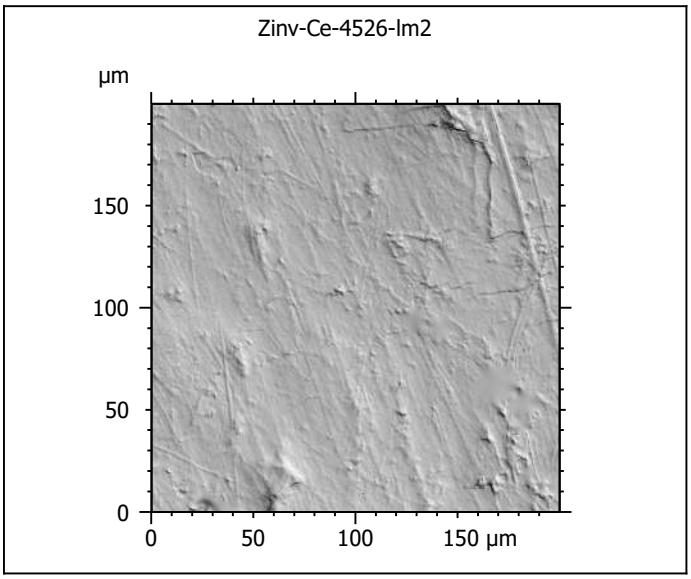

Photosimulations and false color elevation maps of scanned molar facets of the red deer (*Cervus elaphus*) from the Bauges Natural Regional Park, France scanned at the PALEVOPRIM lab by G. Merceron , CNRS and University of Poitiers, France with "TRIDENT", white light confocal microscope Leica DCM8

ANR-13-JSV7-0008-01, PI: G. Merceron

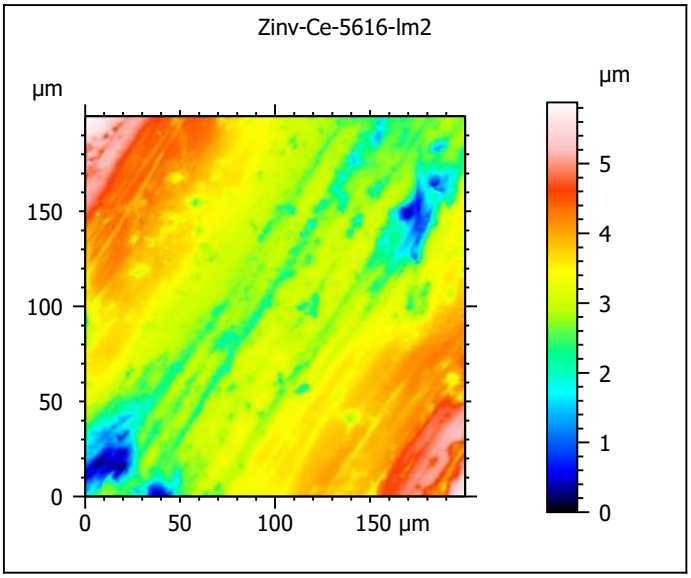

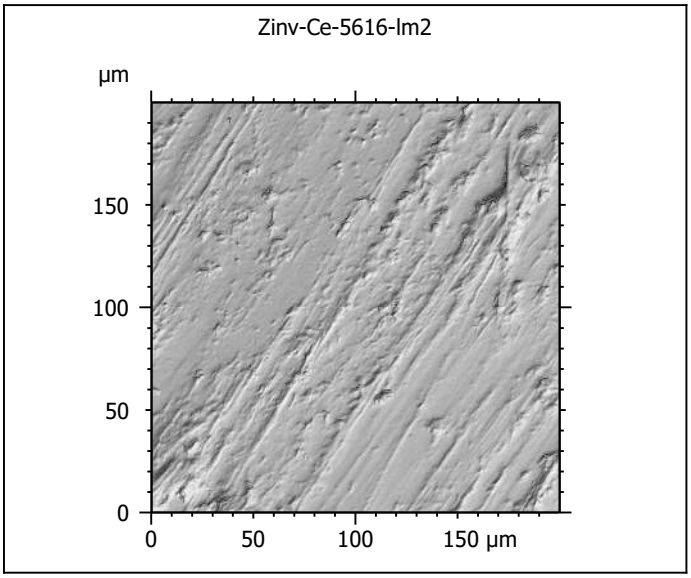

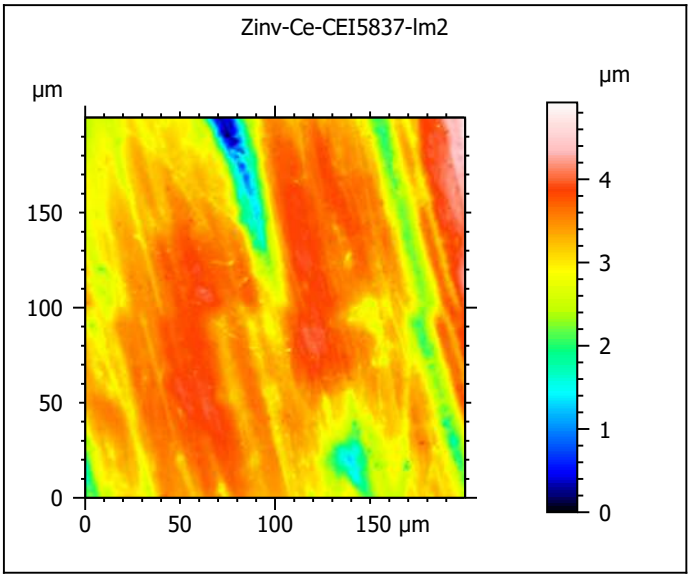

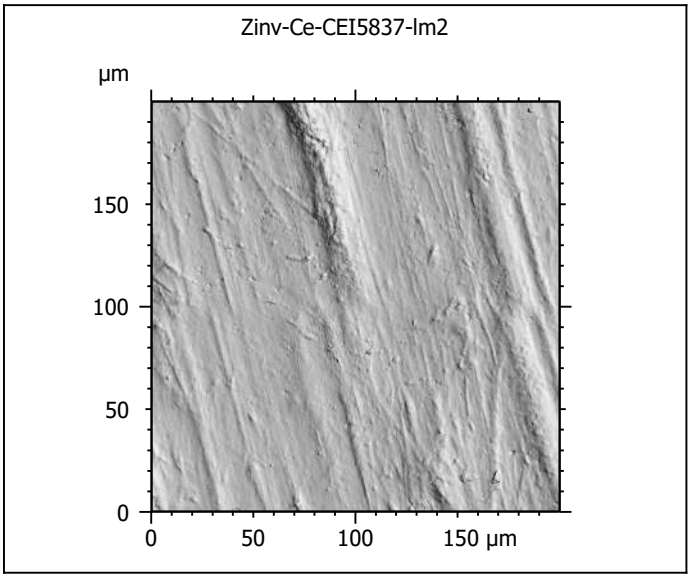

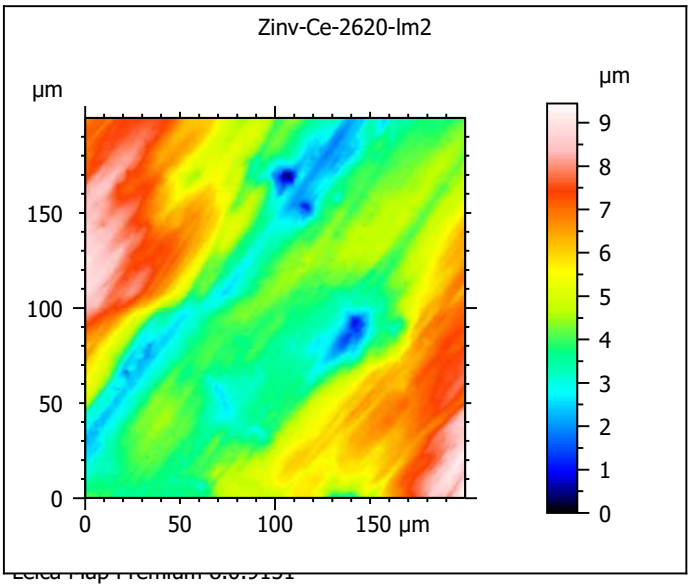

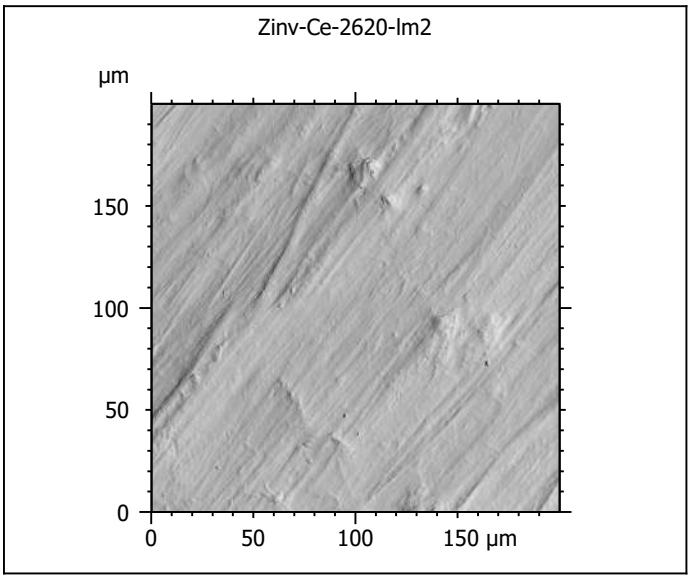

Photosimulations and false color elevation maps of scanned molar facets of the red deer (*Cervus elaphus*) from the Bauges Natural Regional Park, France scanned at the PALEVOPRIM lab by G. Merceron , CNRS and University of Poitiers, France with "TRIDENT", white light confocal microscope Leica DCM8

ANR-13-JSV7-0008-01, PI: G. Merceron

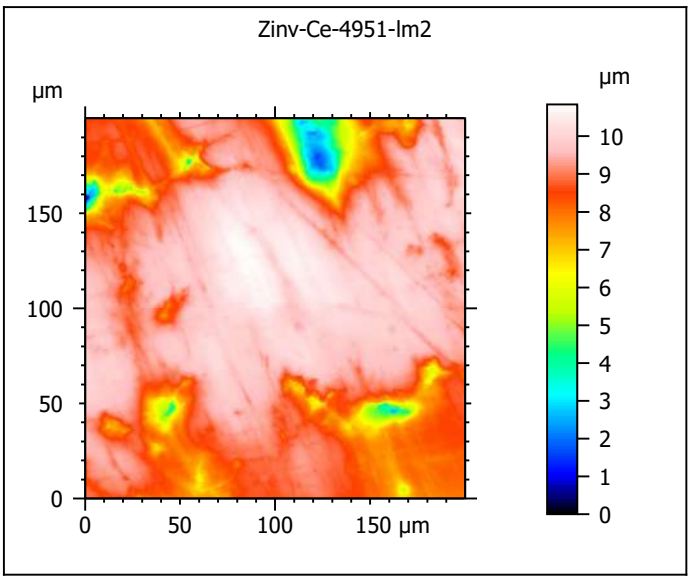

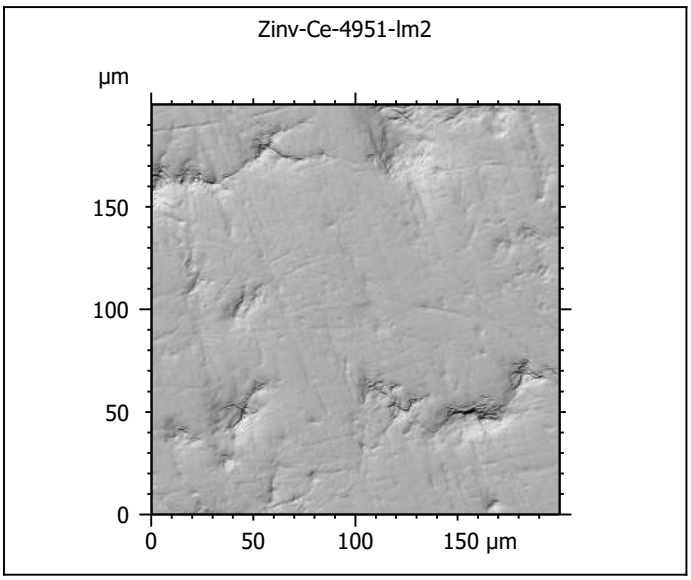

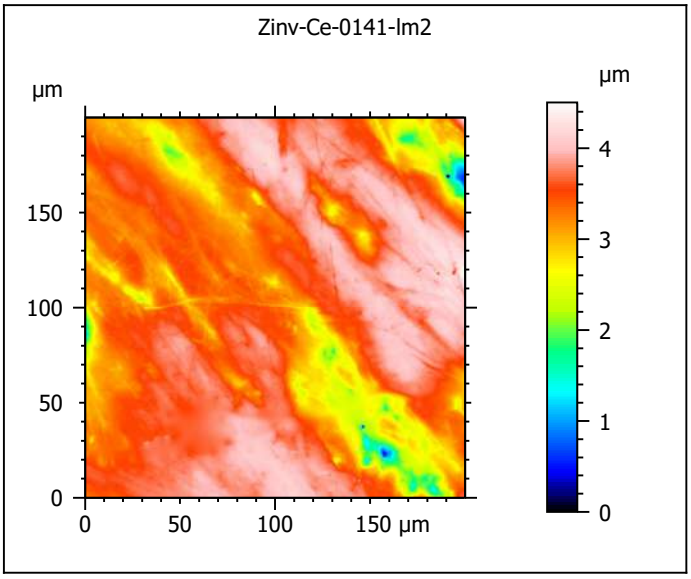

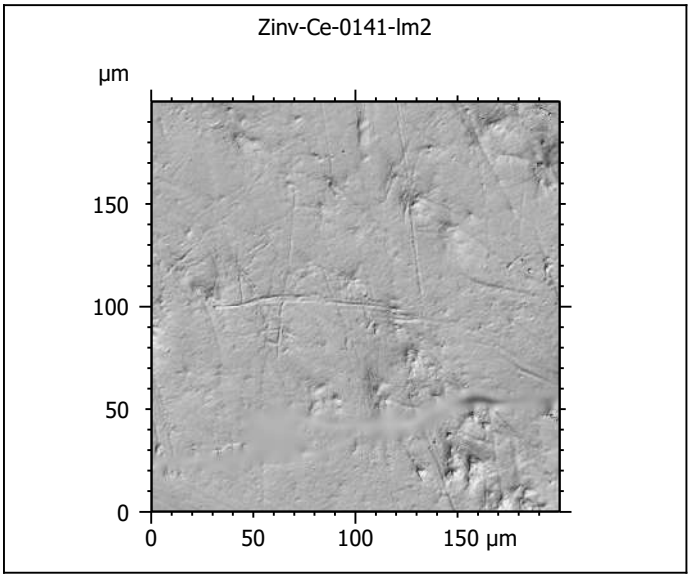

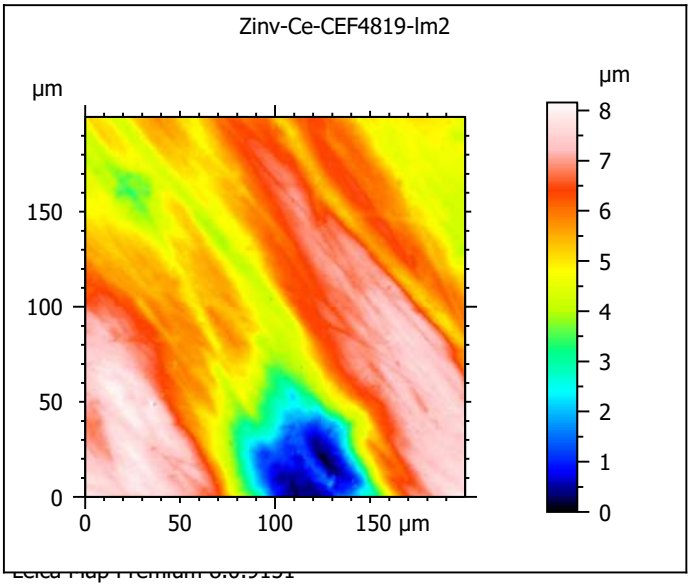

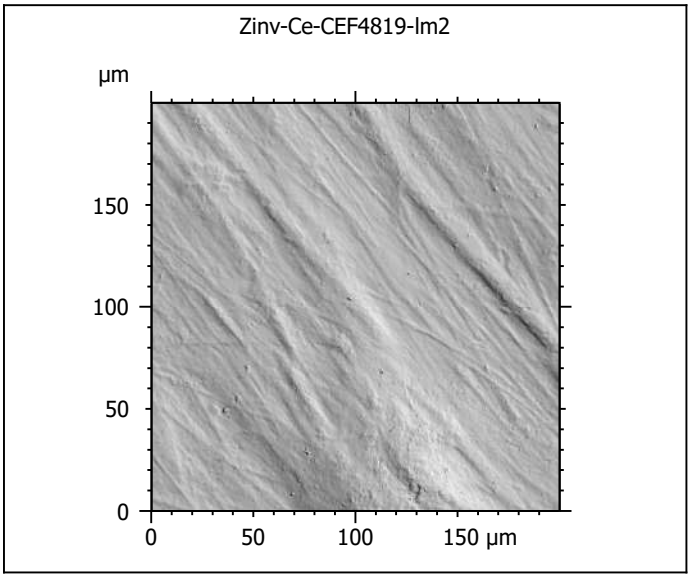

Leica Map Premium 8.0.9151

Photosimulations and false color elevation maps of scanned molar facets of the roe deer (*Capreolus capreolus*) from the Bauges Natural Regional Park, France
scanned at the PALEVOPRIM lab by G. Merceron , CNRS and University of Poitiers, France with "TRIDENT", white light confocal microscope Leica DCM8

ANR-13-JSV7-0008-01, PI: G. Merceron

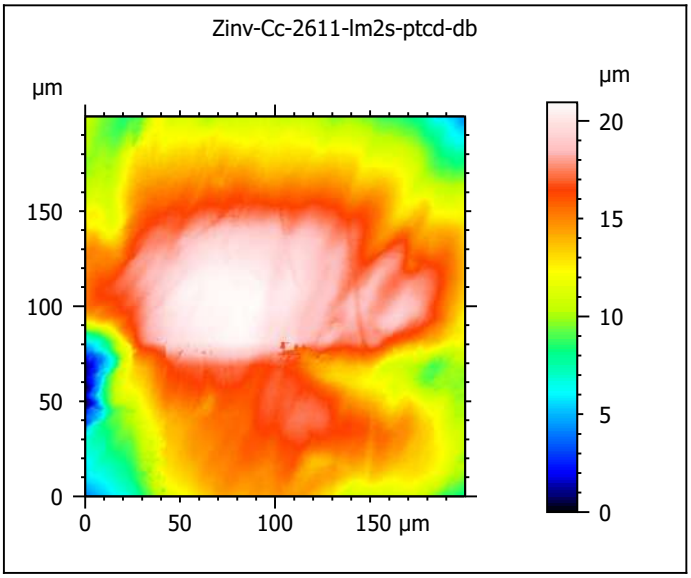

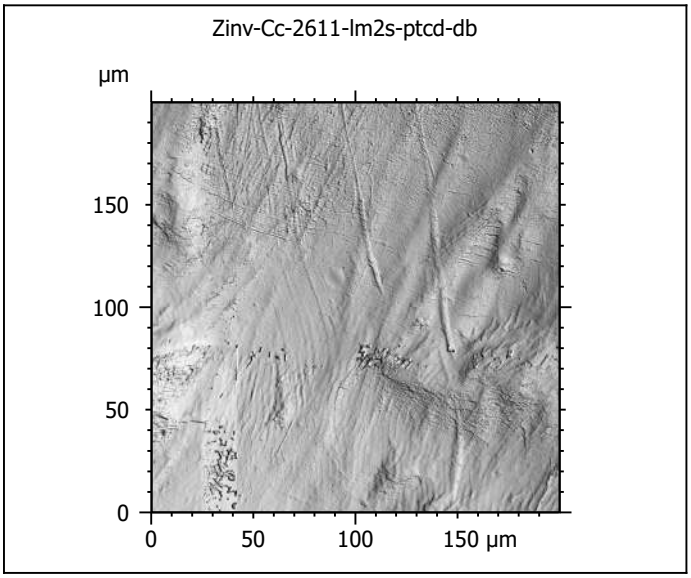

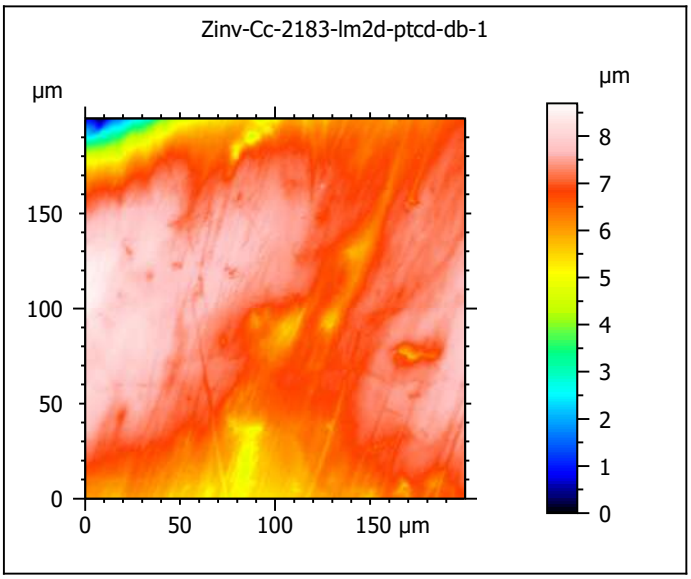

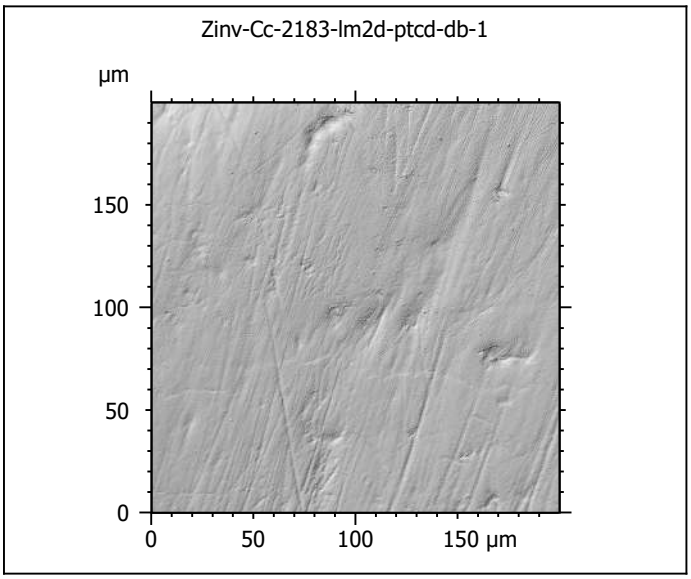

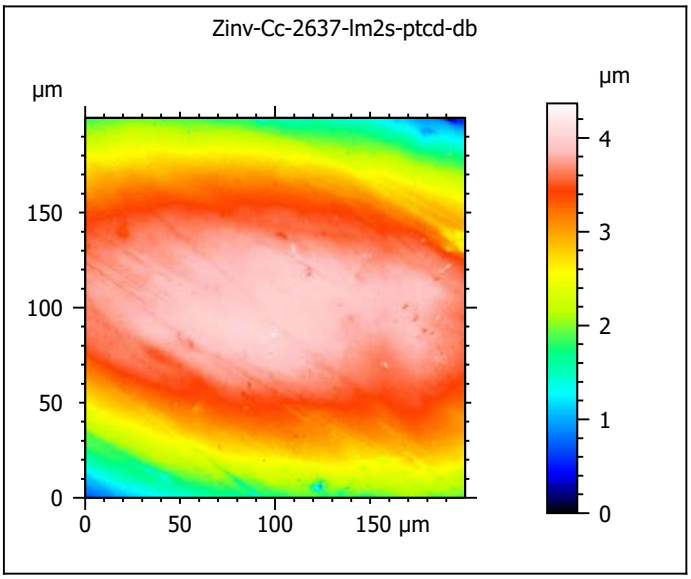

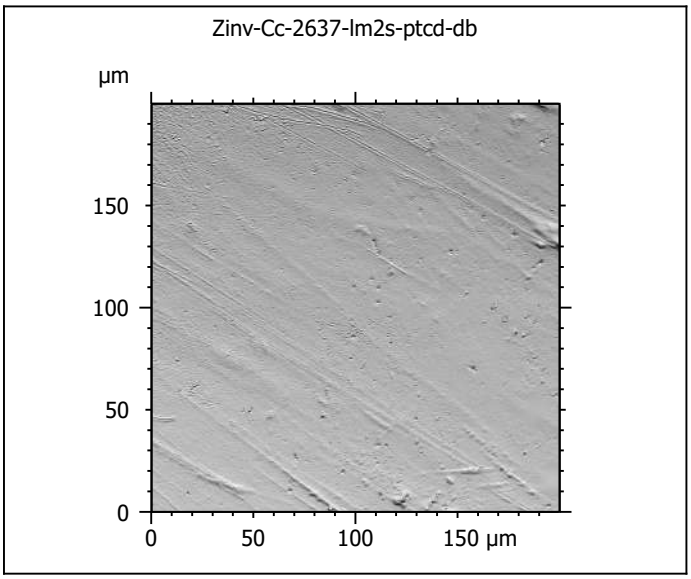

Leica Map Premium 8.0.9151

Photosimulations and false color elevation maps of scanned molar facets of the roe deer (*Capreolus capreolus*) from the Bauges Natural Regional Park, France
scanned at the PALEVOPRIM lab by G. Merceron , CNRS and University of Poitiers, France with "TRIDENT", white light confocal microscope Leica DCM8

ANR-13-JSV7-0008-01, PI: G. Merceron

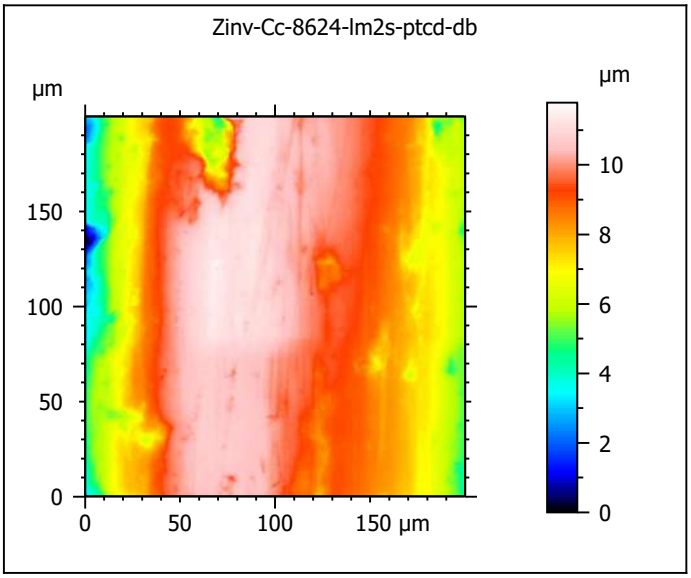

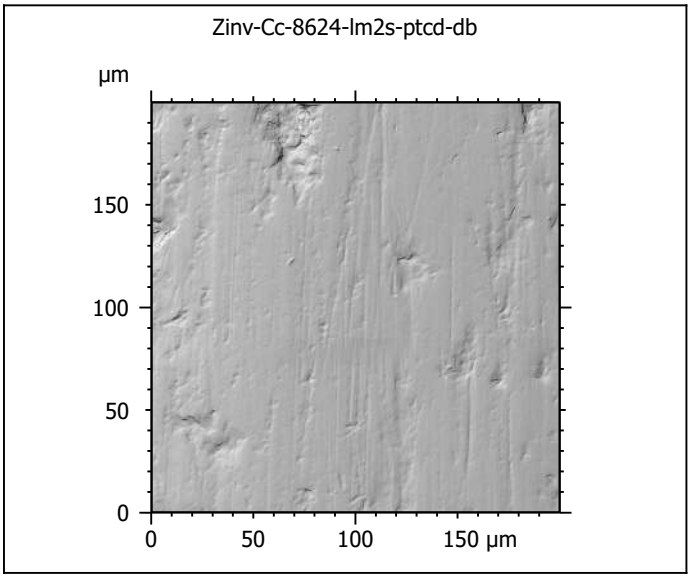

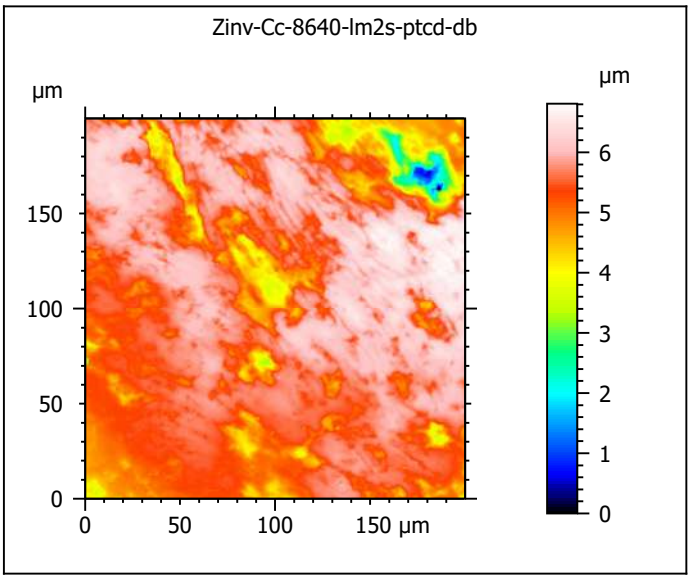

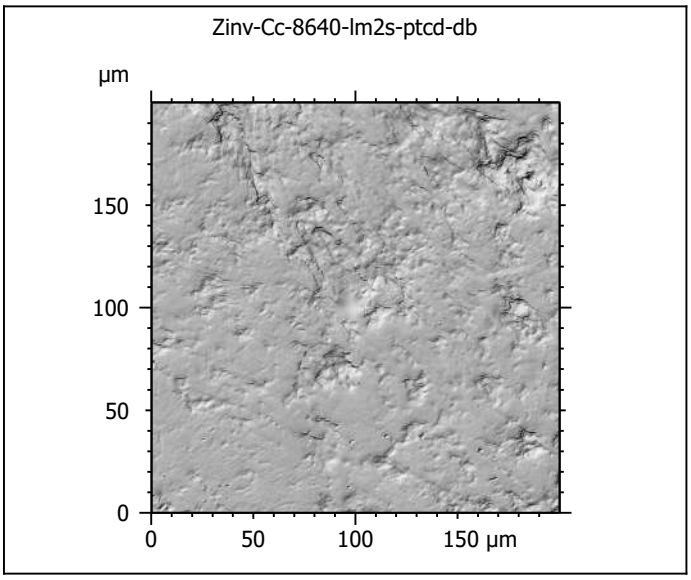

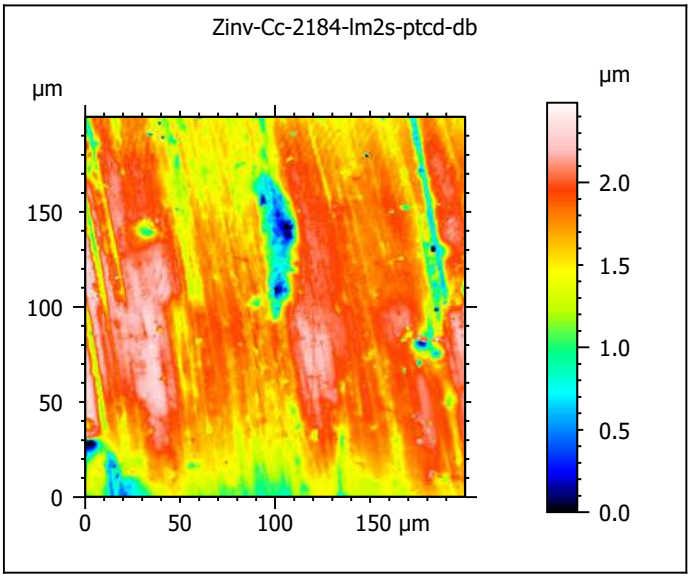

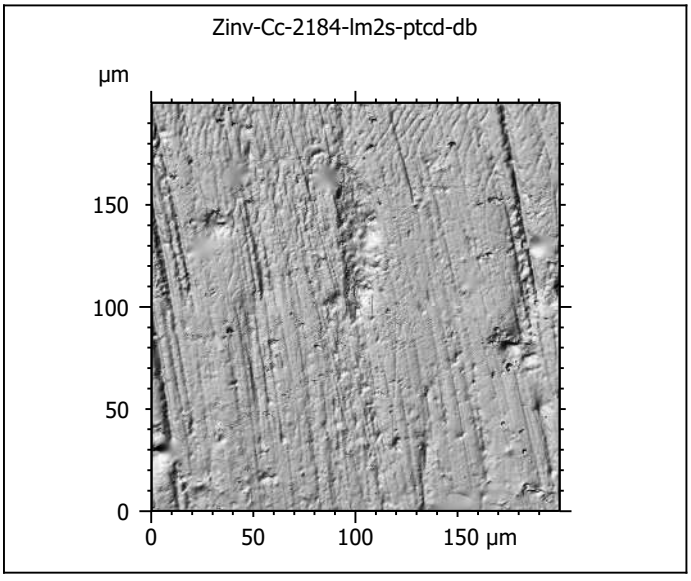

Leica Map Premium 8.0.9151

Photosimulations and false color elevation maps of scanned molar facets of the roe deer (*Capreolus capreolus*) from the Bauges Natural Regional Park, France
scanned at the PALEVOPRIM lab by G. Merceron , CNRS and University of Poitiers, France with "TRIDENT", white light confocal microscope Leica DCM8

ANR-13-JSV7-0008-01, PI: G. Merceron

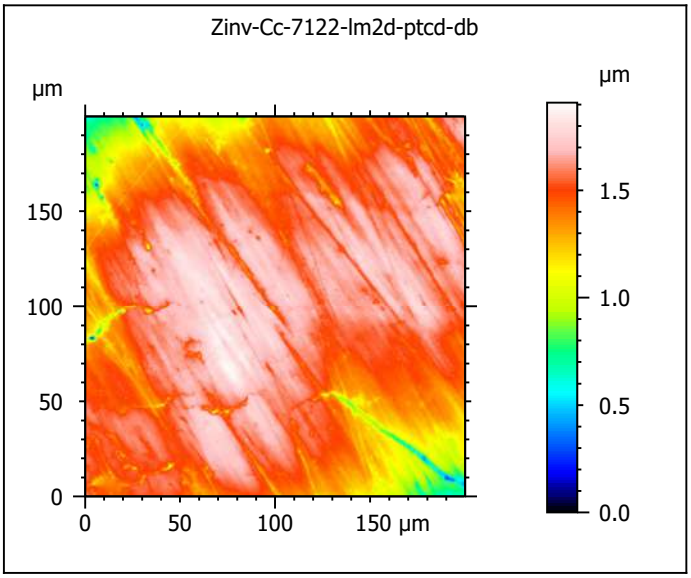

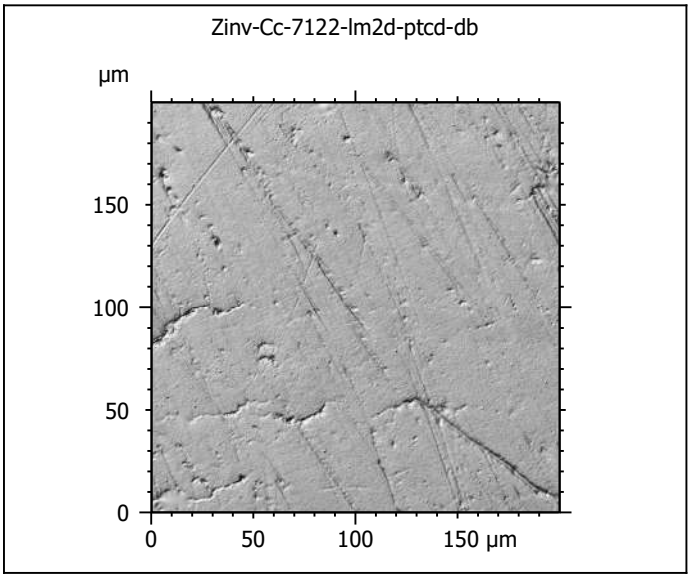

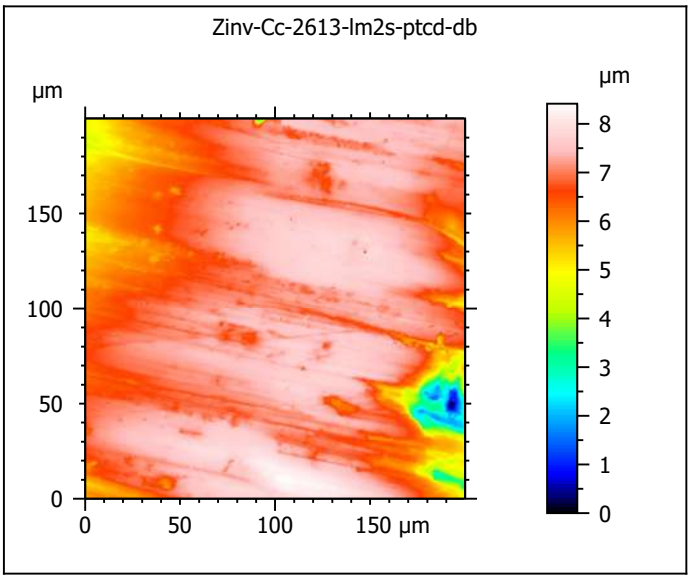

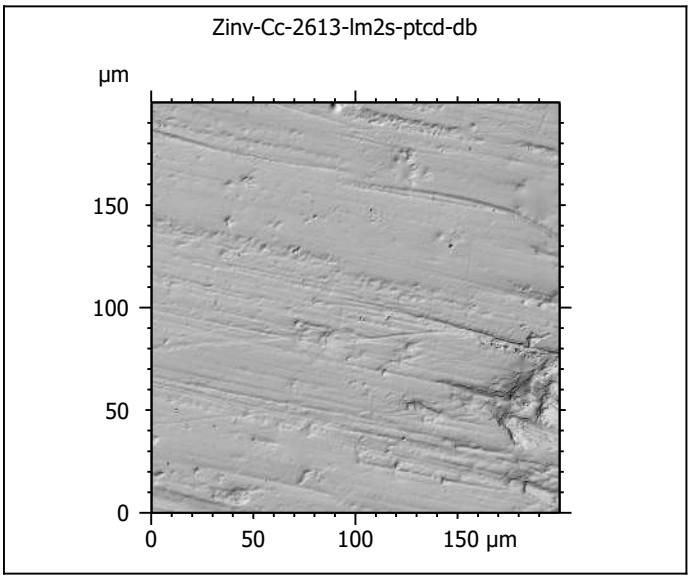

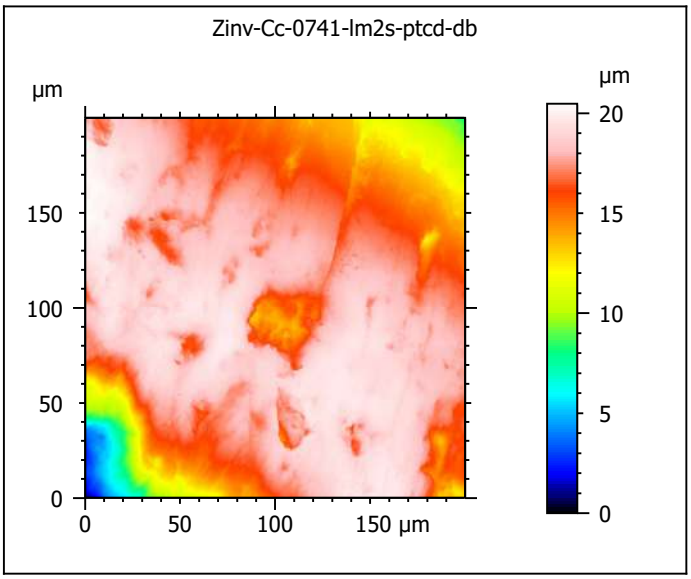

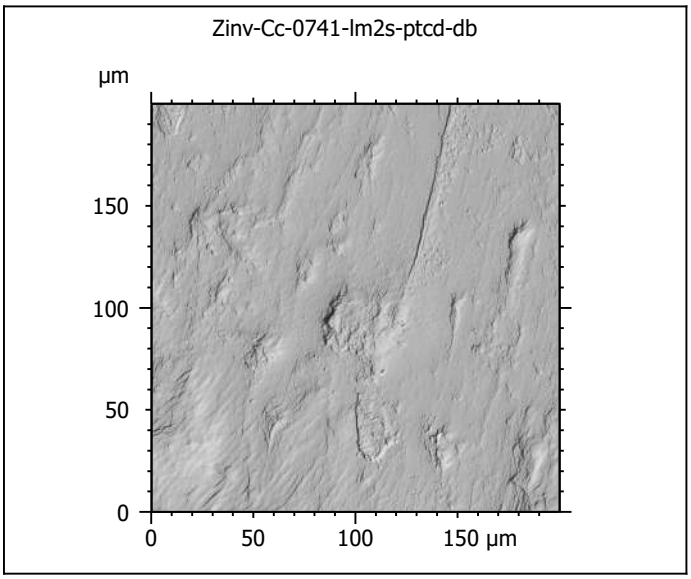

Leica Map Premium 8.0.9151

Photosimulations and false color elevation maps of scanned molar facets of the roe deer (*Capreolus capreolus*) from the Bauges Natural Regional Park, France
scanned at the PALEVOPRIM lab by G. Merceron , CNRS and University of Poitiers, France with "TRIDENT", white light confocal microscope Leica DCM8

ANR-13-JSV7-0008-01, PI: G. Merceron

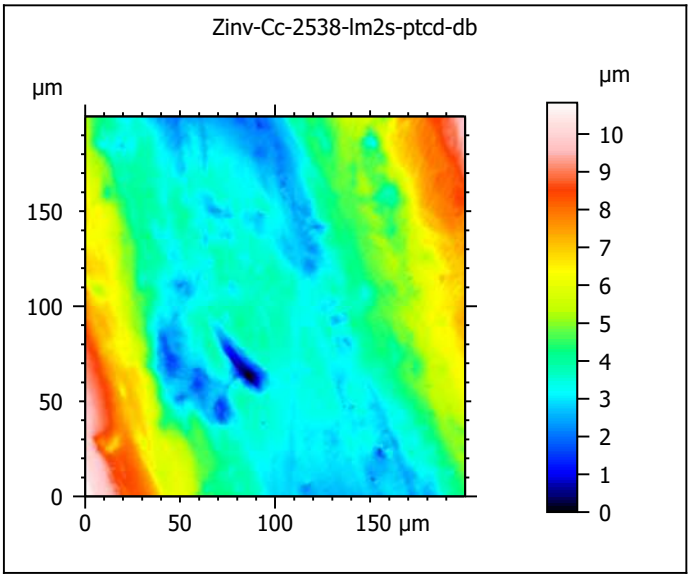

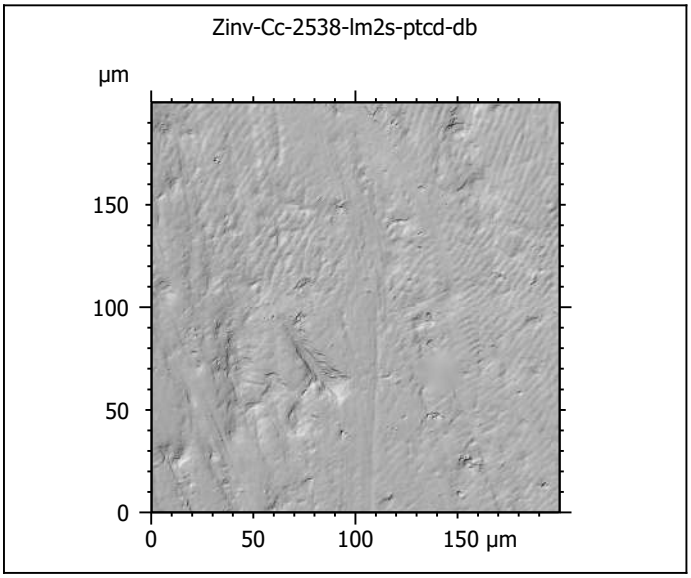

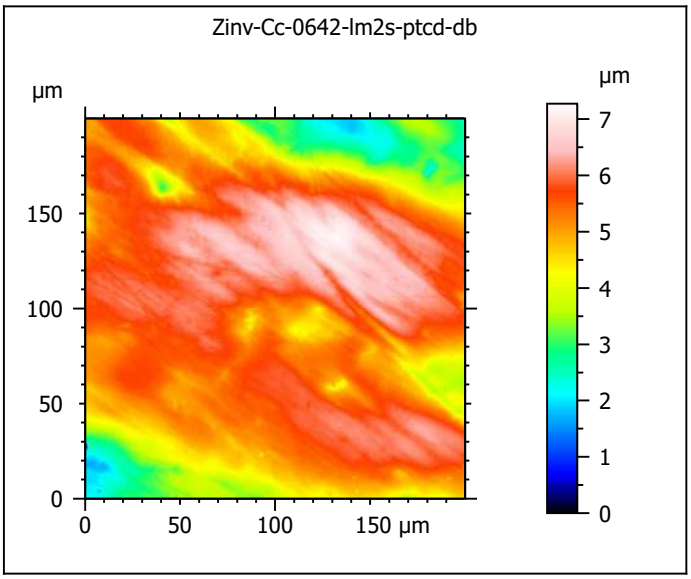

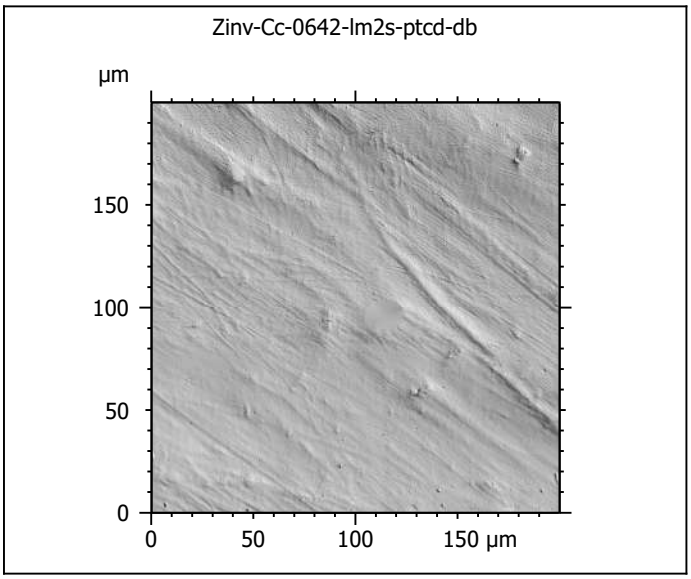

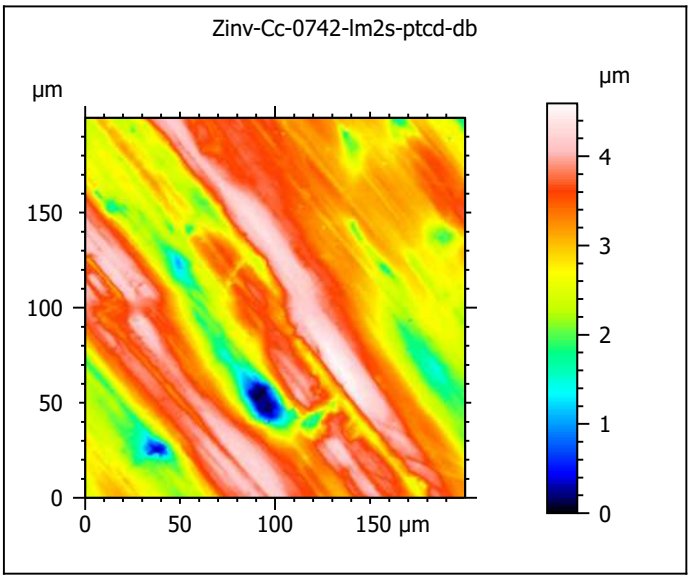

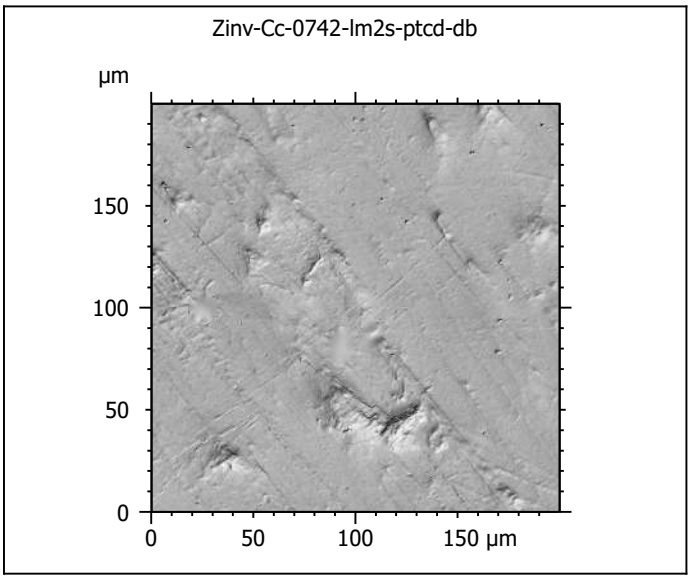

Leica Map Premium 8.0.9151

Photosimulations and false color elevation maps of scanned molar facets of the roe deer (*Capreolus capreolus*) from the Bauges Natural Regional Park, France
scanned at the PALEVOPRIM lab by G. Merceron , CNRS and University of Poitiers, France with "TRIDENT", white light confocal microscope Leica DCM8

ANR-13-JSV7-0008-01, PI: G. Merceron

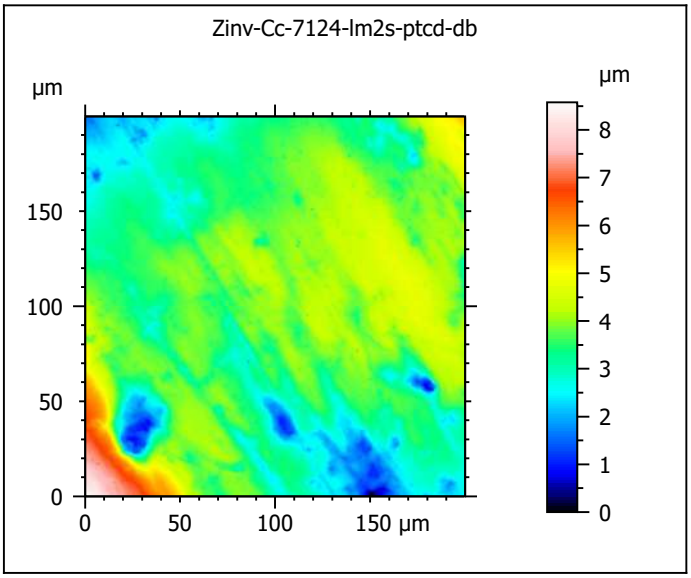

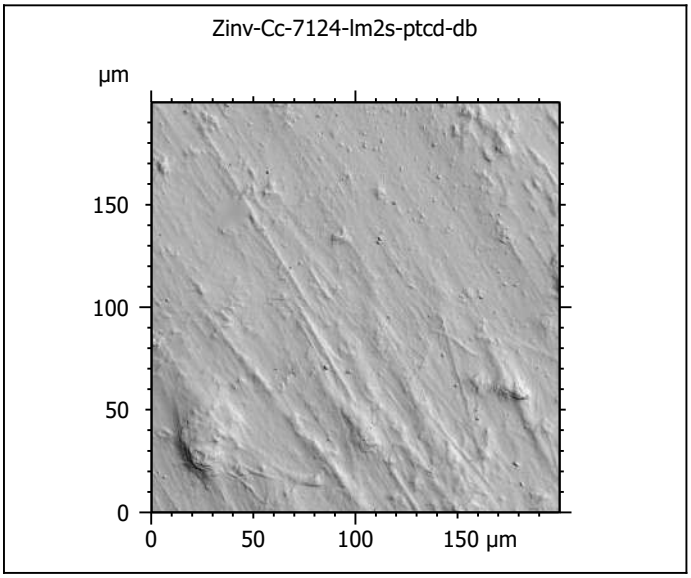

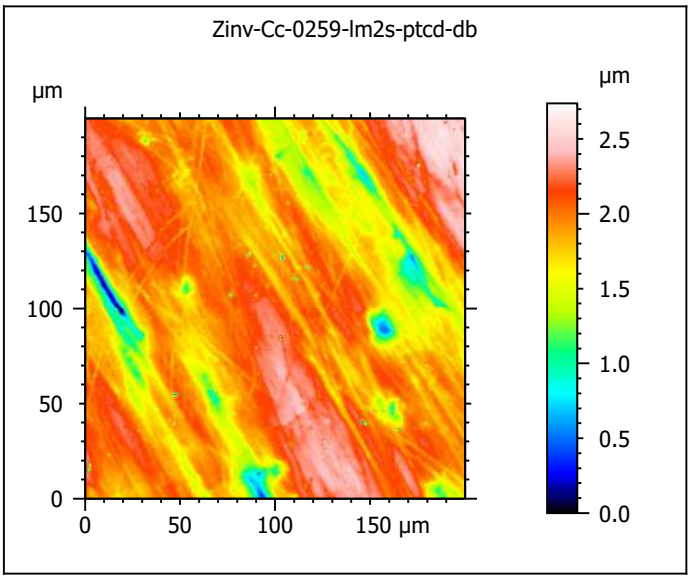

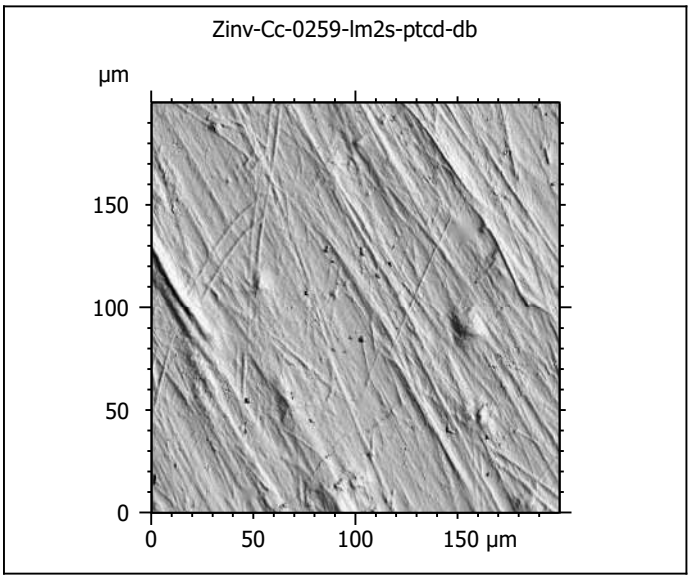

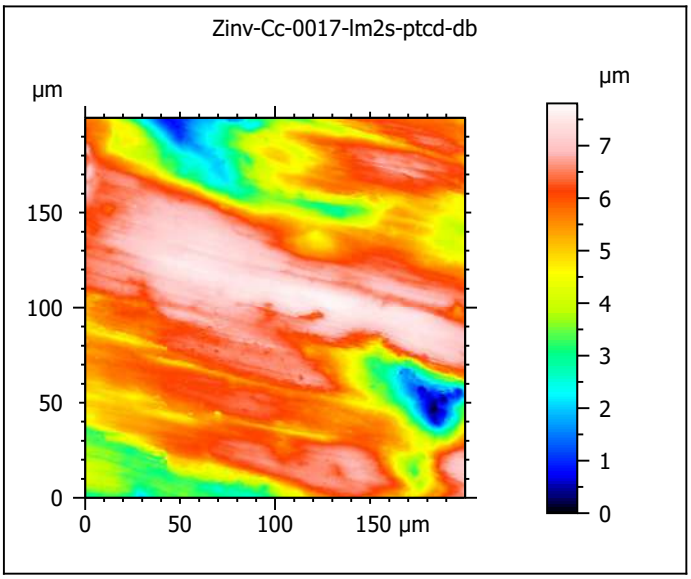

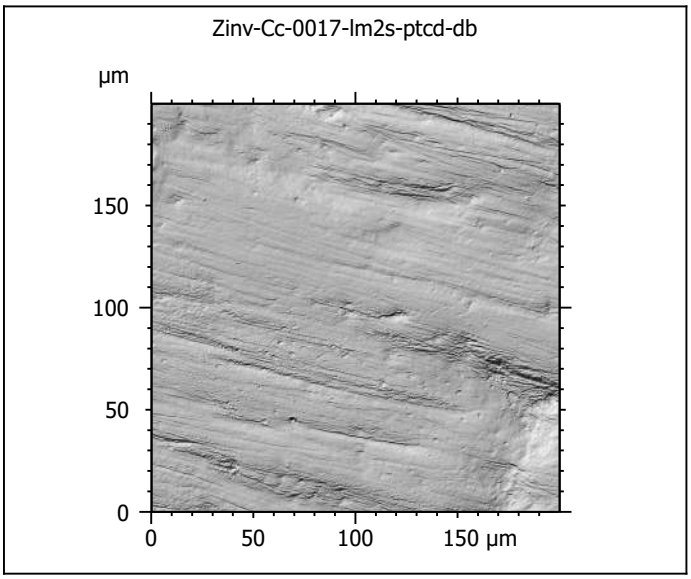

Leica Map Premium 8.0.9151

Photosimulations and false color elevation maps of scanned molar facets of the roe deer (*Capreolus capreolus*) from the Bauges Natural Regional Park, France
scanned at the PALEVOPRIM lab by G. Merceron , CNRS and University of Poitiers, France with "TRIDENT", white light confocal microscope Leica DCM8

ANR-13-JSV7-0008-01, PI: G. Merceron

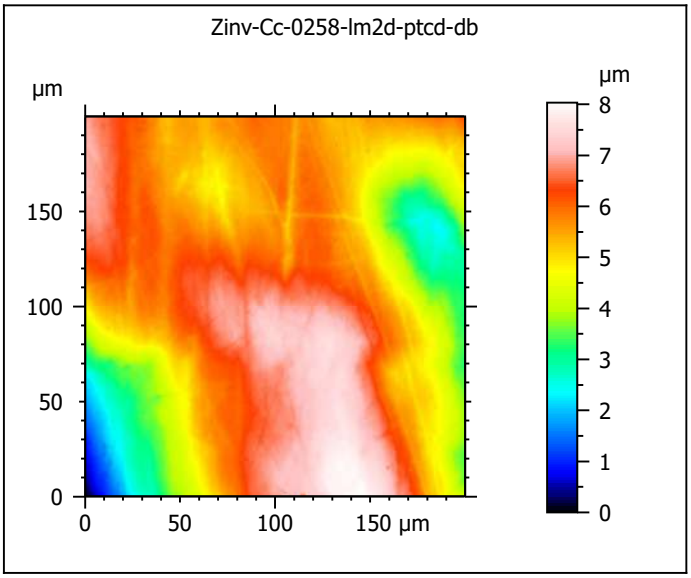

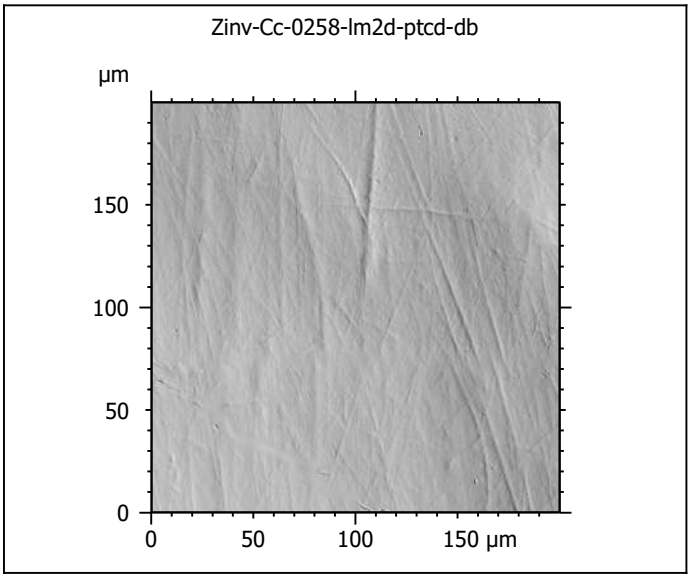

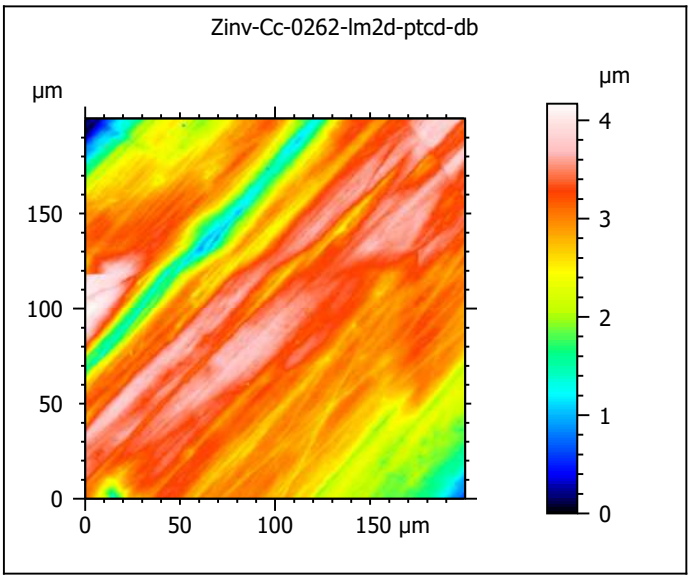

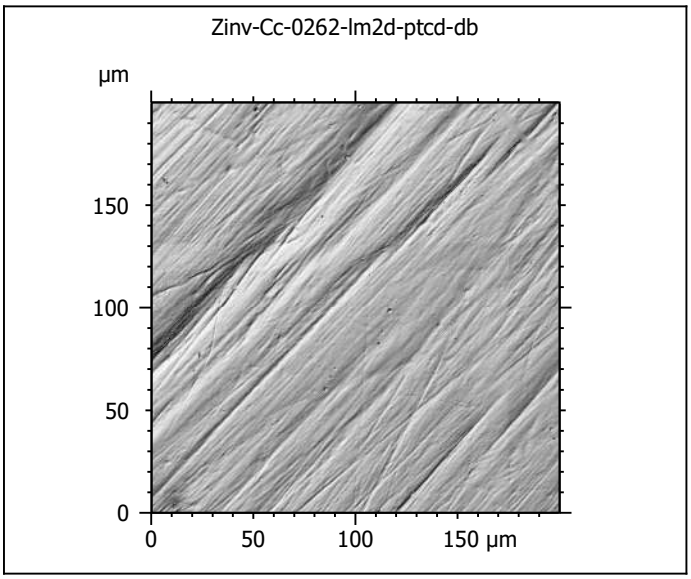

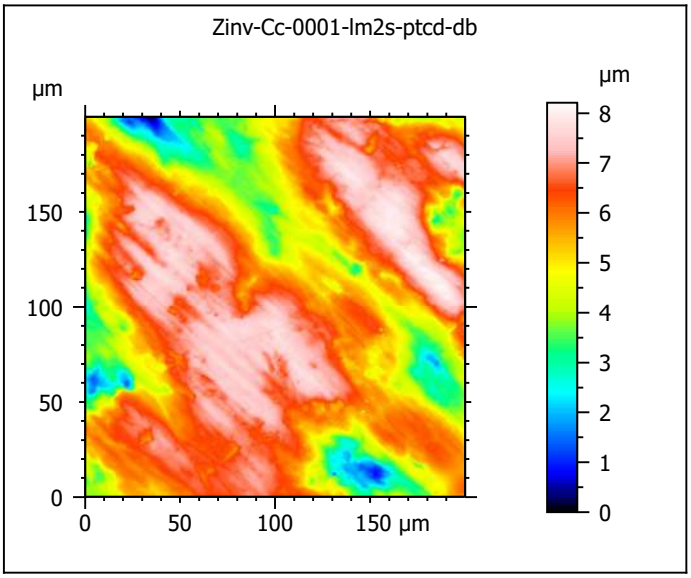

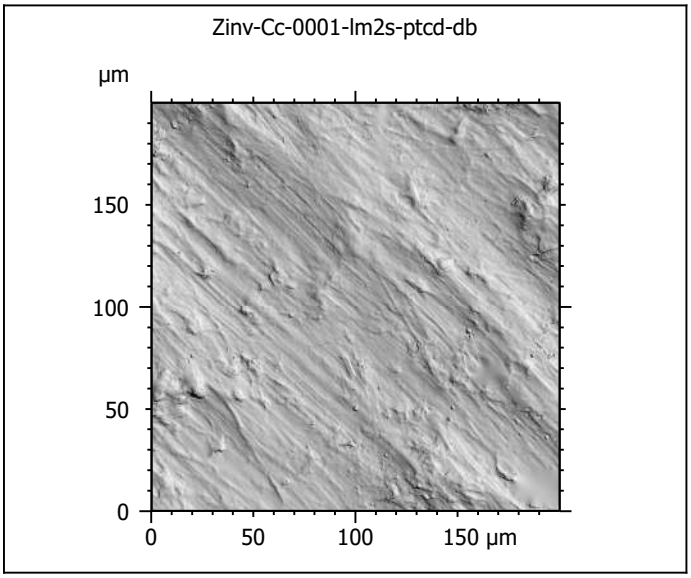

Leica Map Premium 8.0.9151